DEVELOPMENT OF POLYVINYLIDENE FLUORIDE (PVDF) HOLLOW FIBER MEMBRANES BY NOVEL THERMALLY INDUCED PHASE SEPARATION

ZHAO JIE

SCHOOL OF CIVIL AND ENVIRONMENTAL ENGINEERING

2019

DEVELOPMENT OF POLYVINYLIDENE FLUORIDE (PVDF) HOLLOW FIBER MEMBRANES BY NOVEL THERMALLY INDUCED PHASE SEPARATION

ZHAO JIE

School of Civil and Environmental Engineering

A thesis submitted to the Nanyang Technological University

in fulfilment of the requirements for the degree of

Doctor of Philosophy

2019

Statement of Originality

I hereby certify that the work embodied in this thesis is the result of original research, is free of plagiarised materials, and has not been submitted for a higher degree to any other University or Institution.

24/1/2019
.....
Date

Zhao
.....
Zhao Jie

Supervisor Declaration Statement

I have reviewed the content and presentation style of this thesis and declare it is free of plagiarism and of sufficient grammatical clarity to be examined. To the best of my knowledge, the research and writing are those of the candidate except as acknowledged in the Author Attribution Statement. I confirm that the investigations were conducted in accord with the ethics policies and integrity standards of Nanyang Technological University and that the research data are presented honestly and without prejudice.

25/1/19
Date

Supervisor: Wang Rong

Authorship Attribution Statement

This thesis contains material from 2 paper(s) published and 1 paper submitted in the following peer-reviewed journal(s) where I was the first author.

Chapter 4 is published as Zhao, J., Shi, L., Loh, C. H. and Wang, R. Preparation of PVDF/PTFE hollow fiber membranes for direct contact membrane distillation via thermally induced phase separation method. *Desalination* **430**: 86-97 (2018). DOI: 10.1016/j.desal.2017.12.041.

The contributions of the co-authors are as follows:

- Prof. Wang provided the initial project direction and edited the manuscript drafts.
- I prepared the manuscript drafts. The manuscript was revised by Dr. Shi and Dr. Loh.
- I co-designed the study with Prof. Wang and Dr.Shi, and I performed all the laboratory work at the Singapore Membrane Technology Centre (SMTC) and the School of Civil and Environmental Engineering. I also analyzed the data.
- All microscopy, including sample preparation, and other characterization were conducted by me in the Singapore Membrane Technology Centre (SMTC).
- Dr. Shi provided guidance on the fabrication of hollow fiber membranes.
- Dr. Shi and Dr. Loh assisted in the interpretation of the data from the scanning electron spectroscopy and membrane distillation.

Chapter 5 is published as Zhao, J., Chong, J. Y., Shi, L., and Wang, R. Explorations of combined nonsolvent and thermally induced phase separation (N-TIPS) method for fabricating novel PVDF hollow fiber membranes using mixed diluents. *Journal of Membrane Science* **572**: 210-222 (2019). DOI: 10.1016/j.memsci.2018.11.015.

The contributions of the co-authors are as follows:

- Prof. Wang suggested the research area and edited the manuscript drafts.

- I wrote the drafts of the manuscript. The manuscript was revised together with Dr. Chong and Dr. Shi.
- I performed all the membrane fabrication, conducted all the characterization work and data evaluation.
- Dr. Shi provided guidance on the fabrication of hollow fiber membranes.
- Dr. Chong and Dr. Shi assisted in the interpretation of the data from the scanning electron spectroscopy and Fourier transform infrared spectroscopy.
- Dr. Chong provided suggestion on interpretation of membrane formation mechanisms.

Chapter 6 is submitted as Zhao, J., Chong, J. Y., Shi, L., and Wang, R. PTFE-assisted immobilization of Pluronic F127 in PVDF hollow fiber membranes with enhanced antifouling property through N-TIPS method. Submitted.

The contributions of the co-authors are as follows:

- Prof. Wang proposed the initial research direction and edited the manuscript drafts.
- I prepared the drafts of the manuscript. The manuscript was revised by Dr. Chong and Dr. Shi.
- I co-designed the research plan with Prof. Wang conducted all the fabrication of hollow fiber membranes, and all the characterization and performance test. I also analyzed the data collected.
- Dr. Shi provided guidance on the manufacture of hollow fiber membranes.
- Dr. Chong and Dr. Shi advised on the explanation of the data from the scanning electron spectroscopy and fouling test.

24/1/2019 ..... Date

Zhao J ..... Zhao Jie

ACKNOWLEDGEMENTS

In the very first place, I would like to express my sincere appreciation to my supervisor, Prof. Wang Rong, for the support, guidance and encouragement she has extended to me throughout the academic program and research work. It would not have been possible for me to finish my PhD study without her supervision.

Many thanks go to the group members (Prof. Wang's group), especially to Dr. Shi Lei, for his kind help and guidance in experiment trainings, data analysis and writing skills. I also sincerely thank Prof. William Bill Krantz for the helpful guidance with regard to the communication and writing skills. Thanks also go to Prof. Chong Tzyy Haur, Prof. Bae Tae-Hyun, Dr. Loh Chun Heng, Dr. Zhao Shanshan, Dr. Chong Jeng Yi and Dr. Lin Yuqing for their inspiring advices on thesis writing.

I would like to acknowledge the Singapore Membrane Technology Centre (SMTC) for providing me with the necessary facilities. Meanwhile, thanks go to National Research Foundation (NRF) for offering me the Environmental and Water Technologies (EWT) PhD scholarship.

It is my great pleasure to thank everyone for the help and sharing throughout my research work. I sincerely thank Ms. Chan Wai Yee for her support in experiments, Dr. Liu Chang for his suggestions about instrument trainings, Dr. Laurentia , Dr. Liao Yuan, Dr. Tian Miao for their kind sharing in research experience, Dr. Chen Guizi for her advices and instrument training, Dr. Fang Wangxi for his guidance in experiments, Dr. Li Xuesong and Dr. Chou Shuren for useful discussion. Thanks also go to Dr. Li Ye, Dr. Jin Mengyi, Dr. Chen Yunfeng, Ms. Xu Yilin, Mr. Chew Guan Pin Nick, Mr. Chan Tao Guang, Ms. Li Jieling, Ms. Ng Hui Xin Ellen and Ms. Phua Xuan Ru for their endeavors and kind assistance in the research work.

Last but not the least, my fully gratitude is given to my parents for their caring and support to me. I would also like to thank my dearest fiancée, Huan, for her love and constant encouragement. This thesis is dedicated to my beloved grandfather Mr. Zhang Shihua who had passed away during my PhD study.

ZHAO JIE

TABLE OF CONTENTS

LIST OF PUBLICATIONS

- Journals

Zhao, J., Shi, L., Loh, C. H. and Wang, R. (2018). "Preparation of PVDF/PTFE hollow fiber membranes for direct contact membrane distillation via thermally induced phase separation method." Desalination 430: 86-97.

Zhao, J., Chong, J. Y., Shi, L., and Wang, R. (2019). "Explorations of combined nonsolvent and thermally induced phase separation (N-TIPS) method for fabricating novel PVDF hollow fiber membranes using mixed diluents." Journal of Membrane Science 572: 210-222.

Zhao, J., Chong, J. Y., Shi, L., and Wang, R. "PTFE-assisted immobilization of Pluronic F127 in PVDF hollow fiber membranes with enhanced antifouling property through N-TIPS method." Submitted.

- Conferences

Zhao, J., Shi, L., and Wang, R. "Development of PVDF/PTFE hollow fiber membranes for direct contact membrane distillation via thermally induced phase separation method", The 10th Conference of Aseanian Membrane Society (AMS10), Nara, Japan, 26-29 Jul 2016 (Oral and poster presentation; Student Best Poster Award).

Zhao, J., Shi, L., and Wang, R. "Preparation of novel PVDF hollow fiber membranes from a ternary system via combined thermally and nonsolvent induced phase separation (TIPS-NIPS) method", The 9th International Membrane Science and Technology Conference (IMSTEC), Adelaide, Australia, 5-8 Dec 2016 (Oral presentation; Travel Award).

Zhao, J., Shi, L., and Wang, R. "Explorations of combined TIPS and NIPS (N-TIPS) method for development of novel PVDF/PTFE hollow fiber membranes", The 11th International Congress on Membranes and Membrane Processes (ICOM), San Francisco, USA, 29 Jul–4 Aug 2017 (Poster presentation; Student Best Poster Award).

LIST OF TABLES

LIST OF FIGURES

LIST OF SYMBOLS

A	Filtration area of the membrane
D	Estimated diameter of the crystals
d	Pore diameter
f	Flow distribution
F	Permeate flux of DCMD
F_d	Flow rate through dry sample
F_w	Flow rate through wet sample
ΔG^E	Molar excess free energy
ΔH	Fusion enthalpy (melting enthalpy) of the membrane
ΔH_m	Fusion enthalpy (melting enthalpy) of PVDF with 100% crystallinity
ΔH_u	Heat of fusion for the repeat unit
J_w	Permeate flux at each cycle of filtration test
J_w	Pure water flux after cleaning at each cycle of filtration test
K	Scherrer's constant
m_n	Weight of dried hollow fiber after normal post-treatment
m_p	Weight of dried hollow fiber after prolonged post-treatment
M_w	Molecular weight
n	Number of fibers in the module
p	Differential pressure across the pore
ΔP	Pressure difference between the feed side and the permeation side of the membrane
J_{w0}	Pure water permeability
R	Gas constant
R_a	mean roughness parameter
R_e	Reynolds number
R_t	Total flux reduction ratio
Δt	Testing time
T_c	Crystallization temperature of PVDF in dope mixtures
T_m	Melting temperatures of the PVDF in dope mixtures
T_m^0	Melting temperatures of the pure PVDF

V	Volume of permeate taken per determined time, *t*
V_d	Molar volume of the diluent
V_m	Molar volume of the specific repeating unit size of the polymer
V_u	Molar volume of the repeat unit
ΔW	Weight of distillate

Greek

β	Peak width at half height
γ	Surface tension of the wetting liquid
δ_d	Dispersive parameter
δ_p	Polar parameter
δ_h	Hydrogen bonding parameter
θ	Contact angle
θ_d	Diffraction angle
λ	Wavelength of the incident x-rays
ϕ_d	Volume fraction of diluent
ϕ_p	Volume fraction of polymer
χ	Flory–Huggins interaction parameter
χ^*	Flory–Huggins interaction parameter between polymer and the diluent
χ_c	Degree of crystallinity
ω	Weight fraction of Pluronic F127 in the hollow fiber

LIST OF ABBREVIATIONS

ATBC	Acetyl tributyl citrate
BSA	Bovine serum albumin
DCMD	Direct contact membrane distillation
DMP	Dimethyl phthalate
FRR	Flux recovery ratio
ID	Outer diameter of hollow fiber
LEPw	Liquid entry pressure for water
MD	Membrane distillation
MW	Molecular weight
NG	Nucleation and growth
NIPS	Nonsolvent induced phase separation
N-TIPS	Combined TIPS and NIPS
OD	Outer diameter of hollow fiber
PTFE	Polytetrafluoroethylene
PVDF	Polyvinylidene fluoride
PWP	Pure water permeability
SD	Spinodal decomposition
TEP	Triethyl phosphate
TIPS	Thermally induced phase separation

SUMMARY

Polyvinylidene fluoride (PVDF) has received growing attention in hollow fiber membrane preparation for water production and wastewater treatment due to its excellent physical and chemical properties. Currently, the PVDF hollow fiber membranes prepared via the conventional non-solvent phase separation (NIPS) method are often subjected to the formation of macrovoids, resulting in a broad pore size distribution and weak mechanical strength. On the other hand, another method—thermally induced phase separation (TIPS) has gained renewed interest as it can produce robust membranes with a narrow pore size distribution. However, limited studies on TIPS were focused on the control over the surface pore structure, which is the key to the selectivity and permeability of membranes. Therefore, the development of a novel method to fabricate membranes with tailorable surface pore size and strengthened structure has become a crucial issue in improving the feasibility and scalability of PVDF hollow fiber membranes applied in the water industry.

In this study, PVDF hollow fiber membranes were prepared via the TIPS method using mild solvent with a low toxicity as a first trial. Solvent replacement and freeze drying were comparatively used as post-treatment to explore the sustainability aspect of the spinning process. The resultant membranes were subsequently characterized in terms of morphology, mechanical strength, pore size and pure water permeability (PWP). The effects of polymer molecular weight (MW), initial polymer concentration, bore fluid and coagulation conditions on the membrane properties and performance were investigated and discussed. The resultant PVDF hollow fiber membranes exhibited promising pure water permeability values from 663 ± 33 to 878 ± 5 L m^{-2} h^{-1} bar^{-1} with better tensile strength values from 3.8 ± 1.1 to 5.6 ± 0.3 MPa and a mean pore size below 0.2 μm. This study provides a sustainable approach to fabricate PVDF hollow fiber membranes with promising properties using greener solvents.

Further, hydrophobic PVDF-based hollow fiber membranes were developed via TIPS method for direct contact membrane distillation (DCMD). Polytetrafluoroethylene (PTFE) were used as the key additive to enhance the hydrophobicity of membranes. It was found that the crystallization of PVDF was significantly enhanced with

increased nucleation sites provided by PTFE particles, leading to promoted formation of smaller spherulites in a greater density. Furthermore, the improved uniformity and increased amount of cavity between the spherical crystallites coherently facilitated the formation of smaller pores ranging from 0.08 to 0.12 μm. With certain PTFE loading, the membranes exhibited improved porosity, water permeability and hydrophobicity as well as enhanced tensile strength of 9.4 ± 0.3 MPa. During the test of DCMD, a stable permeation flux of 28.3 kg m^{-2} h^{-1} at the feed temperature of 60 ºC with 99.99 % NaCl rejection for over 50 h of operation was achieved, which is comparable with similar type of PVDF membranes while the newly developed membrane exhibited better mechanical strength. This study suggests that the as-spun PVDF/PTFE hollow fiber membranes have great potential in membrane distillation (MD) applications, which require sufficient surface hydrophobicity.

However, it was found that TIPS method could only control the bulk and surface structure as a whole through the thermal effect. Meanwhile, the NIPS method has been demonstrated to be versatile in controlling the pore formation especially on the membrane surface. Therefore, an attempt to combine the TIPS and NIPS (N-TIPS) process was carried out to develop novel microporous PVDF hollow fiber membranes with tunable surface characteristics while maintaining the pore size distribution and mechanical strength. To further control the membrane formation especially near the membrane surface, an amphiphilic additive Pluronic F127 was also added as a potential pore-former and surface hydrophilicity modifier. PVDF hollow fiber membranes with a highly porous structure and a narrow pore size distribution were successfully synthesized by using triethyl phosphate (TEP) and Pluronic F127 in the N-TIPS process. The mechanism of N-TIPS process was thoroughly discussed. The water permeability of the membrane increased significantly from 389 ± 30 to 922 ± 36 L m^{-2} h^{-1} bar^{-1}, with overall porosity improved from 50 ± 2.2 to 69 ± 2.9 %, and a mean pore size of ~0.18 μm. The membranes produced by N-TIPS method also exhibited a good tensile strength ranging from 5.6 ± 0.1 to 6.5 ± 0.2 MPa, showing great potential for a broad range of water applications after further modifications. Besides, the formation of piezoelectric β-phase crystals of the PVDF membrane was observed when the mixed diluent was used, which sheds light on the possible applications of resultant membranes in electrochemical separation process.

Despite that the Pluronic F127 has been successfully used as a pore-former in the N-TIPS process, the stability issue deactivates its hydrophilic modifying function in the membrane preparation from PVDF. In the final part, we developed a novel approach to immobilize F127 in PVDF hollow fiber membranes using PTFE as a binding agent via N-TIPS method. The results suggest that the hydrophobic segment of F127 could adsorb firmly onto PTFE, protruding its hydrophilic segments outwards spontaneously. As a mediating agent, PTFE could allow PVDF to epitaxially crystallize on through fluorine-fluorine interactions. The stability of F127 in the presence of PTFE was confirmed by the analysis of differential scanning calorimetry (DSC) and Fourier transform infrared spectroscopy (FTIR). By using PTFE and F127 conjunctively, the dual functions of F127 were observed in pore formation, surface hydrophilization for PVDF membranes. The water contact angle of PVDF/PTFE/F127 membranes decreased from 101 ± 4 to 69 ± 3° compared with membranes without additives. Compared to the pristine PVDF membranes, the hybrid membranes possess a PWP value of 876 ± 32 L $m^{-2}h^{-1}bar^{-1}$ with a mean pore size of 0.09 ± 0.01 μm. It also has a narrower pore size distribution, a larger porosity, and enhanced antifouling property as well as outstanding tensile strength of 7.1 ± 0.2 MPa, suggesting the potential of N-TIPS method for preparation of membranes with tunable pore structure and improved antifouling properties by using multifunctional additives.

In conclusion, this thesis presents the development of PVDF hollow fiber membranes by discovering new features in TIPS process and exploring its potential in the hybrid process with NIPS. This work contributes to the sustainable development of membrane fabrication technology and facilitates the applications of membrane distillation and microfiltration in water or other related industries.

CHAPTER 1 Introduction

1.1. Background

Water scarcity is one of the largest concerns around the world nowadays, especially the lack of freshwater for drinking. 11 percent of the global population—783 million people—remains without access to an improved source of drinking water and, at the current pace, 605 million people will still lack coverage in 2015 (United-Nations 2012). The global demand for fresh water from daily life, agricultures, industries and other sectors has significantly increased in past decades (Larsen 2009). On the other hand, contamination and deterioration of fresh water resources are becoming worsening factors in adversely affecting fresh water supply. The crucial importance of water to numerous aspects of human health, development and well-being led to the adoption of innovative water sanitation and production technologies (United-Nations 2012). Among those means available today, novel membrane-based technologies have been achieving promising progresses in recent years.

A membrane, as applied to purification and separation, can be defined as a semi-permeable thin film between two phases with preferential transport of some species over others. Modern development of membrane can be traced back to 1963, when the first commercial anisotropic reverse osmosis membrane with properties of defect-free and high flux was made by S. Loeb and S. Sourirajan (Loeb and Sourirajan 1964). Since then, membrane separation processes comprising microfiltration (MF), ultrafiltration (UF), nanofiltration (NF), reverse osmosis (RO), forward osmosis (FO) membrane bioreactor (MBR) and gas separation have been extensively embedded in water treatment, wastewater reclamation, seawater desalination, and other industrial sectors.

The key role in such processes is the membrane. A number of different materials are available to produce membranes. Recently, polyvinylidene fluoride (PVDF) has attracted much attention with regard to its excellent properties including high mechanical strength, thermal stability and chemical resistance, and hydrophobicity compared to other commercial polymer materials (Lloyd *et al.* 1990, Li and Lu 2006, Rajabzadeh *et al.* 2008). Based on related studies, hydrophobic porous membranes have shown great potential in membrane technologies such as membrane contactors

(Bottino *et al.* 2005) and membrane distillation (Gabelman and Hwang 1999). Among common commercial polymer materials, PVDF has higher hydrophobicity (indicated from surface tension) than polysulfone (PS), polyethersulfone (PES), polyimide (PI), but lower hydrophobicity than polytetrafluoroethylene (PTFE). The PVDF membranes can be made into two major types of configurations which include flat sheet and hollow fiber membranes. The hollow fiber modules outweigh flat sheet spiral wound modules with features including a much larger membrane area per unit volume of membrane module, self-mechanical support that can be back-flushed for liquid separation, as well as good flexibility and easy handling during module fabrication, membrane reparation, and system operation (Li and Kim 2008).

Such polymeric hollow fiber membranes can be fabricated via several routes and the phase inversion method is currently the mainstream method. Among the different phase inversion methods, two techniques are frequently used: namely, non-solvent induced phase separation (NIPS) and thermally induced phase separation (TIPS). The NIPS method involves three major components (polymer, solvent, and nonsolvent). The membrane formation starts at the interface between the polymer solution and the nonsolvent driven by the solvent-nonsolvent exchange (van de Witte *et al.* 1996, Setiawan *et al.* 2012, Feng *et al.* 2013). The NIPS technique can expediently adjust the pore size and other surface characteristics of membranes with the help of additives, which has been extensively studied (Shi *et al.* 2008, Wongchitphimon *et al.* 2011). Nevertheless, it is difficult to achieve evenly distributed phase separation along the membrane thickness direction for semi-crystalline polymers such as PVDF, resulting the formation of an asymmetric structure that often contains a supporting layer with finger-like or sponge-like macrovoids due to delayed demixing under supersaturation conditions. Hence, the membrane has poor mechanical strength owing to anisotropic and non-oriented molecules. Furthermore, the inhomogeneous exchange of solvents can lead to a wide pore size distribution, which can negatively affect the selectivity of membrane. On the contrary, the ability to prepare membranes from semi-crystalline polymers is one of the distinct advantages of TIPS over NIPS. The TIPS method is normally employed to fabricate membranes from thermoplastics which include poly(methyl methacrylate) (PMMA) (Rajabzadeh *et al.* 2009), polypropylene (PP) (Matsuyama *et al.* 2002) and PVDF (Cui *et al.* 2014). The phase

separation occurs due to the temperature gradient when the polymer solution (hot front) is in contact with the coagulant (cold front). Subsequently, the pore structure is formed and fixed along with the crystallization of polymer. Therefore, the membranes prepared via TIPS method usually possess a narrow pore size distribution and high mechanical strength (Kim *et al.* 2016). However, the surface properties such as pore size and hydrophilicity cannot be effectively controlled using pore-formers with different functions in the same way as the NIPS method (Shi *et al.* 2007). This can be attributed to the weak mass transfer in the conventional TIPS process as a result of low mutual affinity between commonly used TIPS diluents and the nonsolvent. In addition, a large portion of common diluents used in the TIPS process are considered as non-green solvents in regard to their toxicity to human health and the environment (Figoli *et al.* 2014). Therefore, the key challenge is to modify the TIPS method to sustainably develop desirable PVDF-based hollow fiber membranes which have (1) controllable bulk membrane structure, (2) tailorable surface pore structure and hydrophobicity, (3) good mechanical properties for longer lifetime, (4) and simple and green fabrication for easier scale-up in sustainable mass production.

1.2. Objectives

This research aims to develop PVDF-based hollow fiber membranes via novel thermally induced phase separation. Specifically, the primary objectives of the research are:

- to fabricate PVDF hollow fiber membranes using mild solvents with a low toxicity via TIPS method as a basic step:
  - to study the effect of dope compositions and spinning conditions on membrane properties and performance;
  - to evaluate the feasibility of using green solvents and post-treatment method requiring less solvent consumption as sustainable alternatives;
  - to synthesize PVDF hollow fiber membranes with a robust and porous structure as well as acceptable permeate flux;
- to prepare hydrophobically enhanced PVDF-based hollow fiber membranes with addition of PTFE via TIPS method:

- to synthesize PVDF-based hollow fiber membranes fabricated by using PTFE as an additive;
- to investigate the effect of PTFE on the membrane formation and properties
- to assess the membrane performance by using a direct contact membrane distillation (DCMD) set-up;

➢ to develop PVDF-based hollow fiber membranes with tailorable surface properties by using the combined TIPS and NIPS (N-TIPS) method:

- to fabricate and characterize PVDF-based hollow fiber membranes with a more precisely controlled structure and a better balance between high mechanical strength and permeability;
- to incorporate a typical NIPS additive to understand the underlying phenomena in the membrane formation kinetics during the N-TIPS process

➢ to achieve hydrophilic PVDF-based hollow fiber membranes via N-TIPS method:

- to introduce a multifunctional additive to enhance pore-forming process and the hydrophilicity;
- to develop a solution to immobilize the additive if the stability of the additive in the PVDF-based membrane is an issue;
- to assess the antifouling performance of the prepared membranes by using a microfiltration set-up.

1.3. Thesis outline

This thesis includes five chapters, which are highlighted as follows:

Chapter 1: Introduction - Background information and the objectives of the study are provided.

Chapter 2: Literature review - This chapter is divided into four parts. The first part is the review of PVDF properties. It starts with the introduction of crystalline properties of PVDF followed by its thermal and chemical stability. The second part of the literature study contains the concepts and mechanisms of TIPS process. This is then followed by a more specific review concerning of development of hollow fiber

membranes by TIPS process. The current status of application of PVDF membranes, subsequently, is followed to end this chapter.

Chapter 3: Fabrication of PVDF hollow fiber membranes using mild diluents via TIPS method–PVDF hollow fiber membranes were fabricated using mild diluents with a low toxicity via TIPS method. The effects of polymer molecular weight, initial polymer concentration, air gap and coagulation conditions on the membrane properties and performance were investigated and discussed.

Chapter 4: Preparation of hydrophobically enhanced PVDF-based hollow fiber membranes for membrane distillation (MD) via TIPS method - PVDF/PTFE hollow fiber membranes were fabricated via the TIPS method with various PTFE loadings to thoroughly investigate the impact of PTFE addition on membrane properties and possible mechanisms behind. The characteristics of prepared membranes were examined and the pure water permeability and performance of DCMD were also evaluated.

Chapter 5: Explorations of combined TIPS and NIPS (N-TIPS) method for development of PVDF-based hollow fiber membranes - PVDF hollow fiber membranes were developed via a modified N-TIPS method using the triethyl phosphate (TEP) as a second diluent and Pluronic F127 particles as additives. The pore size and pore size distribution, surface hydrophobicity, mechanical strength and water permeability were characterized.

Chapter 6: Fabrication of hydrophilic PVDF-based hollow fiber membranes with improved antifouling property through N-TIPS method - Novel hydrophilic PVDF hollow fiber membranes were prepared via N-TIPS method using PTFE and Pluronic F127 particles as additives. The individual and combined effect of PTFE and Pluronic F127 on the membrane formation and properties was evaluated. The stability of Pluronic F127 in PVDF membranes with or without the presence of PTFE was studied.

Chapter 7: Conclusions and future work - The important findings of this study and recommendations are summarized in this chapter.

CHAPTER 2 Literature Review

2.1. Properties of PVDF

Polyvinylidene fluoride (PVDF or PVF_2) is the addition polymer of 1,1-difluoroethene, generally known as vinylidene fluoride (VDF or VF_2) (Dohany 2000). PVDF is commonly manufactured by polymerization in aqueous emulsion or suspension using radical generators, forming a repeat unit of–CH_2–CF_2– (Liu *et al.* 2011).

Compared to other perfluorocarbon polymers, PVDF has relatively high mechanical strength and abrasion resistance. Besides, the excellent thermal stability and chemical stability as well as the resistance to nuclear radiation and ultraviolet also make PVDF applicable to a wide range of applications.

2.1.1. Crystalline properties of PVDF

PVDF is a semi-crystalline polymer that typically contains 3 wt% hydrogen and 59.4 wt% fluorine (Dohany 2000) as shown in **Figure 2.1**. The unique properties of PVDF are rooted in its crystalline structure which are contributed by the spatial arrangement of the CH_2 and CF_2 groups along the polymer chains (Liu *et al.* 2011).

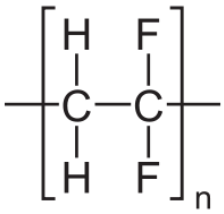

Figure 2.1. Chemical structure of PVDF

Different from other synthetic polymers, PVDF chains can crystallize into at least four chain conformations, which are α (form II), β (form I), γ (form III) and δ (form IV) (Lovinger 1982, Hirschinger *et al.* 1991). α-phase, the trans-gauche (TGTG') molecular chain conformation with H and F atoms placed alternately on each side, is the most common polymorph of PVDF (Dohany 2000), which can be produced during crystallization from the melt (Güell and Davis 1996, Khayet *et al.* 2002, Madaeni and Yeganeh 2003). The four phases can transform from one to the other

under certain conditions (Rajabzadeh *et al.* 2009). Because of the good piezoelectricity and pyroelectricity property of the β phase PVDF, most attention has been paid to obtain more β phase crystalline phases in the prepared samples (Madaeni and Yeganeh 2003). The β phase PVDF can be obtained from non-polar α phase PVDF by various processes such as mechanical deformation, poling under large electric fields, and crystallization from the melt under high pressure or very high cooling rates (Du *et al.* 2007).

The impact resistance and mechanical strength of PVDF are influenced by crystallinity. Spherulite-like crystals of PVDF that can be seen in the optical microscope are crystallographically packed lamellae of polymer chain segments. The crystallinity of PVDF can be measured via the method described below. Polymer-diluent samples weighting about 10 mg closed in aluminum pans were heated from room temperature up to 180 °C at 10 °C/min. The degree of crystallinity of membranes was calculated according to the following equation (Chen *et al.* 2014):

$$\chi_c = \frac{\Delta H}{\Delta H_m} \times 100\% \tag{2.1}$$

where χ_c is the degree of crystallinity (%); ΔH and ΔH_m represent the fusion enthalpy (melting enthalpy) of the membrane and PVDF with 100% crystallinity, respectively; The value of ΔH_m is 104.5 J g^{-1} (Loh and Wang 2014).

2.1.2. Thermal stability of PVDF

The high stability of fluoropolymers is generated from the high electronegativity of fluorine atoms on the chain and the high bond dissociation energy of the C–F bond. PVDF was observed to be among the most thermally stable halogen-containing polymers in the study using a Torsional Braid Analysis (TBA) method (Furusho *et al.* 1974). The thermal stability of a commercial Kynar PVDF ultrafiltration membrane was investigated using spiral-wound modules at an elevated temperature. The PVDF membrane remained in stable state without evidence of thermal degradation was observed during continuous operation at 85.6 °C and constant pressure for 7 months.

Nevertheless, PVDF can be thermally unstable under certain harsh conditions. Rapid thermal decomposition occurs and HF gas evolves if the ambient temperature exceeds 375 °C. The charring phenomenon happens, i.e., the residue ultimately burns entirely to char after 70 wt % loss, at higher temperature (Dohany 2000). Predominated by dehydrofluorination, thermal degradation in PVDF consequently can lead to a variety of chemical reactions comprising the cross-linking of the polymer or formation of (–C=C–) under elevated temperature conditions (Liu *et al.* 2011). Another related phenomenon—inhomogeneous thermal degradation of PVDF—was analyzed (Lovinger and Freed 1980). The elimination of HF with a little chain scission or cross-linking was interpreted as primary mechanism.

2.1.3. Chemical resistance of PVDF

It has been proved that PVDF has chemical stability against a wide range of harsh chemicals, containing oxidants halogens, inorganic acids, as well as aliphatic, aromatic and chlorinated solvents. However, PVDF has poor stability in caustic environments. There are many factors that can affect the chemical resistance of PVDF membranes, including the exposure time, chemical concentrations, temperature, pressure, frequency of the attack cycles, and the type of mechanical stress imposed. The excellent chemical stability of PVDF does not particularly apply to strong base solutions or to esters and ketoneset.

The degradation of PVDF caused by alkaline solutions was mentioned in some early investigations (Komaki 1979, Shinohara 1979, Nguyen 1985). The discolouration of oxyfluorinated PVDF film was observed by Shinohara, showing that the dehydrofluorination led to the formation of carbon-carbon double bonds (Shinohara 1979). Several factors can have an influence on the chemical stability of PVDF membranes, including the concentration of chemicals, the treatment temperature, the treatment pressure, the exposure time, the frequency of the attack cycles, and the strain imposed.

2.2. Thermally induced phase separation (TIPS)

This part of review begins with an overview of the concepts phase inversion, especially the thermally induced phase separation (TIPS), followed by the discussion of different types of TIPS and different processes of TIPS.

2.2.1. Concept of phase separation

Phase inversion, which is a demixing process, transforms the initially homogeneous polymer solution from a liquid state to solid state under controlled conditions. (Mulder 1996). The core process of phase inversion is the formation in a polymer solution of two inter-dispersed liquid phases (a polymer rich phase and a polymer lean phase) attributed to the change of the state of the polymer solution induced by the alteration of its surrounding circumstances or operating conditions, followed by crystallization, gelation or vitrification. In other words, a liquid polymer solution is precipitated into two phases: (a) a polymer-rich phase that forms the matrix of the membrane; (b) a polymer-lean phase that forms the membrane pores in an unstable nascent membrane structure. The morphology of porous asymmetric membrane structure is then fixed with the subsequent solidification process.

- Types of phase separation

To date, four major types of phase inversion methods have been developed, which include TIPS, non-solvent induced phase separation (NIPS), vapor induced phase separation (VIPS), and solvent evaporation. The phase inversion can be induced through cooling, immersion in liquid-phase non-solvent, contact with vapor-phase non-solvent, and evaporation of solvent, respectively. Among them, TIPS and NIPS are most broadly utilized during the past decades (Kim *et al.* 2016):

(1) Thermally induced phase separation (TIPS): the precipitation is achieved by diminishing the temperature of the polymer solution. This process is suitable for membrane preparation from semi-crystalline polymers such as PVDF, which can not be easily dissolved in common solvents at room temperature. TIPS is also one of chief methods for the fabrication of microporous membranes. In the general TIPS process, a homogeneous solution is formed by dissolving a polymer

in a high boiling point, low molecular weight diluent, which could be a single water-immiscible solvent or a mixture of solvent and non-solvent at high temperature (Liu *et al.* 2011). By cooling down or quenching (cooling down at rapid rate) the homogeneous solution, the phase separation is induced. After the solidification of polymer-rich phase the morphology of porous membrane structure can be created by extracting the solvent (Mulder 1996).

(2) NIPS or diffusion induced phase separation (DIPS): diffusional mass exchange, due to the contact of the polymer solution with a non-solvent, leads to a change in the polymer film composition and then precipitation is induced.

The major difference between the TIPS and NIPS is that the removal of thermal energy to convert the solution into a two-phase mixture is required in the former process, while an exchange between non-solvent and solvent for membrane formation is involved in the latter method (Liu *et al.* 2011).

- Advantages of TIPS over NIPS

(1) The TIPS process is applicable to a wide range of polymers that could not be formed into membranes due to poor solubility by conventional NIPS process. Based on this concern, the ability to prepare membranes from semi-crystalline polymers is one of the distinct advantages of TIPS over NIPS;

(2) TIPS method is able to create a variety of microporous structures with high porosity, sometimes exceeding 90% (Lloyd *et al.* 1990);

(3) TIPS method can generate relatively thick isotropic structures. On the other hand, if a thermal gradient is induced in TIPS process, it is also possible to develop anisotropic structures;

(4) Smaller number of variables is needed to be controlled when the preparation follows TIPS process (Lloyd *et al.* 1990);

(5) Membranes developed by TIPS method usually exhibit a higher mechanical strength and narrower pore size distribution than those prepared by NIPS method.

2.2.2. Principles of TIPS method

- Types of TIPS method

TIPS method can be categorized into two types: (1) solid–liquid (S–L) separation with subsequent crystallization (generally); (2) liquid–liquid (L-L) separation with subsequent crystallization. The miscibility of the system, which is correlated with the strength of polymer–diluent interactions, is the major factor determining the type of phase separation (Kim and Lloyd 1992). When thermal energy is removed from a homogeneous polymer–diluent mixture, the TIPS can occur via S-L or L-L phase separation according to several crucial conditions including polymer–diluent interaction, polymer com-position, and thermal diving force. The ultimate morphology of membrane in TIPS process is in hinges on the kinetics and the thermodynamics of the phase separation (Ji *et al.* 2007).

- Solid-liquid (S-L) phase separation

For binary systems whereby the polymeric component in polymer-diluent mixture is able to crystallize, the melting point of the polymer can be described as follows (Flory 1953):

$$\frac{1}{T_m} - \frac{1}{T_m^o} = \frac{RV_u}{\Delta H_u V_d}(\phi_d - \chi\phi_d^2) \tag{2.2}$$

where T_m^o and $T_m$are the melting temperatures of the crystalline polymer in the pure crystalline polymer and solution, respectively; V_d is the molar volume of the diluent, V_u is the molar volume of the repeat unit, ΔH_u is the heat of fusion for the repeat unit, ϕ_d is the volume fraction of the diluent, and χ is the Flory-Huggins interaction parameter.

Equation 2.2 can be worked out to give:

$$T_m = \frac{1}{\frac{RV_u}{\Delta H_u V_d}(\phi_d - \chi\phi_d^2) + \frac{1}{T_m^o}} \tag{2.3}$$

It can be plotted as a function of $\phi_p(= 1 - \phi_d)$ as shown in **Figure 2.2**. The line differentiating the homogeneous one-phase region at raised temperatures. The heterogeneous, two-phase, solid-liquid region is referred to as the melting point

depression curve. As illustrated in **Figure 2.2**, three diluents (represented in curves +/0/-) can have different strengths of interaction with the polymer (Y).

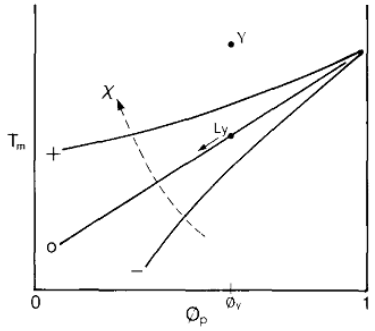

Figure 2.2. Temperature-composition phase diagram for a polymer-diluent system (polymer is semi-crystalline, Y indicates the initial temperature and concentration of polymer, Ly indicates the route that the polymer-diluent system would follow upon reaching the temperature) (With permission from Elsevier for non-commercial purposes (Lloyd *et al.* 1990))

The temperature at which phase separation takes place rises when the strength of interaction drops (χ rises). When $\chi \leq 0$, the relationship shows concave curvature with respect to the composition axis. When $\chi = 0$, the relationship is essentially linear. When $\chi \geq 0$, convex curvature is observed. In terms of greater positive χ, the plot has a tendency to level off at low concentrations of polymer. Stable nuclei grow in size, succeeding primary nucleation of the pure polymer phase, through secondary nucleation into spherulites. Amorphous polymer and diluents are excluded by the crystals in growth during the process of crystallization. Defined as nucleation and growth (NG), this phase separation mechanism is attained via cooling the solution rapidly (defined as quenching) or slowly (Lloyd *et al.* 1990).

- Liquid-liquid (L-L) phase separation

L-L phase separation occurs in a polymer rich phase and a polymer lean phase. The binodal curve is generally denoted by the boundary of L-L phase separation region. Attributed to the presence of the binodal curve and the spinodal curve, this phase separation process follows two types of mechanisms (van de Witte *et al.* 1996).The system of solution is stable to lesser fluctuation when the solution composition

locates at the area between the binodal curve and the spinodal curve (meta-stable region). However, liquid-liquid phase separation occurs following NG mechanism when the fluctuation is large enough. All fluctuations in composition bring about a lessening of free energy as well as L-L phase separation takes place following spinodal decomposition (SD) mechanism when the solution is rapidly cooled into the region surrounded by spinodal curve (unstable region) (Song *et al.* 2012).

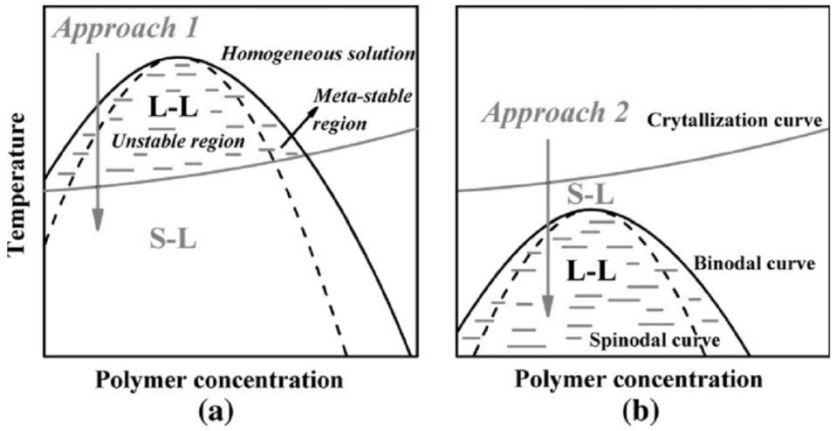

Figure 2.3. Different approaches for L–L and S–L phase separation occurring in different systems: (a) system with weak interaction (enter meta-stable/unstable region before crystallization) and (b) system with strong interaction (reach crystallization and then enter unstable region) (With permission from Elsevier for non-commercial purposes (Song *et al.* 2012))

The structures are strongly influenced by the arrangement of S-L and L-L phase separation. When the crystallization curve is reached as the solution temperature rises, S-L phase separation takes place following NG mechanism. The structures generated by L-L phase separation are stabilized by the crystallization process. Bicontinuous or cellular structures are attained when L-L phase separation is followed by S-L phase separation (Approach 1 in **Figure 2.3(a)**). In contrast (Approach 2 in **Figure 2.3(b)**), governed by S-L phase separation mechanism, the formation of spherulitic structures takes place (Song *et al.* 2012). The position of the binodal curve is determined by the affinity between the polymer and diluent, which is defined as the interaction parameter of the system. When the strength of interaction is high (**Figure 2.3(b)**), the system follows S-L phase separation. When the strength

of interaction is not sufficiently high (**Figure 2.3(a)**), the system follows L-L phase separation with successive crystallization of polymer (Song *et al.* 2012).

The phase separation is induced when the homogeneous solution is cooled down under controlled conditions. The morphology of porous membrane structure can be produced by removing the diluent using extractant when the solidification of polymer-rich phase has taken place.

- Gelation and vitrification

The solidification of polymer solutions is commonly designated by the term "gelation". However, the definition of "gelation" is ambiguous sometimes when it is applied to cases where the formation of "glasses" occurs. A "gel" can be denoted as a matrix of polymer chains cross-linked with diluent trapped in the network (van de Witte *et al.* 1996).

Interconnected polymer matrix, in this case, the gels, can form via a variety of intermolecular interactions, including ionic interactions, microcrystallites, dipolar interactions, hydrogen bonding, solvent bridging, and hydrophobic interactions (Miles 1988, Guenet 1992, Tanaka 1992).

- Combination of liquid-liquid phase separation and crystallization or liquid-liquid phase separation and gelation

Phase transitions usually come across in combination with L-L phase separation are gelation or vitrification, crystallization of the polymer-diluent system. These transitions are helpful in most cases to make the structure of the solution system at certain stage fixed during L-L phase separation. When L-L phase separation and the other phase transitions take place concurrently, desired structures are also able to be attained. Corresponding theoretical phase diagrams are shown in **Figure 2.4** (van de Witte *et al.* 1996).

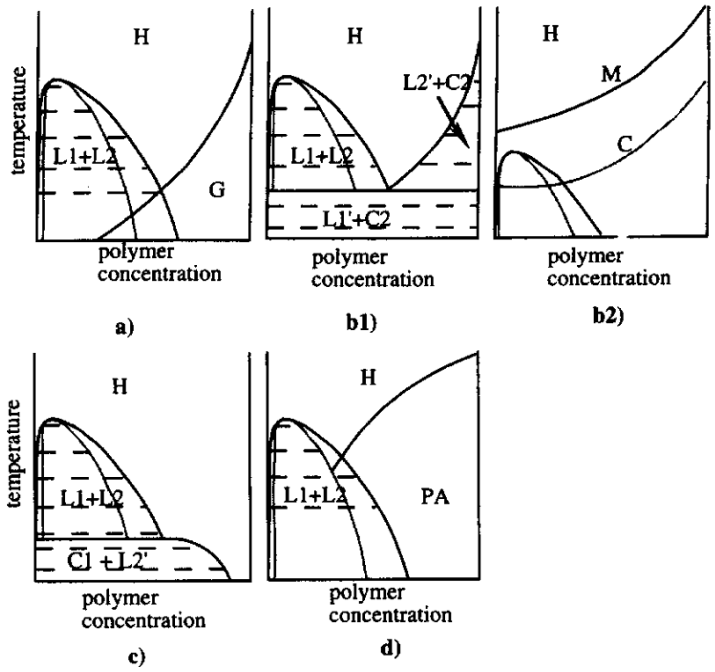

Figure 2.4. Phase diagrams for combinations of phase transitions: (a) combination of liquid-liquid demixing and glass transition; (b1) equilibrium phase diagram for a combination of liquid-liquid demixing and crystallization of the polymer; (b2) non-equilibrium phase diagram for a combination of liquid-liquid demixing and crystallization of the polymer; (c) combination of liquid-liquid demixing and crystallization of the solvent; (d) combination of liquid-liquid demixing and polymer association. Symbols: H, homogeneous solution; L1, dilute polymer solution; L2, concentrated polymer solution; G, glassy state; C2, polymer crystallites; PA, polymer association; M, curve describing equilibrium melting point depression; C, crystallization curve (With permission from Elsevier for non-commercial purposes (van de Witte *et al.* 1996)

2.3. Development of hollow fiber membranes via TIPS method

This part of review begins with an overview of hollow fiber membrane preparation techniques, followed by the discussion of the fabrication conditions and parameters involved in making PVDF hollow fiber substrates via thermally induced phase separation.

Generally, the preparation for hollow fiber membranes via TIPS method follows steps described below:

(1) Homogeneous solution formation at elevated temperature. A homogeneous solution is prepared by dissolving a polymer in a high boiling point, low molecular weight liquid or solid referred as the diluent, which could be a single

solvent or a mixture of solvent and non-solvent at high temperature (Liu *et al.* 2011);

(2) The solution is then cast into the desired shape, flat or hollow fiber membrane (Rajabzadeh *et al.* 2008);

(3) The solution is cooled at a controlled rate or quenched to induce phase separation;

(4) The diluent is removed (typically by solvent extraction);

(5) The extractant is removed (typically by evaporation) to generate a microporous structure (Lloyd *et al.* 1990).

Matsuyama *et al*. prepared polyethylene hollow fiber membrane via thermally induced phase separation using a batch-type extrusion apparatus (**Figure 2.5**) (Matsuyama *et al.* 2003). Rajabzadeh *et al*. adopted this method in their studies on preparation of PVDF hollow fiber membrane via TIPS method under different fabrication conditions (Fane *et al.* , Rajabzadeh *et al.* 2008, Rajabzadeh *et al.* 2009, Rajabzadeh *et al.* 2012).

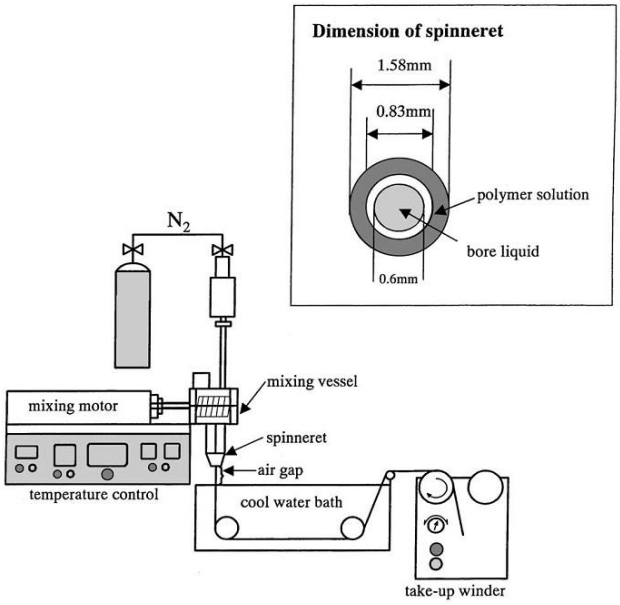

Figure 2.5. Schematic diagram of batch-type extrusion apparatus for hollow fiber membranes preparation (With permission from Elsevier for non-commercial purposes (Matsuyama *et al.* 2003))

2.3.1. Effect of dope compositions

- Diluent selection

The diluent used in TIPS process can be a single solvent or a mixture of solvent and non-solvent with high boiling point, low molecular weight. The selection of diluents shows significant effects on polymer crystallization process and the resulting membrane morphology, and further effects on membrane properties, including pore size, water permeability, mechanical strength, etc. The selection and application of diluents can be categorized into two types: (1) single diluent, which forms binary solution system with the polymer material; (2) mixed diluents, commonly two different diluents, which form ternary solution system with the polymer material (Ji *et al.* 2007).

Based on recent studies, a variety of diluents was employed by researchers, such as cyclohexanone (CO), dibutyl phthalate(DBP), dibutyl sebacate (DBS), diethyl phthalate (DEP), dioctyl adipate (DOA), dioctyl phthalate (DOP), dibutyl sebacate (DBS or KD) dioctyl sebacate (DOS), di(2-ethylhexyl) phthalate (DEHP), diphenyl ketone (DPK), γ-butyrolactone (GBL), Propylene carbonate (PC) (Gu *et al.* 2006, Su *et al.* 2007, Cui *et al.* 2008, Yang *et al.* 2008). The diluents were used individually or in mixtures. By using different types of diluents, the crystallization temperature was altered. With such change of T_c, various membrane structures ranging from spherulite-like crystallites to sheaf-like crystallites were attained (Su *et al.* 2007).

- Toxicity concerns

A major portion of conventional diluents used in the TIPS process are considered as non-green solvents in regard to their toxicity to human health and the environment (Figoli *et al.* 2014). For example, DEP, DBP, DOP, DPK have been found to be carcinogenic to human health upon long-term exposure (Jung *et al.* 2018). Therefore, efforts have been made to replace such highly toxic solvents for the use of diluent in the TIPS process (Cui *et al.* 2013, Figoli *et al.* 2014, Hassankiadeh *et al.* 2014, Cui *et al.* 2015, Hassankiadeh *et al.* 2015, Jung *et al.* 2016, Chang *et al.* 2017). Cui *et al.* tried to utilize a low toxic triethylene glycol diacetate (TEGDA) as diluent and achieved PVDF membranes with comparable permeability (Cui *et al.* 2015). Hassankiadeh *et al.* developed PVDF membranes with a novel green solvent—

PolarClean and demonstrated the possible usage of additives (Hassankiadeh *et al.* 2014). However, the membranes prepared using these non-toxic solvents often possessed a relatively inferior property especially in mechanical strength compared to the ones obtained using conventional solvents (Cui *et al.* 2013).

- Initial polymer concentration

The initial polymer concentration affects the polymer-diluent interaction, which can result in the alteration in the phase-separation mechanism. Furthermore, the morphology of resultant membrane can be substantially influenced. The analysis on the effect of initial polymer concentration can be made based on two scenarios in terms of the position of the phase diagram. When the initial polymer concentration is lower than the upper critical solution concentration (the critical temperature above which the components of mixture are miscible in all proportions), the solution will undergo solid-liquid phase separation (Nic *et al.* 2012). NG of crystals in the polymer-rich phase will lead to the formation of spherulitic morphology. On the other hand, when the initial polymer concentration is greater than the upper critical solution concentration, L-L phase separation can precede crystallization. Under such condition, interconnected bicontinuous structure will form while the formation of polymer particles will be inhibited (Li *et al.* 2008).

In the study of Yang *et al*., S-L phase separation mechanism dominated when that the PVDF concentration was larger than 30 wt % (Yang *et al.* 2008). Ji and co-workers obtained spherulites structure at the initial polymer concentration of 30 wt %. Meanwhile, the cellular structure was found when the initial polymer was concentrated (Ji *et al.* 2007). Su and co-workers found that the crystallization temperature of PVDF increased when increased polymer concentrations were applied (Su *et al.* 2007).

- Blending

The further development and applications of PVDF membranes are limited by numerous problems. Due to the low surface energy, the strongly hydrophobic nature of PVDF results in serious membrane fouling during the process of filtration, which is initiated by different types of hydrophobic solutes and colloids (termed foulants), including natural organic matters (NOMs), proteins and microorganisms. Hence,

improving the hydrophilicity of PVDF membranes should be taken into account in certain applications (Rajabzadeh *et al.* 2012).

Numerous attempts, in terms of modification, have been taken to improve the hydrophilicity of PVDF. The modification for hydrophilicity improvement can be categorized into two groups: surface modification and blending modification. First of all, surface modification, which consists of coating and grafting has been taken into account, such as alkaline solution treatment (Bottino *et al.* 2000), chitosan coating (Boributh *et al.* 2009) and plasma treatment (Yang *et al.* 2011). Blending modification, in comparison with surface modification, can be more practical in industrial fabrication since it is able to maintain the membrane preparation process unchanged. Hydrophilic polymers, such as polyethylene glycol (PEG) (Kim and Lee 1998), perfluorosulfonic acid (PFSA) (Kim and Lee 1998), sulfonated polycarbonate (SPC) (Masuelli *et al.* 2009) and, poly(methyl methacrylate) (PMMA) were used as hydrophilic additives in the modification of PVDF membranes (Rajabzadeh *et al.* 2012). In addition to improving the hydrophilicity, the kinetics and thermodynamics conditions can be altered during the TIPS process to control membrane structure, pore size and pore size distribution (Kim and Lee 1998, Lang *et al.* 2007, Yuan and Dan-Li 2008, Masuelli *et al.* 2009).

Compared with the blending of polymers, the blending of inorganic particles can be easier in the preparation process. The isodimensional nanoparticles are considered to be introduced to the membrane network by blending them with polymer-diluent solution in the TIPS processes. Recent studies have studied the introduction of isodimensional nanoparticles such as ZrO_2 (Bottino *et al.* 2002), SiO_2 (Bottino *et al.* 2001, Cui *et al.* 2010), $CaCO_3$ (Li and Lu 2006),TiO_2 (Cao *et al.* 2006, Damodar *et al.* 2009, Oh *et al.* 2009, Shi *et al.* 2012), Al_2O_3 (Yan *et al.* 2006, Cui *et al.* 2008, Liu *et al.* 2011), $Mg(OH)_2$ (Dong *et al.* 2012), one dimensional TiO_2 nanowires (Wei *et al.* 2011), two dimensional clay platelets (Li and Kim 2008).

Due to its semi-crystalline property, the nucleation and crystallization of PVDF could play a significant role in the formation of membrane microstructures during thermal processes such as the TIPS. Therefore, in recent studies of the TIPS method, a number of additives have been used in PVDF/diluent systems to adjust these two processes

during membrane formation, as summarized in **Table 2.1**. Based on the effects of the additives on membrane formation, they can be generally classified into two major types: nucleating agents and crystallization inhibitors. In the first category, the nucleating agents represent those additives that can enhance the NG of the polymer-rich phase, as they are able to act as crystal nuclei during the nucleation process. The additives with such functions include $CaCO_3$ (Li and Lu 2006, Song *et al.* 2016), TiO_2 (Shi *et al.* 2012), montmorillonite (MMT) (Ma *et al.* 2013), polytetrafluoroethylene (PTFE) (Ma *et al.* 2013), oxidized multi-wall carbon nanotubes (O-MWCNTs) (Xu *et al.* 2014), etc. The additives in the second category normally act as crystallization inhibitors due to their ability on suppressing the crystallization process of PVDF crystalline phase. Examples from previous study include blending PVDF with poly(vinylpyrrolidone) PVP (Cha and Yang 2006, Rajabzadeh *et al.* 2012), poly(methyl methacrylate) PMMA (Cui *et al.* 2008, Rajabzadeh *et al.* 2012), SiO_2 (Cui *et al.* 2010), glycerol (Rajabzadeh *et al.* 2008, Ghasem *et al.* 2011), etc.

Table 2.1. Effects of additives on PVDF membranes through TIPS method[a]

Type of additive	Additive	Solvent	Structure	Spherulite formation	Tensile strength	Hydrophilicity	Porosity	Water permeability	Ref.
Nucleating agent	$CaCO_3$	DBP, GBL/DOP	Cellular	Decrease size, improve uniformity	Increase	Decrease	Increase	Increase	(Li and Lu 2006, Song *et al.* 2016)
	TiO_2	DMP	Spherulitic	Decrease size, increase amount	Increase	Decrease	Increase	Increase	(Shi *et al.* 2012)
	MMT	DPK	Spherulitic	Decrease size, increase amount	Increase	-[b]	-[b]	-[b]	(Ma *et al.* 2013)
	PTFE	DPK	Spherulitic	Decrease size, increase amount	Increase	-[b]	-[b]	-[b]	(Ma *et al.* 2013)
	O-MWCNTs	DBP	Cellular	Decrease size, increase amount	Increase	Increase	Decrease	Decrease	(Xu *et al.* 2014)
Crystallization inhibitor	PVP	GBL, DEP	Spherulitic	Decrease size, improve uniformity	Increase	Increase	-[b]	Decrease	(Cha and Yang 2006, Rajabzadeh *et al.* 2012)
	PMMA	Sulfolane, DEP	Cellular (sulfolane), spherulitic (DEP)	Decrease size, improve uniformity	Decrease	Increase	-[b]	Decrease	(Cui *et al.* 2008, Rajabzadeh *et al.* 2012)
	SiO_2	DBP	Spherulitic	Decrease size, improve uniformity	Increase	Increase	Increase	Increase	(Cui *et al.* 2010)
	Glycerol	Triacetin	Spherulitic	Improve connectivity	Decrease	-[b]	Increase	Increase	(Rajabzadeh *et al.* 2008, Ghasem *et al.* 2011)

Notes:

[a)] This summary is based on the effects of additives before the occurrence of aggregation above the optimum loading;

[b)] The effect is not discussed in the cited reference.

2.3.2. Effect of spinning conditions

- Polymer extrusion temperature

Fewer studies on the effect of polymer extrusion temperature have been carried out compared to other relevant fabrication factors. Nevertheless, the polymer extrusion temperature is rather important in controlling the TIPS process since it has a crucial impact on the evaporation of diluent. Rajabzadeh *et al*. studied effects of polymer extrusion temperature on the morphology and performance of PVDF hollow fiber membranes. They found that the effects of the increase in polymer extrusion temperature on the membrane structure and water permeability were quite different even contradictory in different polymer-diluent solution systems (Rajabzadeh *et al.* 2008, Rajabzadeh *et al.* 2009, Rajabzadeh *et al.* 2012).

- Effect of air gap distance

Following the previous section, air gap distance is another critical factor influencing the evaporation process of diluent. In the same study of Rajabzadeh and co-workers, the effect of air gap distance was also discussed together with polymer extrusion temperature. For PVDF/triacetin/glycerol ternary system, the water permeability lessened by increasing air gap distance (Rajabzadeh *et al.* 2008). In this scenario, the higher air gap distance, the higher the evaporation at the outer surface of the membrane. This led to the higher concentration of the polymer and the lower surface porosity, which resulted in lower permeability of the membrane. Except for evaporation of the diluent at the outer surface of the membrane, other phenomena also may have an impact on the membrane structure during the air gap distance. Die swell and relaxation takes place after being extruded from spinneret caused by the relaxation of polymeric macromolecules (Chung 1997).

- Effect of cooling condition

In TIPS process, the cooling and the quenching condition are important factors affecting the crystallization of PVDF membranes. Different quenching (rapid cooling) conditions also affect the polymer crystallization structure (Barton and McHugh 2000). With the increase of cooling rate, the crystallization temperature of PVDF lessened gradually (Su *et al.* 2007). Lloyd *et al*. indicated that the supercooling

was initiated by increasing the cooling rate, i.e., prior to the actual crystallization of the polymer from solution, the polymer solution might cool to temperature below its corresponding equilibrium crystallization temperature (Lloyd *et al.* 1990, Lloyd *et al.* 1991). Su *et al*. reported that the PVDF crystallization rate rose and the crystallinity lessened with the increase of cooling rate when GBL was used as a diluent. However, the PVDF crystallization rate only exhibited a slight rise and the crystallinity had no noticeable variation when KD was used as a diluent (Su *et al.* 2007).

- Effect of coarsening

The polymer-diluent system will carry on to evolve to lessen the surface energy when the development of the porous structure via phase separation has taken place earlier on (Song and Torkelson 1995). This process, defined as coarsening, brings about a decrease in the amount of droplets and an increase in their diameter (Voorhees 1992) which can be observed from the increase in their pore size (Aubert 1990, Song and Torkelson 1995). Coarsening is of great importance, in the TIPS process, since it may dominate the mechanism of the phase separation, either SD or NG, at early stage within the first few minutes.

The coarsening effects were studied by Gu *et al*. at 368 K (Gu *et al.* 2006). As a result, the rich polymer phase had the ability to congregate. There was noticeable spherulitic structure at of the phase separation, either SD or NG, at early stage within the first. The diameter of the spherulities increased as the duration increased, while the size of the pore remained unchanged. Two different types of cooling approaches were adopted by Yang *et al*. to induce phase separation of homogeneous PVDF-DPK solution (Yang *et al.* 2008). Small pores were in greater amount due to the shortage of growing time.

- Effect of take-up speed

High-Speed spinning is more desirable in industrial hollow fiber membrane manufacture in order to increase the efficiency of production. On the other hand, the origin of macrovoids formation has remained to be controversial. Macrovoids are unfavorable in the fabrication of asymmetric hollow fiber membranes as they can weaken the mechanical strength of the membrane, resulting in membrane failure at high pressures. A number of studies have been carried out to modify the phase

inversion conditions to yield a sponge-like structure to diminish macrovoids, including (1) high concentration of polymer solutions, (2) the addition of components with high viscosity (Liu *et al.* 2003), (3) the induction of delayed phase separation or gelation, (4) spinning at high shear rates, and (5) the addition of surfactants.

Wang *et al*. observed that the formation of finger-like macrovoids structure was able to be inhibited or eliminated in hollow fiber membranes using high-speed take up techniques (Wang *et al.* 2004). Shang *et al*. studied the effect of take-up speed on the structure and performance of the hollow fiber membranes prepared via TIPS process (Shang *et al.* 2003). The effect of the take-up speed on the permeability was more sensitive at the elevated temperature condition.

2.4. Applications of PVDF hollow fiber membranes

PVDF has been widely used in a variety of industries comprising membrane-based filtrations (Güell and Davis 1996, Khayet *et al.* 2002, Madaeni and Yeganeh 2003), membrane distillation (Khayet *et al.* 2004, Bonyadi and Chung 2007, Wang *et al.* 2008), pervaporation (Jian and Pintauro 1997), membrane gas absorption (Li *et al.* 1999, Atchariyawut *et al.* 2006), polymer electrolyte (Cui *et al.* 2008).

2.4.1. Membrane filtration process

The pore size of PVDF membrane is normally at a microfiltration (MF) level. If the hydrophilicity can be improved, such PVDF membranes with good chemical resistance can also be used for water and wastewater treatment process such as MF or membrane bioreactor (MBR). These applications require membranes with a narrow pore size distribution for a good permeability against selectivity, as well as mechanical durability and fouling resistance for long-term operation.

- Microfiltration (MF) and ultrafiltration (UF)

PVDF was used as membrane material for crossflow microfiltration of protein mixtures by Güell and co-workers (Güell and Davis 1996). Furthermore, Madaeni and Yeganeh employed hydrophilic PVDF membranes for emulsified oil wastewater

(Madaeni and Yeganeh 2003). Khayet *et al*. reported that PVDF hollow fiber membranes could be used for ultrafiltration (Khayet *et al.* 2002).

- Membrane bioreactor (MBR)

MBR combines the conventional biological wastewater treatment with membrane separation. It is an attractive alternative to the conventional activated sludge treatment using secondary sedimentation. The types of membranes used are different depending on the size contaminants contacting during the treatment process. Basically, membranes employed in MBR are typically UF or MF membranes. For example, Badani *et al*. and Brik *et al*. used commercial PVDF UF membranes for the treatment of textile wastewater towards reuse by MBR technology (Kang and Cao 2014). This process showed superior performance compared to other biological treatment systems. Nevertheless, a postprocessing such as nanofiltration (NF) was recommended by the authors to treat the recalcitrant chemical oxygen demand (COD) and color components.

2.4.2. Membrane contactor process

Due to its hydrophobic nature and thermal stability, PVDF membranes is a good candidate for membrane distillation.

- Membrane distillation

Membrane distillation (MD) is a membrane-based separation process which could drive water vapor to pass through the hydrophobic membrane by the temperature difference on two sides of the membrane. It has been considered as a potential alternative to the current major desalination technique-reverse osmosis (RO), thanks to its ability of making use of waste and less fouling due to larger pore sizes and lower operating pressure. The MD process suffers from some drawbacks such as low permeate flux, wetting problems, as well as fouling and scaling. Khayet and co-workers prepared PVDF membranes for MD (Khayet *et al.* 2004). The mean pore sizes obtained with tapping mode atomic force microscopy (TM-AFM) were 1.2 to 2.1 times larger than those determined from gas permeation test. For the first time, co-extrusion was applied for the fabrication of dual layer hydrophilic–hydrophobic

hollow fibers using PVDF as membrane material especially for the direct contact membrane distillation (DCMD) process in the study of Bonyadi and Chung (Bonyadi and Chung 2007). The fabricated hollow fibers were tested for the DCMD process and flux as high as 55 kg m^{-2} h^{-1} at 90 °C was achieved in the test. Yu Wang *et al*. used hydrophobic PVDF hollow fiber membranes with narrow pore size distribution and ultra-skin for the fresh water production through membrane distillation (Wang *et al.* 2008).

- Gas adsorption

Li *et al*. employed tailor-made PVDF asymmetric hollow fiber membranes and their membrane modules for soluble gas removal, such as H_2S from waste gas streams (Li *et al.* 1999). In another study conducted by Atchariyawut *et al*., PVDF microporous hollow fiber membranes were fabricated to gain a better understanding of the membrane's role in the whole process of mass-transfer in membrane gas–liquid contacting systems (Atchariyawut *et al.* 2006).

2.4.3. Membrane pervaporation process

Jian and Pintauro prepared asymmetric PVDF hollow fiber pervaporation membranes with an inner diameter of 0.05–0.06 cm, an outer diameter of 0.07–0.08 cm and a dense layer (≈ 3 μm in thickness) on the inner fiber wall for the removal of ppm concentrations of organics from water (Jian and Pintauro 1997). A small module containing 6–30 PVDF hollow fiber membranes performed equally well for organic extraction from water with either a bore-side or shell-side feed when the feed flowrate was adequately high to eliminate concentration polarization. It was found that the changes in organic flux and separation factor for variations were qualitatively comparable to those perceived with asymmetric PVDF pervaporation membranes in the configuration of flat sheet.

2.4.4. Other applications

PVDF has been widely applied as the polymer microporous matrix (or membrane) of polymer electrolyte in lithium ion batteries due to its desirable properties. Ji *et al*. have found that TIPS process is a practical method to fabricate PVDF matrix used as

polymer electrolyte, and ionic conductivity of resultant polymer electrolyte reached 10^{-3} S/cm at room temperature (Ji *et al.* 2007).

In order to achieve polymer electrolyte with higher ionic conductivity, Cui and co-workers took attempts to increase the electrolyte uptake (Cui *et al.* 2008). They prepared microporous PVDF/polyethylene oxide-co-polypropylene oxide-co-polyethylene oxide (PVDF/PEO-PPO-PEO, or PVDF/F127) blend membranes using sulfolane as the diluent via TIPS process. Then the resultant membranes were soaked in a liquid electrolyte to form polymer electrolytes for the application of lithium ion battery.

CHAPTER 3 Fabrication of PVDF Hollow Fiber Membranes Using Mild Diluents via TIPS Method

3.1. Introduction

As described in **Chapter 2**, membranes have been prepared from PVDF via TIPS method during the past decades (Cui *et al.* 2013). However, PVDF membranes in the configuration of hollow fiber did not receive proportionate attention in the TIPS field considering its superior potential compared to flat sheet membranes as stated in **Section 1.1** (Li and Kim 2008). Most TIPS studies focused on the flat sheet configuration when developing formulas of dope compositions probably thanks to its relatively simple procedures during preparation (Cui *et al.* 2013). A comprehensive knowledge is yet to be developed on the principles and mechanisms of TIPS process during the fabrication of PVDF hollow fiber membranes. In addition, conventional solvents used as diluents in the TIPS process are often considered as non-green due to their toxicity, which could cause serious damage to human health and the environment over long-term usage (Jung *et al.* 2018). In the first part of this work, PVDF hollow fiber membranes were developed using mild solvents with low toxicity via TIPS method as a basic trial. The dope compositions and spinning conditions were optimized to achieve a porous structure, high water flux and good mechanical strength. This research aims to discover the general principles of TIPS process by looking into its thermodynamic or kinetic characteristics on an experimental basis.

3.2. Methodology and experiments

3.2.1. Materials

Polyvinylidene fluoride (PVDF Solef® 1015, M_w = 570-600 kDa, and Solef® 6020, M_w = 670-700 kDa, Solvay) and PVDF (Solef® 6020, M_w = 670-700 kDa, Solvay) were used to make porous hollow fiber membranes. Dimethyl phthalate (DMP, Merck KGaA, Germany), Acetyl tributyl citrate (ATBC, Merck KGaA, Germany), and triethyl phosphate (TEP, Merck KGaA, Germany) were used as both diluents and bore fluids. Ethanol (Merck KGaA, Germany) and n-hexane (Merck KGaA, Germany) were used to perform post-treatment of the porous hollow fiber

membranes. For pure water permeability (PWP) experiments, purified water by a Milli-Q system (18 MΩcm) was used. All the reagents were used as received.

3.2.2. Phase diagram determination

The samples of polymer/diluent dope solution were prepared separately using a StarFish Workstation (Heidolph Instruments, Germany) at 220 °C. The cloud point (T_{cloud}) measurement of the polymer-diluent system was conducted following the method used in a previous study (Ji *et al.* 2007). The cooled dope mixture was sliced into small pieces of samples (diameter around 0.5 cm) and carefully sandwiched between two transparent cover slips. The prepared sample was mounted on a hot stage (Linkam THMS600, UK) and heated up to 220 °C and then cooled down to 40 °C. The cooling rate was controlled at 10 °C min^{-1}. Through the observation under an optical microscope (Nikon Eclipse 50i, Japan), the T_{cloud} can be determined visually at the point of the first appearance of liquid droplets.

Thermal behavior analysis of polymer/diluent dope mixtures was performed by using a differential scanning calorimeter (DSC, Q20, TA Instruments, USA) in a dry nitrogen atmosphere. For each measurement, about 5 mg of dope mixture was tightly encapsulated into an aluminum pan (Tzero pan and Tzero hermetic lid, TA Instruments, USA). The thermal history of the sample was removed by a rapid ramp to 200 °C at a controlled rate of 40 °C min^{-1} prior to the melting tests. The dynamic crystallization temperature (T_c) (the point at which that the system begins to crystallize) was determined as the onset temperature of the exothermic peak during the cooling process (Ma *et al.* 2013). The crystallization curve was subsequently obtained by cooling to 40 °C at a rate of 10 °C min^{-1} after equilibrating at 200 °C for 2 min (Rajabzadeh *et al.* 2012, Cui *et al.* 2013, Ma *et al.* 2013). The phase diagrams of both polymer/diluent systems were obtained by depicting the cloud points (if any) along with the crystallization curve. Following the cooling process, the melting behavior of polymer/diluent samples was also analyzed at a heating rate of 10 °C min^{-1}.

3.2.3. Preparation of hollow fiber membranes

Hollow fiber membranes were fabricated by a set of spinning apparatus shown in **Figure 3.1** (Rajabzadeh *et al.* 2012). The polymer powder was firstly degassed in the heated oven over 24 h. Measured amounts of PVDF and diluent with predetermined composition were fed to the vessel, heated up to a certain temperature that was higher than cloud point and then mixed under determined conditions. After the dope solution was prepared, the dope solution in the dope tank was heated up to a certain temperature. The spinneret was also heated up to same temperature as the dope tank. Next, nitrogen gas was supplied to the dope tank to provide a positive pressure and the hot dope solution was dispensed into the spinneret by gear pump. The desired bore fluid was then pumped into the spinneret at room temperature using a syringe pump (Teledyne ISCO Inc., Model 1000D) at a certain rate. Together with the bore fluid, the hot polymer solution extruded into the coagulation bath to induce phase separation and solidify the membrane. Tap water was used as coagulant for fabrication. The dope compositions and spinning conditions are described in **Table 3.1**.

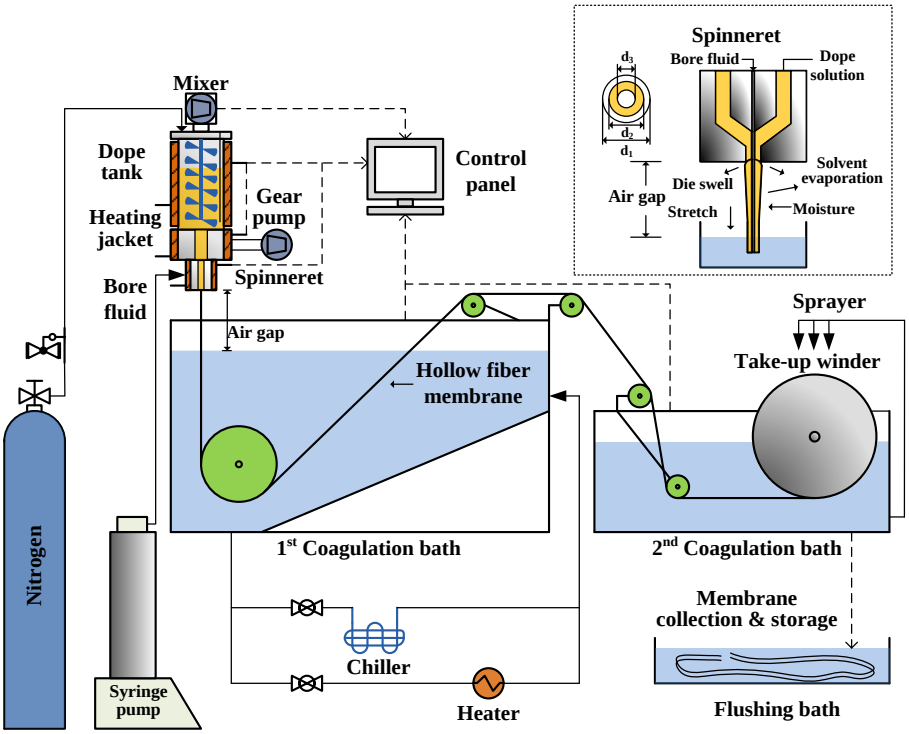

Figure 3.1. Schematic diagram of spinning apparatus for hollow fiber membranes preparation

Table 3.1. Dope compositions and spinning conditions

Code	Dope compositions		Spinning conditions		
	PVDF (wt%)	Diluent (wt%)	Bore fluid composition (wt%)	Air gap (cm)	Coagulation temperature (°C)
M1AW30	1015 (30)	ATBC (70)	ATBC (100)	1	30
M1TW30		TEP (70)	TEP (100)		
M1DW30		DMP (70)	DMP (100)	1,5,10,15	5,30,45,60
M6DW25	6020 (25)	DMP (75)		1	30
M6DW27	6020 (27)	DMP (73)			
M6DW30	6020 (30)	DMP (70)			
M6DW35	6020 (35)	DMP (65)			
M6DW40	6020 (40)	DMP (60)			

Notes:
Extrusion rate (g min^{-1}): 5.3; OD/ID of spinneret (mm): 1.84/0.92; Bore fluid flow rate (mL min^{-1}): 2.0, 3.0; The take-up speed was adjusted according to the air gap to ensure the moderate tightness of spinning line.

3.2.4. Post-treatment

In order to alleviate the membrane shrinkage during the drying process at ambient condition for some characterizations, which required the hollow fiber membranes to be dried, the hollow fiber membranes were post-treated by solvent replacement or freeze drying respectively. Prepared hollow membranes were immersed into ethanol for 24 h to extract the residual diluent from the membranes and were then immersed in turn into n-hexane for 3 h. During the process, water in the membrane pores was gradually replaced with the exchanged reagents, which have a lower surface tension. The hollow fiber membranes were subsequently air-dried at room temperature (26 °C) before characterization tests (Shi *et al.* 2007). Another post treatment method is freeze-drying where membranes were dried in low temperature and under vacuum condition. The hollow fiber membranes were cut into desired length and then bundled. The bundled hollow fibers were enfolded with Aluminum foil and put in a -20 °C

freezer to make sure that the samples were totally frozen before the freeze drying process. The frozen samples were loaded into a freeze dryer (Brand & model: Martin Christ Alpha 2-4; Supplier: ITS Science & Medical Pte Ltd). The samples were subsequently dried before characterization tests.

3.2.5. Characterization of PVDF hollow fiber membranes

The dimension of hollow fiber membranes was measured by a digital microscope (Keyence, VHX-500F). Two different fibers were taken and a mean value was calculated for each sample measurement. The structure and morphology of resultant membranes were examined by a scanning electron microscope (SEM) (Zeiss EVO 50). The dried membrane samples were frozen in liquid nitrogen and subsequently cracked in order to obtain the cross sections. The samples were then carefully mounted on the SEM stubs and dried overnight in a 50 °C vacuum oven. An Emitech SC7620 gold sputter coater was used to deposit a layer of gold on the samples under argon environment (Wongchitphimon *et al.* 2011, Setiawan *et al.* 2012).

The tensile strength of the membrane under room temperature was carried out using a tensile tester (Zwick/Roell Z 0.5 kN Universal Testing Machine). The sample was camped at the both ends and pulled in tension at a constant elongation velocity of 50 mm min^{-1} under room temperature (26 °C). Tensile modulus, tensile strength, and elongation were measured to indicate the mechanical strength of the fibers (Wongchitphimon *et al.* 2011).

Four pieces of hollow fibers were potted into a module and sealed to prepare a lab-scale module with an effective length of 16.3 cm. PWP experiments were performed by using two to three modules from the same batch of the membrane spinning process. Milli-Q ultra pure water was circulated through the shell side of the membrane module under a pressure of 1 bar for 30 min to compact the membrane prior to PWP measurement (Setiawan *et al.* 2012). The PWP of the membranes (L m^{-2} h^{-1} bar^{-1}) was calculated by：

$$PWP = \frac{V}{tA\Delta P} = \frac{V}{tn\pi ODl\Delta P} \tag{3.1}$$

where V is the volume of permeate taken (L) per determined time, t (h); A is the filtration area of the dual-layer membrane (m^2); n is the number of fibers in the module; OD is the outer diameter of hollow fiber (m); l is the effective length of hollow fibers (m); ΔP represents the pressure difference between the feed side and the permeation side of the membrane (bar).

The pore size of membranes was determined by a capillary flow porometer (model CFP 1500A, from Porous Material. Inc. (PMI) in Singapore) (Wongchitphimon *et al.* 2011). Its working principle is shown in **Figure 3.2**.

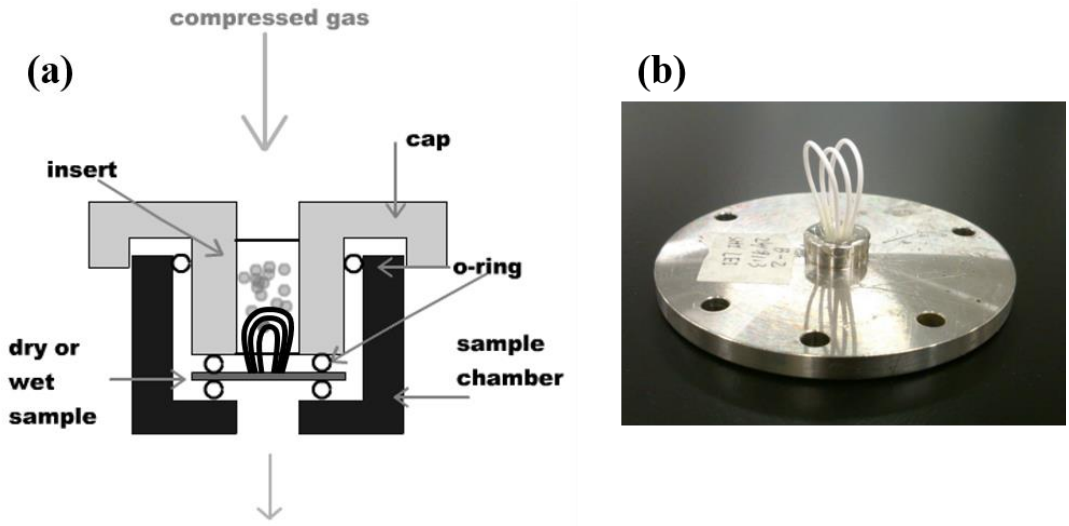

Figure 3.2. Schematic diagram of working principle of the capillary flow porometer for pore size distribution of hollow fiber membranes. (a) Illustration of the mechanisms; (b) sample holder for hollow fiber membranes

A fully wetted sample was placed in the sample chamber and the chamber was sealed. Gas was then allowed to flow into the chamber behind the sample. When the pressure reached a point that could overcome the capillary action of the fluid within the largest pore, the bubble point had been found. After determination of the bubble point, the pressure was increased and the flow was measured until all pores were empty, and the sample was considered dry. Gas pressure and flow rates through the dry sample were also measured. Each sample was tested twice.

The amount of gas flow was then measured to determine the pore size of the membrane. The definition of the pore diameter, d is as follows.

$$d = 4\gamma \cos\theta / p \tag{3.2}$$

where γ is the surface tension of the wetting liquid; θ is the contact angle; p is the differential pressure across the pore; The flow distribution, f is determined from:

$$f = -d[100 \times (F_w / F_d)] / dD \tag{3.3}$$

where F_w and F_d are flow rates through wet and dry samples; The area under the curve in any pore diameter range indicates the percentage of flow through that range (Akshaya Jena 2002).

3.3. Results and discussion

This section aims to evaluate the effect of dope compositions, spinning conditions and post-treatment conditions. A conclusive discussion on the optimization of relevant parameters will be made in **Section 3.3.4**.

3.3.1. Effect of dope compositions

The thermodynamic properties of dope solutions are majorly affected by the dope compositions (Lloyd *et al.* 1990, Lloyd *et al.* 1991). To determine the dope composition, we firstly selected an appropriate solvent for the diluent and then weighed the effect of polymer molecular weight and concentration on the membrane properties.

- Diluent selection

The selection of an appropriate solvent as the diluent is normally based on the interaction between polymer and the diluents (Kim and Lloyd 1991). In the TIPS process for PVDF membrane preparation, a poor solvent is necessary since it can only dissolve PVDF at a high temperature. For the same chemical, the terms “diluent” (in TIPS) and “solvent” (in NIPS) are used interchangeably in this thesis to emphasize its function in different processes. The transform of solubility of PVDF in the solvent from high (solvent) to low (only diluent) temperature creates the possibility for the phase inversion to occur. Therefore, it is preferred to have a relatively low affinity of

PVDF with the solvent. Basically, the mutual affinity of a polymer and a solvent can be estimated by the Hansen's solubility parameter (δ_t) which comprises of three dimensional components: polar (δ_p), dispersion force (δ_d), and hydrogen bonding (δ_h) (Hansen 2012). The individual relative affinity of PVDF with solvents can be examined by the following equation (Bottino *et al.* 1991, Wongchitphimon *et al.* 2011):

$$\Delta\delta_{ps} = ((\delta_{ps} - \delta_{pp})^2 + (\delta_{ds} - \delta_{dp})^2 + (\delta_{hs} - \delta_{hp})^2)^{1/2} \quad (3.4)$$

where *p* and *s* represent the polymer and solvent, respectively. Normally, smaller value indicates better interaction.

It can be seen from **Table 3.2** that the conventional solvents (dibutyl phthalate(DBP), diethyl phthalate (DEP), dioctyl phthalate (DOP), and diphenyl ketone (DPK)) have a lower mutual affinity with PVDF than DMP, ATBC and TEP. However, such conventional solvents might induce a carcinogenic effect over long-term usage. To eliminate the potential hazard to lab users, we selected mild solvents—DMP, ATBC and TEP which are less toxic and can be considered as mild solvents. In the following studies, we will examine whether comparable properties and performance can be achieved or not by using mild solvents with relatively higher affinity with PVDF than conventional solvents.

Table 3.2. Solubility parameters and toxicity of common chemicals used in TIPS process

Chemical	δ_d	δ_p	δ_h	$\Delta\delta_{ps}$	Toxicity	Ref.
	(MPa)$^{1/2}$					
PVDF	17.2	12.5	9.2	\	\	(Xiao *et al.* 2015)
DBP	17.8	8.6	4.1	6.4	Carcinogenic effect	(Figoli *et al.* 2014)
DEP	17.6	9.6	4.5	5.5	Carcinogenic effect	(Jung *et al.* 2018)
DOP	16.6	7.0	3.1	8.2	Carcinogenic effect	(Figoli *et al.* 2014)
DPK	19.6	8.6	5.7	5.8	Carcinogenic effect	(Figoli *et al.* 2014)
DMP	18.6	10.8	4.9	4.8	Organ damage by repeated exposure	(Yang *et al.* 2008)
ATBC	16.8	2.6	8.6	10.0	No distinctive effect	(Jung *et al.* 2018)
TEP	16.8	11.5	9.2	1.1	No distinctive effect	(Figoli *et al.* 2014)

Figure 3.3 shows the cross-sectional morphology of PVDF hollow fiber membranes spun using DMP (M1DW30) or ATBC (M1AW30) as diluents. A typical spherulitic structure can be spotted in the morphology of the M1DW30 membrane. Clearly different from the M1DW30, M1AW30 exhibited a structure with loosely connected lamellae. The principles of TIPS method for semi-crystalline polymers can be better illustrated from a thermodynamic perspective by using a two-dimensional phase diagram as shown in **Figure 3.4** (Rajabzadeh *et al.* 2008, Yang *et al.* 2008, Kim *et al.* 2016). Governed by nucleation and growth (NG) or spinodal decomposition (SD) mechanisms, the phase separation normally occurs following two major modes: liquid-liquid (L-L) separation and solid-liquid (S-L) separation. When the process undergoes the metastable region (route A and C), L-L phase separation normally

occurs with the NG mechanism. As the compositions varies, the system can also be quenched through the unstable region (route B). In this case, the SD mechanism often dominates when L-L phase separation takes place, resulting in membranes with bicontinuous cellular structure (Yang *et al.* 2008). When the system reaches the crystallization curve directly (route D), S-L phase separation occurs with NG mechanism, facilitating the formation of spherulites (Rajabzadeh *et al.* 2008). As shown in **Table 3.2**, DMP possesses a higher mutual affinity with PVDF compared to ATBC. Therefore, ATBC was more likely to induce the phase separation following the L-L route through metastable region. This also explains the formation of spherulites in membranes spun using DMP as the diluent since the S-L phase separation was probably dominant due to strong interactions between DMP and PVDF.

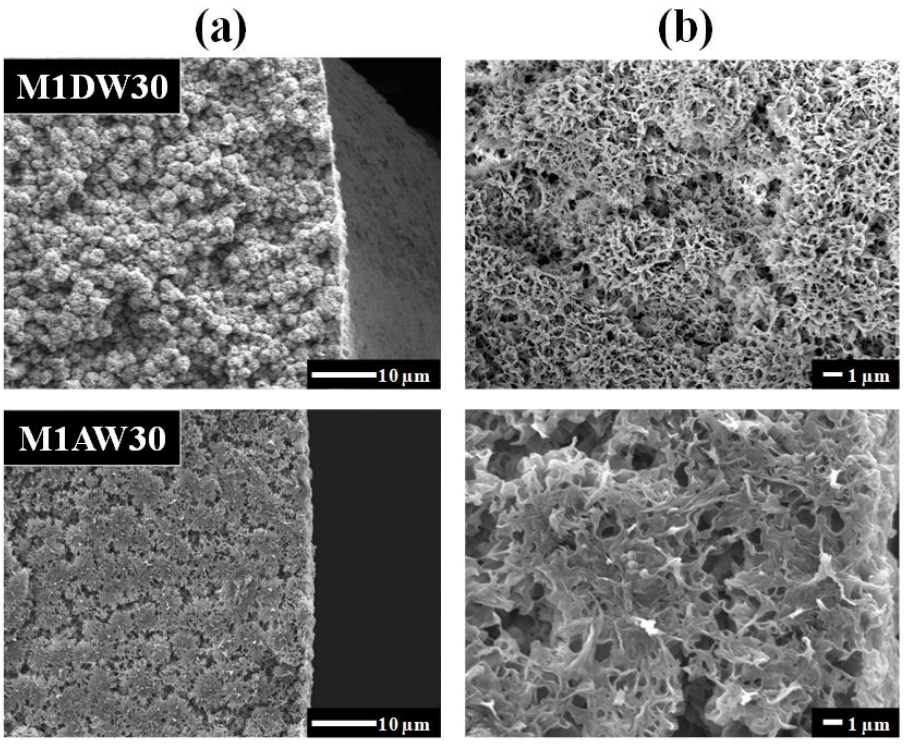

Figure 3.3. Cross-section morphology of hollow fiber membranes spun using DMP or ATBC as diluents with magnification at: (a) x1,500; (b) x7,000 (Dope compositions: PVDF 1015 (30 wt%); Air gap: 1 cm; Coagulation temperature: 30 °C)

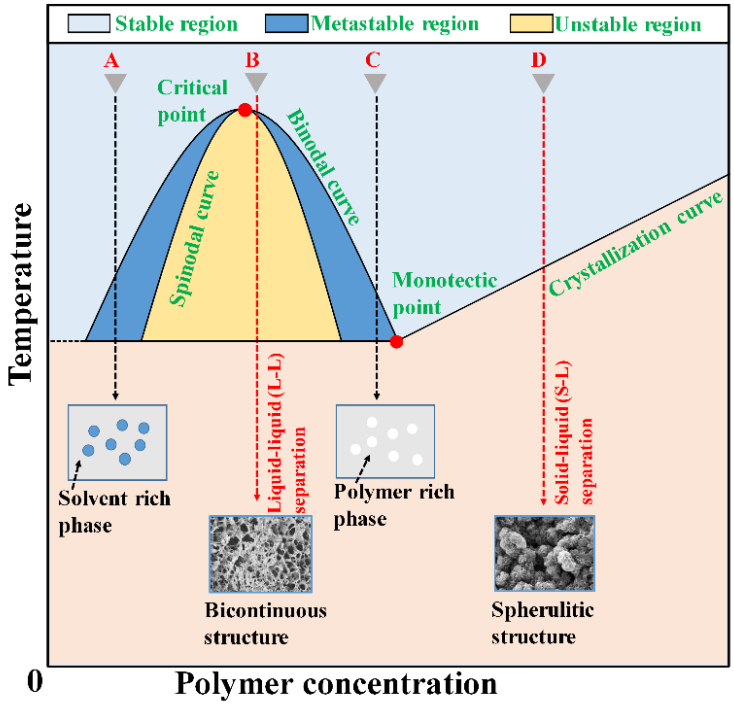

Figure 3.4. Conceptual illustration of TIPS process adapted from literature (Lloyd *et al.* 1990, Lloyd *et al.* 1991, Song *et al.* 2012)

Table 3.3 shows the properties of PVDF hollow fiber membranes fabricated using ATBC, TEP and DMP, respectively. It can be seen that membranes with similar mean pore size can be obtained by using ATBC and DMP under same spinning conditions. However, they have vastly different features in terms of mechanical strength and PWP. M1AW30 membranes have a higher PWP value of 1428 ± 43 L m^{-2} h^{-1} bar^{-1} with a weaker tensile strength value of 2.3 ± 0.1 MPa. On the contrary, M1DW30 membranes possess a moderate value of PWP but a better robustness with tensile strength as high as 3.5 ± 0.1 MPa. Besides, the use of TEP was demonstrated to be ineffective in opening up the pore structure since nearly no flux was observed by using M1TW30 membranes. In conclusion, we selected DMP as the major solvent for diluent in the following studies considering its feasibility in developing membranes with robust structure and acceptable level of permeability.

Table 3.3. Properties of PVDF membranes spun using different diluents

Code	Diluent (wt%)	Tensile strength (MPa)	Mean pore size (μm)	Overall porosity (%)	PWP (L m^{-2} h^{-1} bar^{-1})
M1AW30	ATBC (70)	2.3 ± 0.1	0.26 ± 0.01	68 ± 3	1428 ± 43
M1TW30	TEP (70)	1.9 ± 0.1	0.08 ± 0.01	41 ± 2	0
M1DW30	DMP (70)	3.5 ± 0.1	0.26 ± 0.03	52 ± 6	724 ± 29

Notes:
Dope compositions: PVDF 1015 (30 wt%); Air gap: 1 cm; Coagulation temperature: 30 °C.

- Effect of polymer molecular weight and concentration

Having selected the appropriate solvent for diluent, the effect of the polymer molecular weight and concentration on membrane properties were studied respectively. The phase diagrams for the PVDF/DMP binary system and PVDF/PTFE/DMP ternary system are shown in **Figure 3.5**. It can be seen that the monotectic point of the binary system without the addition of PTFE particles is around 28 wt%. As described previously, the phase separation occurs following different routes: L-L separation (route A), S-L separation (route B) or their combination (route through the monotectic point). The concentrations of PVDF used in this study were greater than 30 wt%, suggesting the occurrence of S-L phase separation (Shi *et al.* 2012). This finding can be used to explain the formation of spherulitic structure when DMP was used as the diluent as observed in **Figure 3.3**.

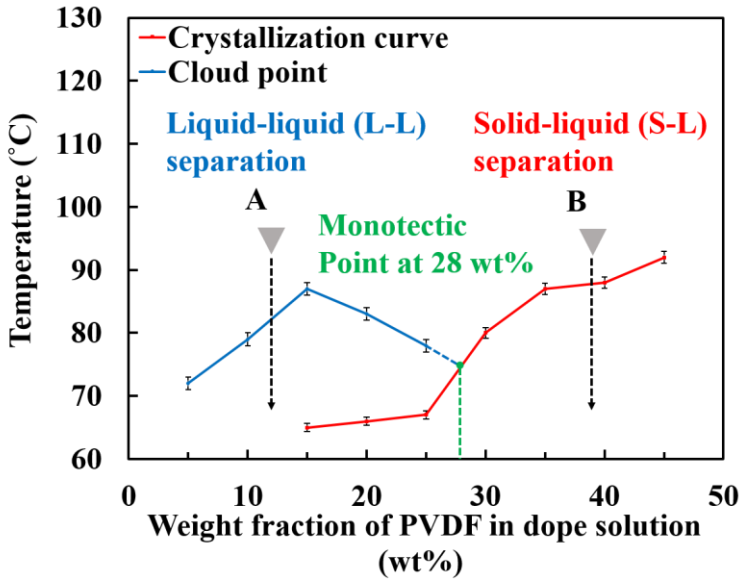

Figure 3.5. Phase diagram for PVDF/DMP binary system

The effects of the polymer molecular weight and concentration on membrane properties and performance are shown in **Figure 3.6**, **Figure 3.7** and **Table 3.4**. It can be seen that the molecular weight and concentration played similar roles in affecting the mechanical strength, pore size and PWP. Membranes spun from PVDF of a higher molecular weight or concentration generally possess smaller spherulites, pore sizes and PWP with stronger mechanical properties. During the S-L phase separation, the crystal NG determine the formation of membrane structure and further affect the rigidity of the membrane (Heo *et al.* 2007). With a higher nucleation density, pores formed within membrane became more compact with smaller mean sizes. The reduction in pore size increased the resistance when water passes through pore under certain pressure, leading to the decrease in the water permeability. In addition, a larger molecular weight of polymer was likely to result in a higher solution viscosity, which could possibly slow down the movement of diluent molecules, giving more time for the crystalline structure to stabilize and grow into more regular shapes (Hassankiadeh *et al.* 2014). Moreover, increasing of polymer concentration might lead to a higher nucleation density, which can further strengthen the connections among crystals. Thus, mechanical properties of membrane could be improved when fabricated from a dope solution with a larger polymer molecular weight or a higher polymer concentration. Overall, the tensile strength (stretch

resistance) went up with the increase of the molecular weight and concentration of the polymer, indicating a better long-term stability.

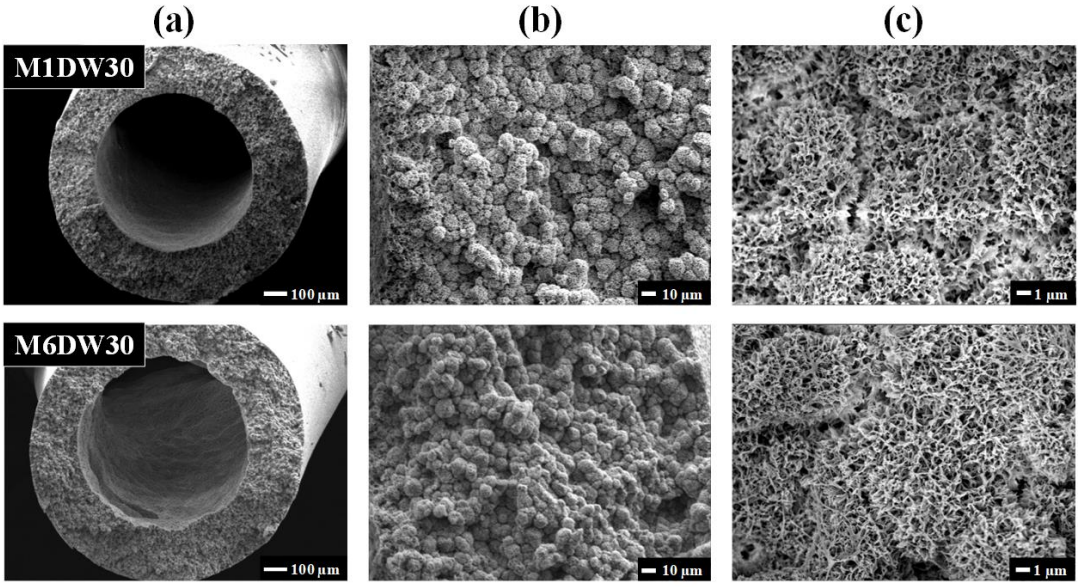

Figure 3.6. Cross-section morphology of hollow fiber membranes spun from the PVDF/DMP (30/70 wt%) dopes using PVDF of different grades (1015 or 6020) with magnification at: (a) x80; (b) x500; (c) x5,000 (Diluent: DMP; Air gap: 1 cm; Coagulation temperature: 30 °C)

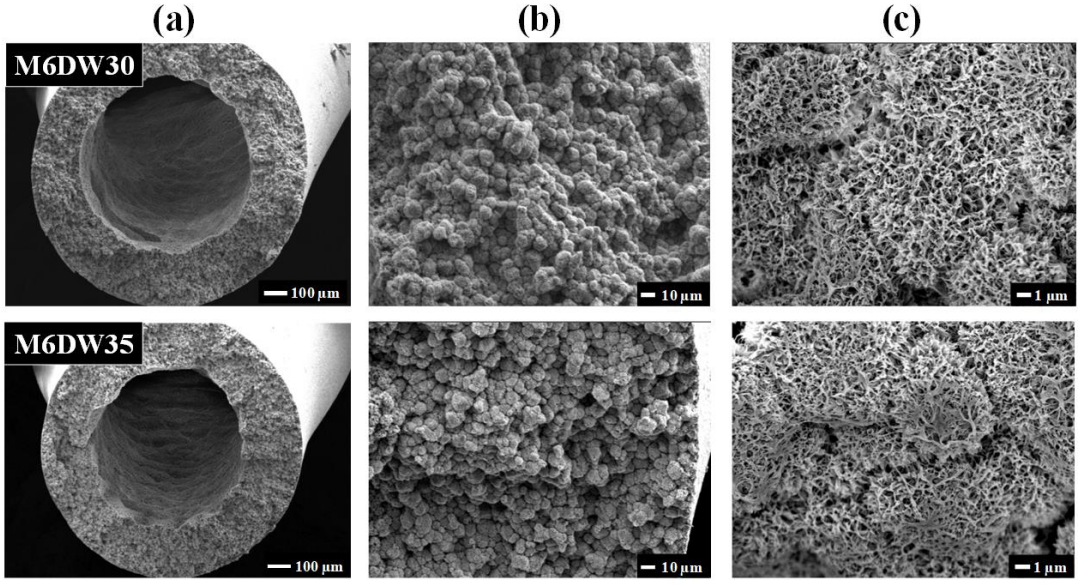

Figure 3.7. Cross-section morphology of hollow fiber membranes spun from the dopes at various polymer concentrations (30 or 35 wt%) with magnification at: (a) x80; (b) x500; (c) x5,000. PVDF grades: 1015. (Diluent: DMP; Air gap: 1 cm; Coagulation temperature: 30 °C)

Table 3.4. Properties of membrane fabricated using different polymer molecular weight and polymer concentration solutions

Code	PVDF M_w (kDa)	PVDF concentration (%)	Tensile modulus (MPa)	Mean pore size (μm)	PWP (L m^{-2} h^{-1} bar^{-1})
M1DW30	570-600	30	3.5 ± 0.1	0.26 ± 0.03	724 ± 29
M6DW25	670-700	25	Fiber too weak for continuous spinning		
M6DW27		27	1.7 ± 0.1	0.35 ± 0.03	1079 ± 62
M6DW30		30	4.0 ± 0.3	0.17 ± 0.01	320 ± 19
M6DW35		35	4.6 ± 0.1	0.16 ± 0.01	274 ± 29
M6DW40		40	Inhomogeneous solution due to insufficient mixing at high viscosity		

Notes:
Diluent: DMP; Air gap: 1 cm; Coagulation temperature: 30 °C.

3.3.2. Effect of spinning conditions

As described in **Section 2.2**, the thermodynamic and kinetic characteristics of hollow fiber spinning via TIPS process can be significantly affected by the temperature gradient along the spinning line from the spinneret (hot end) to the coagulant (cold end) (Lloyd *et al.* 1990, Alwattari and Lloyd 1991, Kim *et al.* 1991, Lloyd *et al.* 1991, McGuire *et al.* 1993). To determine the quenching conditions for spinning, we investigated the effect of air gap and coagulation temperature.

Figure 3.8 shows the cross-sectional images of the membranes obtained from PVDF/DMP system at air gaps of 1 or 10 cm, respectively.

Table 3.5 displays the properties of membranes spun at air gaps of 1, 5, 10, 15 cm, respectively. It can be seen that the membranes spun at a longer air gap (10 cm) has an evidently smaller dimension and spherulites in smaller sizes compared to the ones fabricated at a shorter air gap (1cm). As shown in

Table 3.5, the outer (OD) and inner diameters (ID) decreased gradually with increasing the air gap probably due to amplified stretching force. Normally a relatively smaller dimension can result in a better mechanical strength since the

membranes were developed in the hollow fiber configuration. Moreover, it has been found that a stronger stretching applied can enhance the alignment of polymer chains and thus strengthen the mechanical properties (Mulder 1996). This can explain the improved tensile strength of membranes obtained at higher air gaps. On the other hand, a longer air gaps generally indicates a lower cooling rate, which is correlated with more sufficient time for the growth of crystallites. A slow solidification can subsequently generate pore structure with a better interconnectivity, which links to the real permeability of membranes. It can be seen from

Table 3.5 that the PWP values went up first and then dropped significantly when the air gap was adjusted from 1 to 15 cm. This up-down trend observed implies that there might be other factors in addition to the cooling rate. It was suggested that the tightly aligned polymer chains at a longer air gap might confine the overgrowth of crystallites, resulting in smaller spherulites and mean pore sizes (Mulder 1996). Counteractively, the cooling rate and stretching force might had an antagonistic effect on the performance of membranes. Therefore, a higher permeability could be obtained with a smaller mean pore size at an optimal air gap. It can be found that the best PWP value of 878 ± 5 L m^{-2} h^{-1} bar^{-1} was achieved at the air gap of 10 cm. Besides, it is worth mentioning that, in the future work, the possible effect of the humidity of the air should be considered on the evaporation along the air gap as sometimes the humidity in our lab can be as high as 70%.

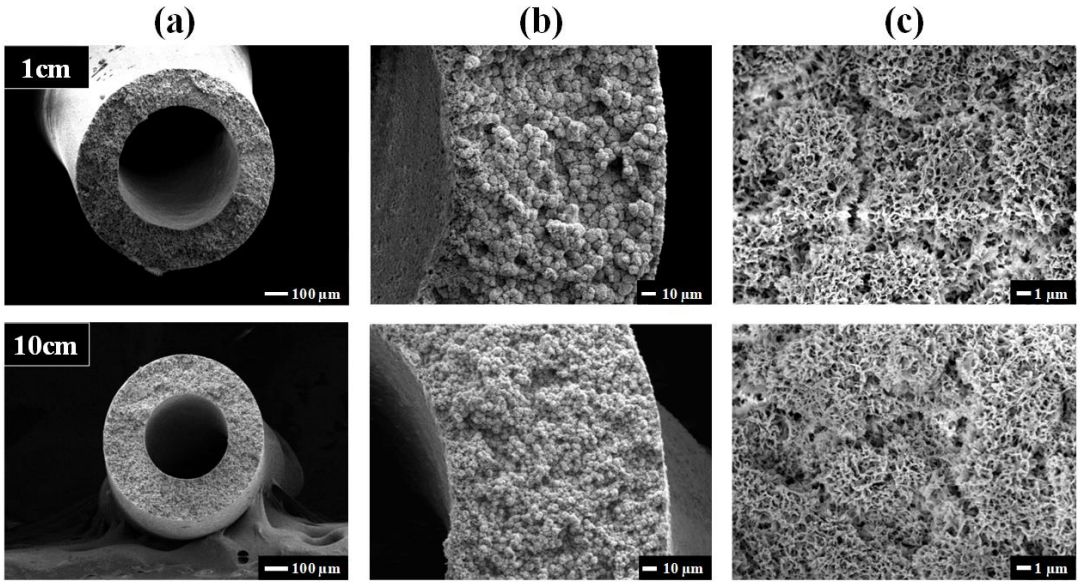

Figure 3.8. Cross-section morphology of hollow fiber membranes spun at different air gaps (1 or 10 cm) with magnification at: (a) x80; (b) x500; (c) x5,000 (Dope compositions: PVDF 1015/DMP (30/70 wt%/wt%); Coagulation temperature: 30 °C)

Table 3.5. Properties of PVDF membranes spun at different air gaps

Air gap	Dimension		Tensile strength	Mean pore size	PWP
(cm)	OD/(mm)	ID/(mm)	(MPa)	(μm)	(L m^{-2} h^{-1} bar^{-1})
1	915 ± 0.1	544 ± 0.1	3.5 ± 0.1	0.26 ± 0.03	724 ± 29
5	891 ± 0.1	495 ± 0.1	3.3 ± 0.1	0.22 ± 0.03	832 ± 39
10	725 ± 0.1	385 ± 0.1	3.8 ± 1.1	0.18 ± 0.01	878 ± 5
15	617 ± 0.1	324 ± 0.1	5.6 ± 0.3	0.12 ± 0.05	663 ± 33

Notes:
Dope compositions: PVDF 1015/DMP (30/70 wt%/wt%); Coagulation temperature: 30 °C.

Figure 3.9 shows the morphologies of the membranes obtained from PVDF/DMP dopes quenched at different coagulation temperatures. **Table 3.6** summarizes the properties of membranes spun at 5, 30, 45 and 60 °C, respectively. It can be seen from **Figure 3.9** that the membranes exhibited a more obvious spherical structure containing spherulites in greater sizes as the coagulation temperature was elevated from 5 to 60 °C. In addition, the mean pore sizes and PWP values gradually increased

accompanying with the decrease in the tensile strength as presented in **Table 3.6**. Upon entering the coagulation bath, the well-heated dope mixtures experiences a high undercooling process, which promotes the extensive formation of crystal nuclei. In this process, the cooling rate of dope mixtures is dependent on the coagulation temperature. Generally, a higher coagulation temperatures provides a lower temperature gradient between the spinneret (hot end) and coagulant (cold end), indicating a lower cooling rate. A lower cooling rate is likely to result in lower solidification rate of the polymer-rich phase, which allows a longer time for the spherulite and polymer-lean phase to grow. Therefore, a higher coagulation temperature (lower cooling rate) could increase the size of spherulites, resulting in a more porous membrane structure with a higher water permeability. In the meantime, the growth of polymer-lean phase was possibly contribute to weaken the interconnectivity of the spherulites, which could lead to a lower tensile strength of the resultant membranes.

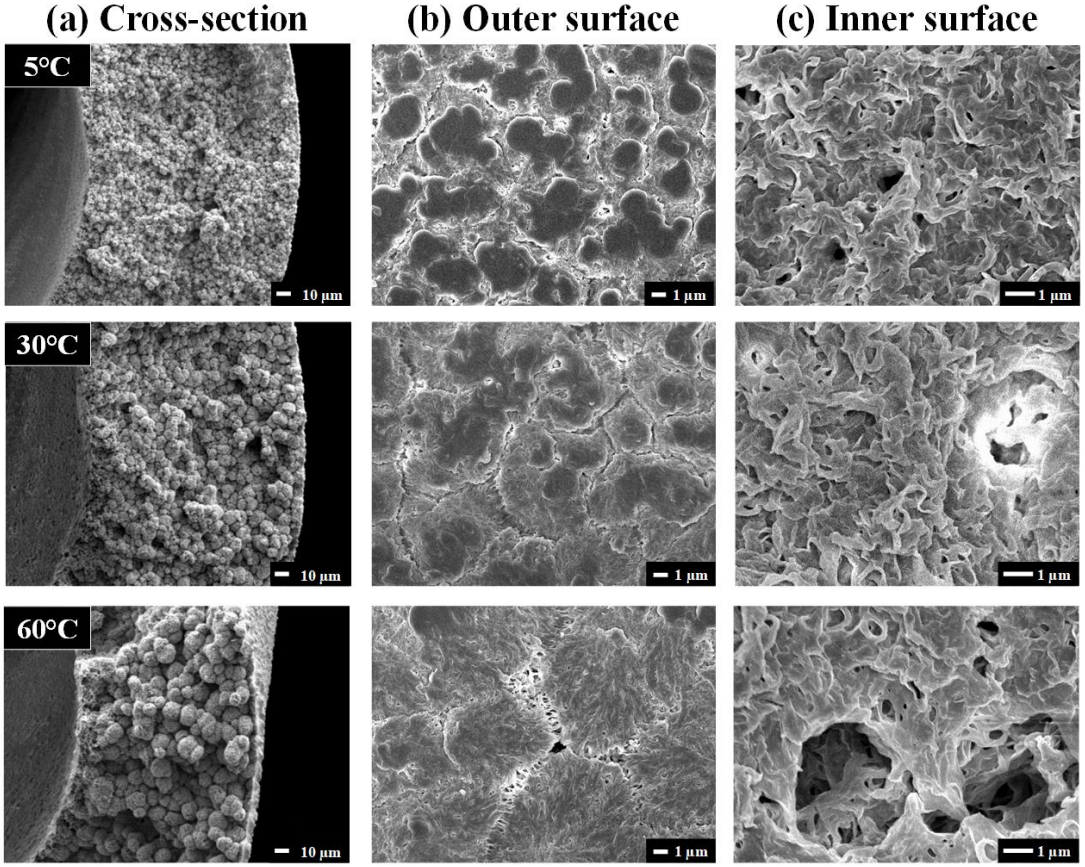

Figure 3.9. Cross-section morphology of hollow fiber membranes spun at different coagulation temperatures (5, 30 or 60 °C): (a) cross-section; (b) outer surface; (c)

inner surface (Dope compositions: PVDF 1015/DMP (30/70 wt%/wt%); Air gap: 1 cm)

Table 3.6. Properties of PVDF membranes spun at different coagulation temperatures

Coagulation temperature (°C)	Tensile strength (MPa)	Mean pore size (μm)	Maximum pore size (μm)	PWP ($L\ m^{-2}\ h^{-1}\ bar^{-1}$)
5	4.5 ± 0.1	0.18 ± 0.05	0.30 ± 0.10	334 ± 5
30	3.5 ± 0.1	0.26 ± 0.03	0.55 ± 0.07	724 ± 29
45	2.2 ± 0.2	0.49 ± 0.05	0.94 ± 0.06	953 ± 33
60	2.0 ± 0.1	0.82 ± 0.06	1.02 ± 0.16	1022 ± 35

Notes:
Dope compositions: PVDF 1015/DMP (30/70 wt%/wt%); Air gap: 1 cm.

3.3.3. Effect of post-treatment conditions

In general TIPS practices, a solvent replacement using ethanol and n-hexane in sequence is commonly used as the post-treatment for PVDF membranes (Rajabzadeh *et al.* 2008, Cui *et al.* 2013). The post-treatment is performed to extract the diluent out from the membrane and thus to make the pore structure vacant and available for potential mass transfer (Rajabzadeh *et al.* 2012). However, a large amount of solvent is consumed and can hardly be recycled after the post-treatment. This raises concerns over the sustainability of the whole membrane production process. Therefore, we proposed to use freeze drying as an alternative to the solvent replacement and compared their effect on the pore size, PWP and mechanical properties of membranes. The corresponding results are summarized in **Table 3.7**. It can be seen that the solvent replacement still possess significantly better performance than freeze drying in rigidity (tensile modulus), stretch resistance (tensile strength). With regard to ductility, the membranes treated by freeze-drying exhibited a higher value of elongation than that of membranes processed using the solvent replacement. It worth noting that the pore size and PWP of freeze-dried membranes were detectable although both of them were smaller compared to those of membranes treated by

solvent replacement. This suggests that the freeze drying was moderately effective in extracting the residual diluents. Admittedly, the PWP results of the same batch of membranes indicate that the full potential of permeability cannot be realized by using freeze drying. The compromised mechanical strength and PWP might be attributed to the possible collapse of pore structure during the quick freeze-drying process. In order to be consistent with previous studies in the literature, we still adopted the solvent replacement as the post-treatment method. It is recommended that methods similar to freeze drying with better sustainability should be developed for the post-treatment in the future.

Table 3.7. Properties of PVDF membranes processed through different post-treatments (Dope compositions: PVDF 1015/DMP (30/70 wt%/wt%); Air gap: 1 cm; Coagulation temperature: 30 °C)

Post-treatment	Tensile modulus (MPa)	Tensile strength (MPa)	Elongation (%)	Mean pore size (μm)	PWP (L m^{-2} h^{-1} bar^{-1})
Solvent replacement	62.6 ± 3.2	3.5 ± 0.1	116.3 ± 9.2	0.26 ± 0.03	724 ± 29
Freeze drying	22.7 ± 5.8	2.8 ± 0.1	127.8 ± 6.2	0.24 ± 0.01	356 ± 16

3.3.4. General principles for optimized spinning

It is important to understand the basic principles of TIPS process in order to optimize the dope compositions and spinning conditions for the preparation of PVDF hollow fiber membranes. Having evaluated the individual effect of each relevant parameters, we combined the results and analyzed them systematically. At this initial stage, a *desirable* hollow fiber membrane in this context is defined as a membrane with robust mechanical properties, porous structure and high water permeability. To conduct a systematic evaluation, we selected several parameters for the control variate study, which includes dope composition parameters such as polymer MW and polymer concentration, spinning conditions such as air gap, coagulation temperature, and post-

treatment methods such as solvent replacement and freeze-drying. The systematic effect was studied on some representative membrane properties, which contain dimension, tensile strength, mean pore size and PWP. The corresponding results are summarized in **Table 3.8**. Based on the results and discussion stated in previous sections, we proposed some guidelines for the following studies using PVDF/DMP system as a starting formula:

(1) Polymer MW and concentration can affect the nucleation density during the crystallization and the viscosity of dope mixture, respectively. PVDF of grades 1015 and 6020 are both recommended. A dope of concentration lower than 25 wt% can produce fibers too weak for continuous spinning. A dope of concentration higher than 40 wt% can be inhomogeneous due to insufficient mixing power at high viscosity. PVDF concentrations ranging from 30 to 35% are recommended. To achieve membranes with small pore sizes and high mechanical strength, a high MW or concentration is recommended. An excessively high MW or concentration can compromise the PWP.

(2) Air gap and coagulation temperature can affect the cooling rate of dope mixture. Besides, the air gap can be used to induce an adjustable stretching force to directly control the dimension of hollow fibers. To achieve membranes with small pore size and high mechanical strength, a long air gap or a low coagulation temperature is recommended. To optimize the PWP, the air gap (coagulation temperature) cannot be set too long (low). For fibers that easy to break, a low coagulation temperature is recommended to ensure the continuous spinning.

(3) Solvent replacement and freeze drying can both be used as the post-treatment for extraction of residual diluent. The solvent replacement can be more effective than the freeze drying. Upon long-term production, the consumption of solvent should be taken into consideration. The energy consumption of freeze drying is recommended for future study.

Conclusively, various PVDF hollow fiber membranes were fabricated using a mild diluent—DMP. Compared with the membranes reported in the literature, our in-house spun membranes exhibited outstanding properties as shown in **Table 3.9**. This

indicates the promising possibility that greener can also be used as alternatives to the conventional toxic solvents to achieve comparable performance of membranes.

Table 3.8. General principles for optimized spinning

Parameter	Effect	Dimension	Tensile strength	Mean pore size	PWP
Dope compositions	Thermodynamics				
Polymer MW ↑	Nucleation density ↑	Easier to increase	↑	↓	↓
Polymer concentration ↑	Viscosity ↑	Easier to increase	↑	↓	↓
Spinning conditions	Thermodynamic and kinetics				
Air gap ↑	Cooling rate↓ Stretching ↑	↓	↑	↓	↑
Coagulation temperature ↑	Cooling rate↓	Not obvious	↓	↑	↑
Post-treatment	Sustainability				
Solvent replacement	Solvent consumption	Not obvious	Higher	Slightly larger	Higher
Freeze drying	Energy consumption	Not obvious	Lower	Slightly smaller	Lower

Table 3.9. Comparison of various PVDF hollow fiber membranes prepared via TIPS method

Diluent	Mean pore size (μm)	Tensile stress (MPa)	Elongation (%)	PWP (L m^{-2} h^{-1} bar^{-1})	Ref.
GBL/DOP	0.27	~5.3[a]	-[b]	~650[a]	(Wang *et al.* 2014)
DEP	-[b]	~4[a]	~100[a]	~500[a]	(Rajabzadeh *et al.* 2012)
DBP/DEHP	0.12	0.4	68.7	542	(Ji *et al.* 2008)
DMP	0.12	5.6	330.3	663	This work
DMP	0.18	3.8	148.1	878	This work

Notes:
[a)] The data were collected from figures in the literature by using the Digitizer function in *Origin* 9.1;
[b)] The data were not shown in the paper.

3.4. Conclusions

The purpose of systematically investigating the factors associated with TIPS process to produce PVDF membranes using mild diluents has been fulfilled by the successful production of membranes with a porous structure, high permeability and robust mechanical strength. The effects of polymer molecular weight, initial polymer concentration, air gap and coagulation conditions on the membrane properties and performance have been investigated and discussed.

The major findings and conclusions are summarized as follows:

- The prepared PVDF hollow fiber membranes possess promising pure water permeability values from 663 ± 33 to 878 ± 5 L m^{-2} h^{-1} bar^{-1} with reinforced tensile strength values from 3.8 ± 1.1 to 5.6 ± 0.3 MPa and a mean pore size below 0.2 μm. This is comparable with the performance of those membranes reported in the literature using TIPS method.

- The mild solvents with a lower toxicity such as DMP can also be utilized as alternatives to the conventional toxic solvents to obtain comparable properties and performance of membranes via TIPS process.
- The spherulitic structures were found from the cross-section morphology, which indicated that the TIPS process might be governed by S-L phase separation mechanism. The packing density of spherulites increased when increasing PVDF MW or initial polymer concentration, resulting in membranes with smaller sizes and better tensile strength.
- The TIPS process can be controlled thermodynamically and kinetically by adjusting the air gap and coagulation temperature. The air gap can have a dual effect on both stretching force and cooling rate. The cooling rate can also be affected by the coagulation temperature. Robust hollow fiber membranes with a small pore size and high PWP can be achieved with a moderate air gap and coagulation temperature.

This study offers a basic understanding of hollow fiber membrane preparation from PVDF via TIPS process. It also suggests that the TIPS spinning process can be sustainably enhanced by using greener solvents and post-treatment method.

CHAPTER 4 Preparation of Hydrophobically Enhanced PVDF-based Hollow Fiber Membranes for Membrane Distillation (MD) via TIPS Method

This chapter has been published as **Zhao, J.**, Shi, L., Loh, C. H. and Wang, R. (2018). "Preparation of PVDF/PTFE hollow fiber membranes for direct contact membrane distillation via thermally induced phase separation method." Desalination 430: 86-97. Permission has been granted by the licensed content publisher "Elsevier" to use the published content as a chapter in this thesis for non commercial purposes.

4.1. Introduction

As described in **Section 2.4.2**, membrane distillation (MD) is a non-isothermal membrane-based separation process involving vapor transport through non-wetted microporous membranes thermally driven by vapor pressure difference between two sides of the membranes (Khayet and Matsuura 2011). It provides attractive features such as theoretically 100% rejection of salts and less fouling as compared with pressure driven membrane processes, insensitivity to salt concentration and lower requirements on membrane mechanical properties in comparison with other separation techniques (Wang and Chung 2015). To maintain the effectiveness and stability of the MD process over a long-term operation, the membrane should possess reasonably high water vapor transfer with minimized tendency of wetting and fouling (Drioli *et al.* 2005). With regard to the materials utilized for MD membrane development, fluoropolymers, such as PVDF, have been well-investigated owing to their notable chemical and thermal stabilities, hydrophobicity and good mechanical properties (Fan and Peng 2012).

Among those additives described in **Section 2.3.1**, PTFE was found to be an effective enhancer for the heterogeneous nucleation of PVDF (Schneider *et al.* 2001, Ma *et al.* 2013). In the study reported by Schneider *et al*., it was observed that the PVDF matrix could epitaxially crystallized on PTFE chains, resulting in increased nucleation density (Schneider *et al.* 2001). This phenomenon also suggested good compatibility between PVDF and PTFE. Ma et al. examined the effect of PTFE on the

crystallization and melting characteristics of PVDF/diphenyl ketone (DPK) flat sheet membranes (Ma *et al.* 2010, Ma *et al.* 2013). The results showed that the addition of PTFE could enhance the nucleation of PVDF during TIPS process. On the other hand, PTFE was demonstrated to be an effective additive to enhance the anti-wetting property of membranes for MD applications given its outstanding hydrophobicity (Van Oss *et al.* 1986). By using the conventional NIPS method, Teoh *et al*. obtained single-layer and dual-layer PVDF/PTFE hollow fiber membranes with increased hydrophobicity and improved long-term MD performance (Teoh *et al.* 2011). Despite these reports involving PVDF and PTFE blending, there are few studies on how the nucleation enhancing capability of PTFE particles in TIPS affects the properties of PVDF membranes such as pore structure, mechanical strength and water permeability.

In this part of work, PVDF/PTFE hollow fiber membranes were fabricated via TIPS method with various PTFE loadings to thoroughly investigate the impact of PTFE addition on membrane properties and possible mechanisms behind. The addition of PTFE is expected to exert dual effects on PVDF membranes including controlling the microstructures during the TIPS process and enhancing the wetting resistance in MD applications. The characteristics of prepared membranes were examined and the pure water permeability and performance of direct contact membrane distillation (DCMD) were also evaluated. To our best knowledge, there is no report on the development of PVDF/PTFE hollow fiber membranes via TIPS method for MD application. It is anticipated that this work is able to provide a better understanding on the PVDF membrane formation mechanism involving PTFE particles in the TIPS process, and to demonstrate the potential of PVDF/PTFE hollow fiber membranes in MD applications.

4.2. Methodology and experiments

4.2.1. Materials

Polyvinylidene fluoride (PVDF Solef® 6020, M_w = 670–700 kDa, Solvay) were used to make porous hollow fiber membranes. Polytetrafluoroethylene (PTFE microparticles, Microdispers-200, M_w ~ 80,000, Size ~ 200–300 nm, Polysciences)

were used as additives for PVDF membrane fabrication. Dimethyl phthalate (DMP, Merck KGaA, Germany) was used as diluent and bore fluid. Ethanol (Merck KGaA, Germany) and n-hexane (Merck KGaA, Germany) were used to conduct the post-treatment for the porous hollow fiber membranes. For pure water permeability (PWP) experiments, deionized (DI) water by a Milli-Q system (18MΩcm) was used. All the reagents were used as received.

4.2.2. Phase diagram determination

The phase diagram was determined by a method as described in **Section 3.2.2**.

4.2.3. Preparation of hollow fiber membranes

The hollow fiber membranes were fabricated using a TIPS machine as shown in **Figure 3.1**. The detailed procedures of fabrication process have been described in **Section 3.2.3**. The dope compositions and spinning conditions are described in **Table 4.1**.

Table 4.1. Spinning parameters for hollow fiber membranes

Code	PE-0	PE-1	PE-2	PE-5
Dope compositions (PVDF/PTFE/DMP (wt%))	35/0/65	34/1/65	33/2/65	30/5/65
Extrusion rate (g min^{-1})	5.3			
Extrusion temperature (°C)	200			
Bore fluid composition (wt%)	DMP (100)			
Bore fluid flow rate (mL min^{-1})	2.0			
Coagulation temperature (°C)	10			
Air gap (cm)	10			
OD/ID of spinneret (mm)	1.84/0.92			

4.2.4. Characterization of hollow fiber membranes

The degree of crystallinity of the resultant membranes was measured by a DSC. 4–5 mg of dried hollow fibers were sealed in an aluminum pan and then tested using the same cool-heat procedure as described in **Section 3.2.2**. The degree of crystallinity of membranes was calculated according to **Equation 2.1**.

Wide angle X-ray diffraction (WAXD) was conducted to analyze the PVDF crystal structure of the prepared membranes in a Bruker D8-Advance diffractometer (Cu Ka radiation, 40 kV and 40 mA). The scanning angle ranged from 5 to 50 with a scanning velocity of 4 ° min^{-1}. The crystal size of PVDF was estimated by Scherrer's equation as follows (Patterson 1939, Burton *et al.* 2009):

$$D = K\lambda / \beta \cos\theta_d \tag{4.1}$$

where D is the estimated diameter of the crystals (nm); K is the Scherrer's constant (K=0.89); λ is the wavelength of the incident x-rays (nm), which is 0.154 in this study; β is the peak width at half height (rad); θ_d is the diffraction angle (rad).

The hydrophobicity of the resultant membranes was determined through the measurement of the dynamic contact angle using a tensiometer (DCAT11 Dataphysics, Germany) based on the Wilhelmy method (Shi *et al.* 2008). A dried sample fiber with a length of 1–1.5 cm was attached on the suspended mobile arm of an electronic balance. The sample then underwent a cycle of immersion into DI water followed by emersion at an advancing/receding speed of 0.2 mm min^{-1} with an immersion depth of 5–10 mm. The electronic balance continuously recorded the change in weight. Three cycles of advancing-receding were measured for each specimen. At the first cycle of measurement, the membrane surface was dry prior to the immersion into the DI water. The contact angles obtained at the second cycle were lower since some of the surface pores might have been filled with water. This is believed to better represent the real situation in MD applications, and therefore the contact angle of the second advancing was presented in this study to reflect the membrane hydrophobicity (Shi *et al.* 2008). To ensure the reproducibility, each run was repeated 3–5 times for all samples.

The surface topography and roughness of membranes were measured using atomic force microscopy (AFM, NX-10, Park Systems). The images were obtained over both the inner and outer surfaces of each sample using a non-contact mode (NCM) with a consistent scan area of 5 × 5 μm. The mean roughness parameter, R_a, was obtained after each test. The procedure for the analysis of AFM images can be found elsewhere (García-Payo *et al.* 2010, Liao *et al.* 2014).

The pore size distribution of membranes was measured using a capillary flow porometer (CFP 1500A, Porous Material. Inc., USA) as described in **Section 3.2.5**. The overall porosity of membrane was measured according to the density (Loh and Wang 2014). A mean value of 3 times of measurement was recorded to reduce the uncertainty which might result from the inner diameter/outer diameter (ID/OD) deviation along the length of fibers. The specific density of PVDF was 1.75–1.80 g cm^{-3} according to the Solvay product information (Solvay 2014). The surface porosity of the membranes was analyzed based on the SEM images using ImageJ software. The detailed procedures can be found elsewhere (Jung *et al.* 2016). The measurement of liquid entry pressure for water (LEPw) was performed using hollow fiber modules with an effective membrane area of 17.9–19.2 cm^2 in a dead-end configuration. The detailed methodology was well-documented (Smolders and Franken 1989, Liao *et al.* 2013).

Other characterizations have been illustrated in **Section 3.2.5**.

4.2.5. DCMD test of hollow fiber membranes

A direct contact membrane distillation (DCMD) experimental setup was used to test the performance of developed membranes as shown in **Figure 4.1** (Yang *et al.* 2011). Both the feed (synthetic seawater: 3.5 wt% sodium chloride (NaCl) with conductivity around 60 ms cm^{-1}) and permeate (Milli-Q ultra-pure water, with conductivity below 1.0 μs cm^{-1}) solutions were circulated through the hollow fiber module in a counter-current mode. The feed solution on the shell side was heated up to the determined operating temperature and circulated using a customized electrical water heater together with a peristaltic pump (0–12 L min^{-1}). The permeate solution on the lumen side was cooled down to 20 ºC using a water bath and circulated by another peristaltic

pump (0–4 L min^{-1}). The distillate that overflowed from the permeate water bath was weighed by a balance (± 0.1 g). To ensure comparable hydrodynamic conditions for different samples, the flow rates were adjusted to achieve the same Reynolds numbers (*Re*) for feed (*Re* = 2553) and permeate (*Re* = 310) streams, respectively. The permeate flux of membrane distillation was calculated using the following equation (Yang *et al.* 2011, Chen *et al.* 2013):

$$F = \frac{\Delta W}{A\Delta t} \tag{4.2}$$

where F is the permeate flux (kg m^{-2} h^{-1}); ΔW is the weight of distillate (kg); A is the outer surface area of the hollow fiber membranes (m^2); Δt is the testing time (h).

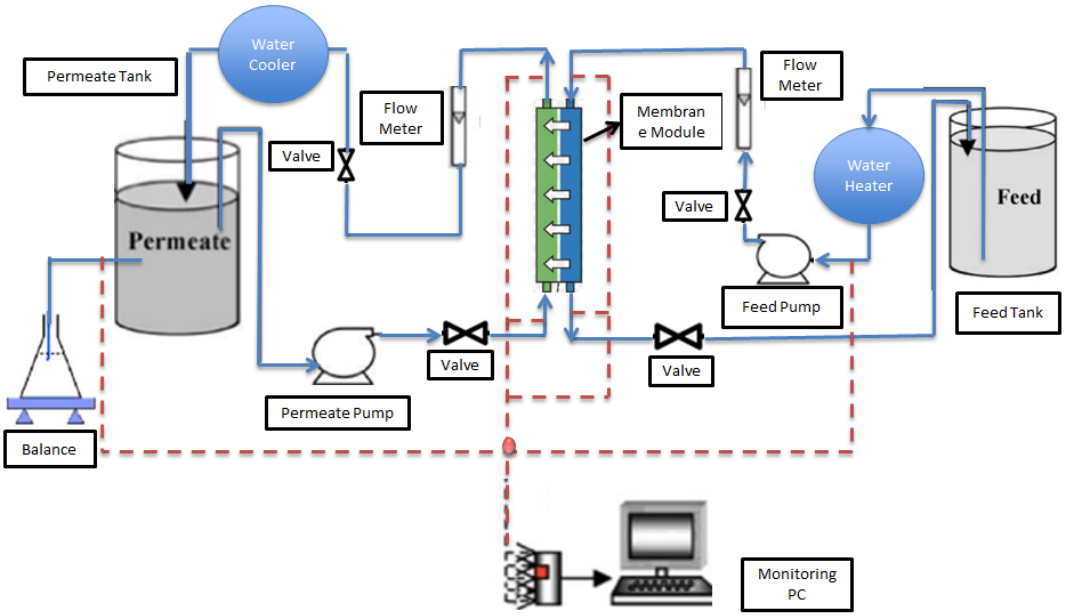

Figure 4.1. Schematic diagram of DCMD experimental set-up

4.3. Results and discussion

4.3.1. Phase diagrams for PVDF/DMP/PTFE ternary system

The phase diagrams for the PVDF/DMP binary system and PVDF/PTFE/DMP ternary system are shown in **Figure 4.2**. As depicted in **Figure 4.2(a)**, the monotectic point of the binary system without the addition of PTFE particles is around 28 wt%.

Governed by nucleation and growth (NG) or spinodal decomposition (SD) mechanisms, the phase separation occurs following different routes: liquid-liquid (L-L) separation (route A), solid-liquid (S-L) separation (route B) or their combination (route through the monotectic point). The concentrations of PVDF used in this study were greater than 30 wt%, suggesting the occurrence of S-L phase separation (Shi *et al.* 2012). Since DMP could not dissolve PTFE particles and the melting point of PTFE particles (326.8 °C) was much higher than the processing temperature (220 °C), the PTFE particles was more considered as an additive in the system that would not play a major role in the phase separation process (Ma *et al.* 2010). However, the impact of PTFE cannot be simply ignored as it might affect the crystallization of PVDF during the phase separation. Therefore, both PVDF/DMP and PVDF/PTFE/DMP systems should be examined by cross-over analysis of their phase diagrams.

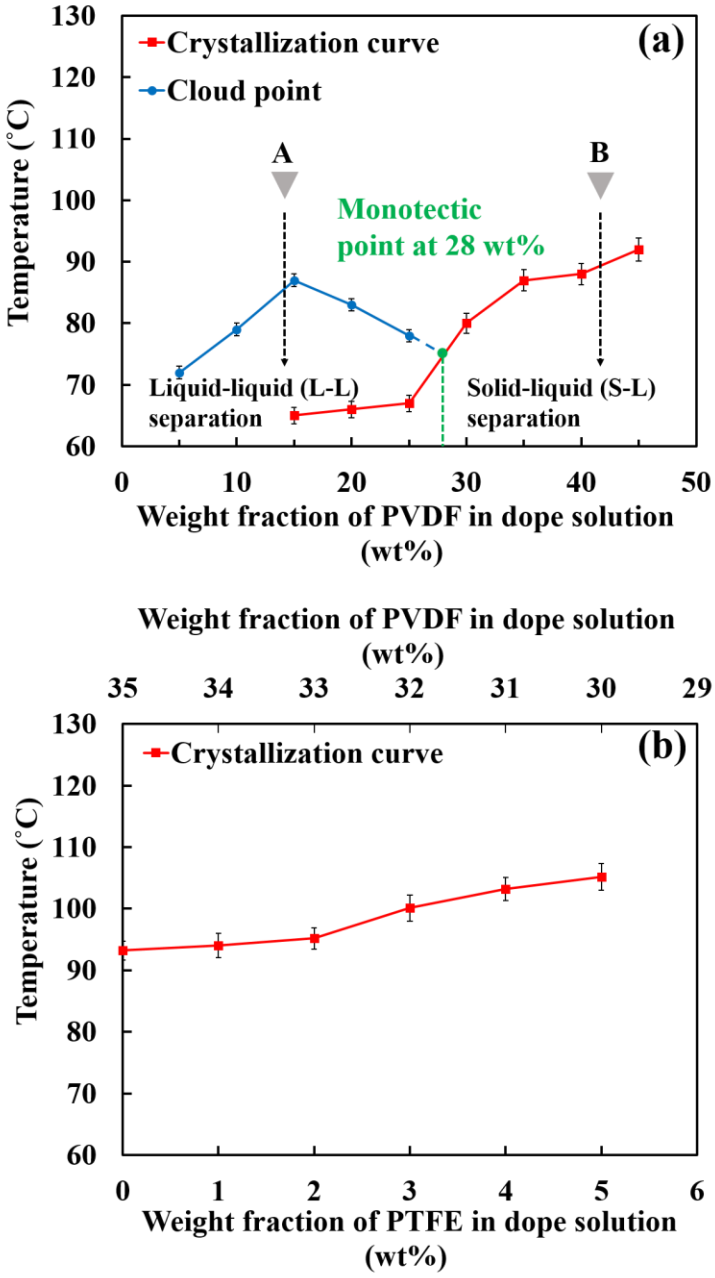

Figure 4.2. Phase diagrams for PVDF/DMP binary system (a) and PVDF/PTFE/DMP system (b), where an increase in PTFE weight fraction was compensated by a decrease in PVDF weight fraction

In this study, the concentration of the diluent was kept constant, while the concentrations of PVDF and PTFE were kept as a whole. Based on previous findings (Matsuyama *et al.* 1999), T_c would increase with increasing PVDF concentration if the effect of additive (in this case, PTFE) was negligible. However, it can be seen from **Figure 4.2(b)** that T_c gradually increased even with the decrease of PVDF

concentration (increase of PTFE loadings), which means PTFE particles played a significant role in the heterogeneous NG. PTFE particles might act as crystal nuclei whereby PVDF crystals could grow and develop due to its good compatibility with PTFE (Schneider *et al.* 2001). Hence, the crystallization process could be accelerated by the addition of PTFE particles. Similar results were found by Ma *et al*. in a comparative study on MMT and PTFE (Ma *et al.* 2013).

4.3.2. Characteristics of the hollow fiber membranes

Figure 4.3 shows the cross-sectional images of the membranes obtained from PVDF/DMP system with various loadings of PTFE. Typical spherulitic structures can be found in all SEM images, indicating that the system might have undergone the S-L phase separation as discussed in **Section 4.3.1**. The spherulites are known as a typical type of monocrystal aggregates in terms of their spherical crystallographic orientation resulted from isotropic and static temperature distribution during the growth of crystals (Teipel 2006). Theoretically, the lamellae are shaped first by the orderly alignment of polymer chains during the crystallization process. The lamellae can grow further in all directions into spherulites in the absence of thermal gradient (Ehrenstein 2012). The amount and size of spherulites can be affected by the nucleation which is the inception of the whole crystallization process (Teipel 2006, Ehrenstein 2012).

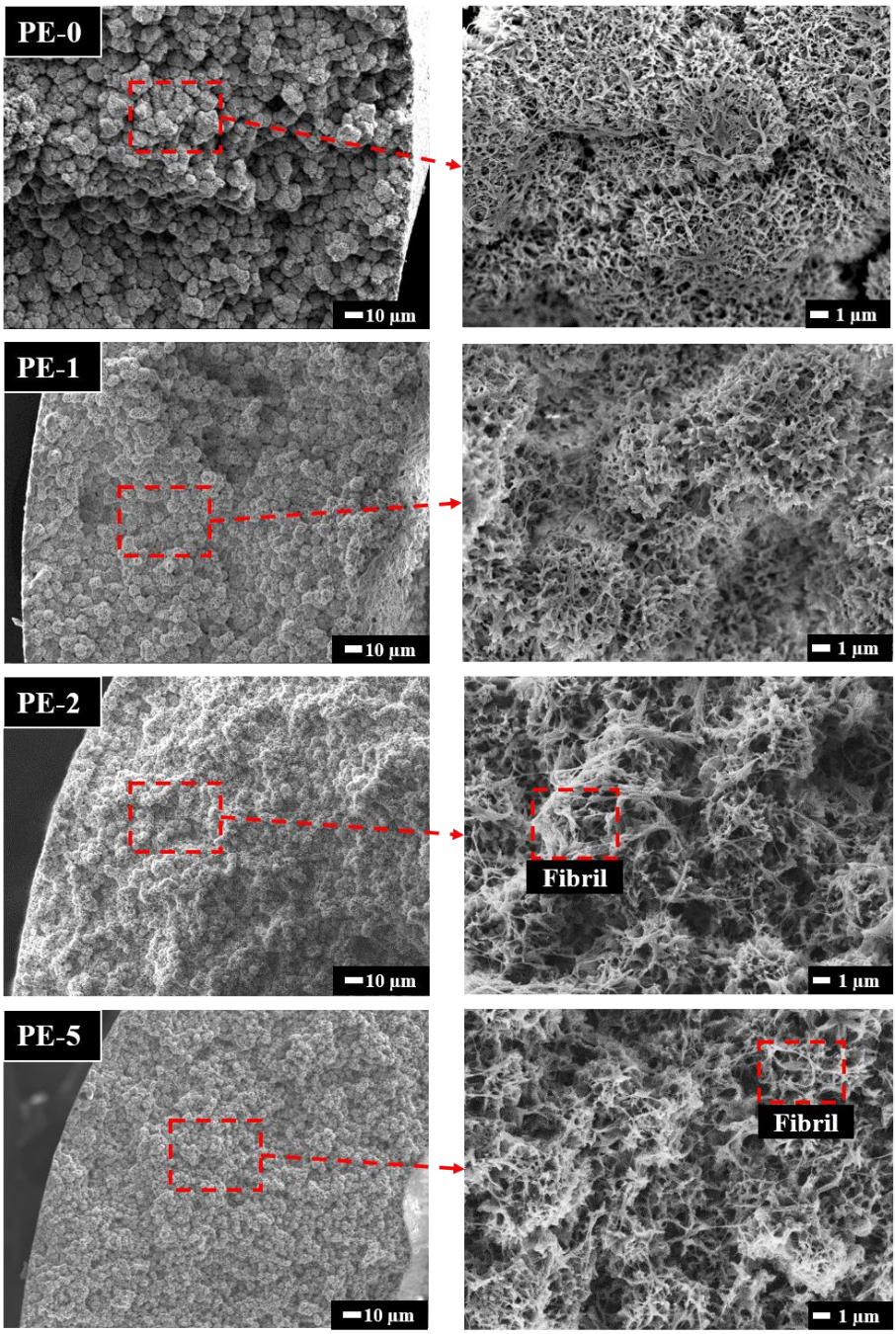

Figure 4.3. Cross-section morphology of hollow fiber membranes spun from the PVDF/DMP dopes with different PTFE loadings

It can be seen in **Figure 4.3** that the virgin PVDF membrane (PE-0) possessed spherulites with large sizes since the homogeneous nucleation was dominant without PTFE addition. As shown in **Figure 4.2(b)**, PE-0 had the lowest T_c, suggesting that it required the longest time to reach the crystallization point, i.e., the highest activation energy for forming crystal nuclei. Due to the smaller number of nuclei

formed, the crystals were able to grow into large diameters before impinging with each other. In contrast, when PTFE particles were incorporated into the blend, a heterogeneous nucleation occurred as the PTFE particles were likely to act as nucleating agents (Shi *et al.* 2012). As such, the crystallization process was probably facilitated with a larger number of nucleation sites supplied, which is consistent with the results of increased T_c at higher PTFE loadings. The larger number of available nuclei might eventually inhibit each spherulites to grow into a larger size, generating spherulites with smaller size and more uniform shape, as shown in **Figure 4.3**. However, when the loading of PTFE exceeded 1 wt%, interconnected fibril structures can be found in the enlarged images, suggesting the planar growth of crystalline lamellae under anisotropic temperature distribution. Therefore, the over-supply of PTFE particles in some regions might affect the temperature gradient.

DSC and WAXD analysis was conducted to study the thermal behaviors of PVDF/PTFE/DMP blends and the crystalline characteristics of resultant membranes. The corresponding results for crystallization and subsequent melting are presented in **Table 4.2** and **Table 4.3**, respectively.

Table 4.2. Crystallization behaviors of polymer dope mixtures with different PTFE loadings

Code	T_c^{on} (°C)	T_c^p (°C)	T_c^f (°C)	ΔT_c (°C)	ΔH_c (J g^{-1})
PE-0	104.3 ± 2.1	93.2 ± 0.8	86.5 ± 0.6	11.1 ± 0.2	34.2 ± 1.2
PE-1	99.5 ± 1.2	94.1 ± 1.1	85.7 ± 0.8	5.4 ± 0.3	35.1 ± 2.1
PE-2	100.2 ± 2.2	95.2 ± 1.0	86.3 ± 1.1	5.0 ± 0.1	35.4 ± 0.6
PE-5	110.3 ± 1.6	105.2 ± 2.1	96.9 ± 1.2	5.1 ± 0.1	30.6 ± 1.1

Notes:
T_c^{on}, onset crystallization temperature of PVDF; T_c^p, peak crystallization temperature of PVDF; T_c^f final crystallization temperature of PVDF; $\Delta T_c = T_c^{on} - T_c^p$.

Table 4.3. Melting behaviors of polymer dope mixtures and crystalline properties of membranes with different PTFE loadings

	Melting behaviors of dope mixtures				Crystalline properties of corresponding membranes		
Code	T_m^{on} (°C)	T_m^p (°C)	T_m^f (°C)	ΔT_m (°C)	ΔH_m (J g^{-1})	χ_c (%)	D (nm)
PE-0	123.1 ± 2.5	144.7 ± 3.2	148.8 ± 2.1	25.7 ± 0.3	45.6 ± 2.1	43.6 ± 2.1	6.42 ± 0.32
PE-1	111.3 ± 2.1	126.5 ± 3.0	136.4 ± 2.2	25.1 ± 0.2	51.9 ± 3.1	49.7 ± 1.9	6.10 ± 0.29
PE-2	112.9 ± 1.5	128.2 ± 2.6	137.7 ± 1.2	24.8 ± 0.1	51.0 ± 2.2	48.8 ± 1.5	5.53 ± 0.15
PE-5	122.1 ± 2.1	137.0 ± 2.2	145.6 ± 3.2	23.5 ± 0.1	49.2 ± 1.6	47.1 ± 2.0	4.52 ± 0.06

Notes:
T_m^{on}: onset melting temperature of PVDF; T_m^p: peak melting temperature of PVDF; T_m^f: final melting temperature of PVDF; $\Delta T_m = T_m^f - T_m^{on}$, ΔH_m: melting enthalpy; χ_c: crystallinity of PVDF; D: crystal size.

As shown in **Table 4.2**, the peak crystallization temperatures, T_c^p, gradually increased as PTFE particles were added into the dope mixtures. The observation indicates that PTFE particles could bring down the threshold of activation energy for crystallization of nuclei (Ma *et al.* 2013). In addition, the difference between the onset and peak temperature of crystallization, ΔT_c, was calculated to further investigate the kinetic characteristics of the crystallization process. It can be seen that the ΔT_c of the dope mixtures decreased with the addition of PTFE particles. This indicates that the crystallization half-time ($t_{1/2}$) for PVDF with PTFE addition was much shorter than that without PTFE addition when the same cooling rate was applied. Hence, the crystallization of PVDF in the mixture was probably promoted due to the accelerated nucleation in the presence of PTFE particles.

From the results of melting scans shown in **Table 4.3**, the peak melting temperature, T_m^p, decreased sharply with 1 wt% PTFE loading, but then gradually bounced back as the PTFE loading was increased to 5 wt%. The T_m^p describes the point at which the heat absorption is happening at the utmost rate (Raimo 2011, Ehrenstein 2012). It indicates the degree of the long-range order in the crystalline structure, which is commonly reflected by the size of spherulites. However, the size of crystal decreased

with increasing amount of PTFE loadings as shown in **Table 4.3**, suggesting a decreasing trend of T_m^p which does not match the experimental observation. This reveals that other factors should also be taken into account. As discussed previously, the planar growth of lamellae probably occurred due to over-supply of PTFE particles. Hence, the increase in T_m^p with increasing PTFE loadings from 1 to 5 wt% may be attributed to the enhanced degree of the long-range order contributed by the lamellae structure. On the other hand, the difference between the final and onset temperatures of melting, ΔTm, decreased with increasing PTFE loading. This suggests that more uniform spherulites could be obtained with PTFE addition (Ma *et al.* 2013), which agrees with the trend observed from the cross-section analysis presented in **Figure 4.3**. Moreover, the crystallinity (χ_c) of the mixture increased first with PTFE addition at 1 wt% and then slightly decreased with further loading, which could be due to the relatively increased fraction of amorphous region between the lamellae structure. This trend also implies that the addition of an appropriate amount of PTFE particles into the PVDF/DMP mixture could facilitate the crystallization of PVDF.

To further interpret the impact of PTFE particles on the crystallization process of PVDF, X-ray diffraction measurement was conducted as depicted in **Figure 4.4**. The peaks at 2θ = 17.66°, 18.30° and 19.90° in the patterns for both virgin and PTFE-incorporated membranes correspond to the diffractions in planes (100), (020), and (110), respectively, suggesting the presence of only the α-phase crystal of PVDF. However, it should be pointed out that the peak of plane (100) and (020) gradually merged together and finally manifested as a single strong peak of plane (100) with increasing PTFE loading from 0 to 5 wt%. The observation suggests that although the crystal types remained to be the α-phase, the crystallographic orientation of crystal growth was actually changed. This supports the speculation stated previously that the lamellae developed sideward without growing into radial-structured spherulites in certain regions with the addition of PTFE particles.

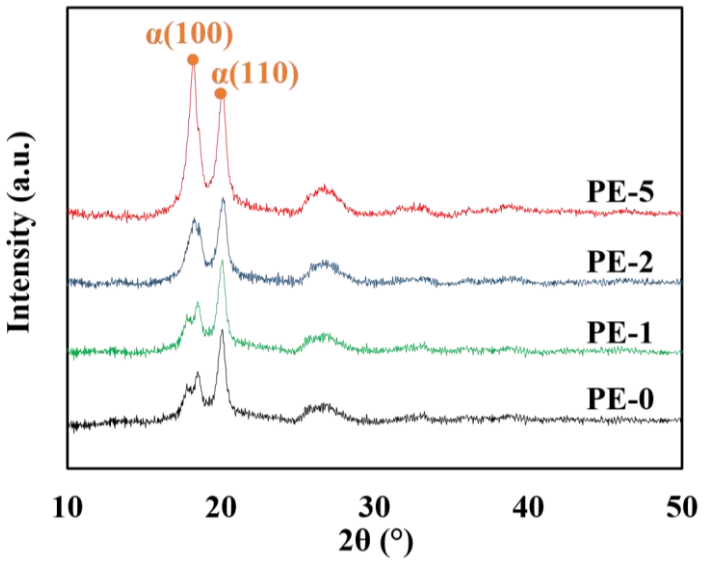

Figure 4.4. X-ray diffraction patterns of membranes obtained with different PTFE loadings

In the S-L phase separation, the pore structure of a membrane forms along with the NG of crystals (Lloyd *et al.* 1990). Thus, the crystallization process could strongly affect the pore structure. The effect of PTFE loading on the mean pore size and pore size distribution of resultant membranes is shown in **Figure 4.5**. The related characteristics of prepared membranes are listed in **Table 4.4**. It can be seen that both mean and maximum pore sizes of membranes decreased first (0 to 2 wt%) and then slightly increased (2 to 5 wt%) with the addition of PTFE particles. As explained earlier, the heterogeneous nucleation promoted by PTFE particles could facilitate the formation of more crystals. Given a faster rate of NG, more spherulites could be shaped with higher uniformity and smaller cavity in between. Therefore, smaller pore diameters and a narrower pore size distribution should be expected. However, the effects of changes in PVDF fraction in the dope system should also be taken into account since the skeleton of membrane is mainly structured by PVDF. In this study, a fixed portion of PVDF/PTFE in the dope mixture was applied so that the PVDF fraction decreased as the PTFE loading went higher. Hence, considering the tradeoff between the promoted density of spherulites and the lowered PVDF fraction, the slight increase in the pore sizes as the PTFE loading was changed from 2 to 5 wt% could be attributed to stronger impact from the decreased PVDF fraction. On the other hand, compared with virgin PVDF membranes, smaller pore sizes and much narrower

pore size distributions can be obtained from the membranes with the addition of PTFE particles.

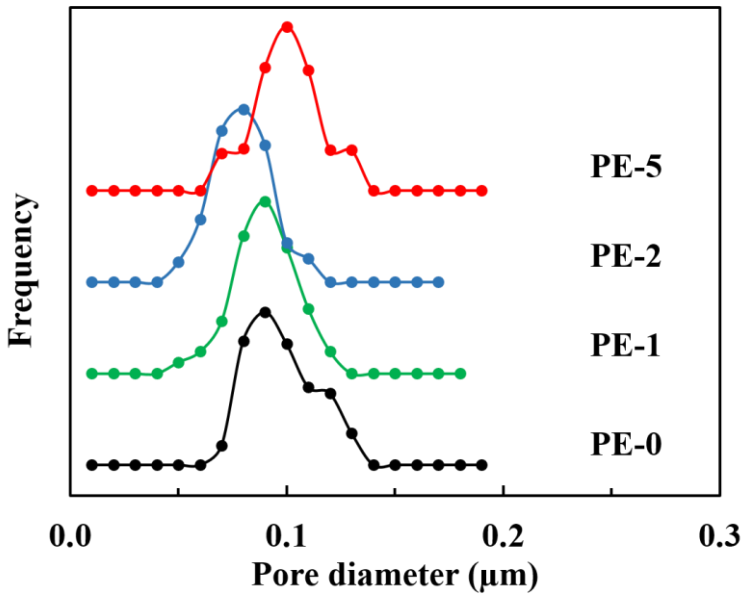

Figure 4.5. Pore size distribution of membranes obtained with different PTFE loadings

Table 4.4. Characteristics of membranes with different PTFE loadings

Code	OD (µm)	ID (µm)	Mean pore size (nm)	Maximum pore size (µm)	LEPw (bar)
PE-0	1032 ± 2	610 ± 4	0.18 ± 0.02	0.21 ± 0.03	0.50 ± 0.01
PE-1	1015 ± 5	547 ± 8	0.10 ± 0.01	0.12 ± 0.02	3.31 ± 0.05
PE-2	1022 ± 11	574 ± 4	0.08 ± 0.01	0.11 ± 0.01	3.54 ± 0.10
PE-5	1098 ± 12	651 ± 9	0.12 ± 0.01	0.15 ± 0.03	2.66 ± 0.06
Commercial[a]	1549 ± 10	855 ± 5	0.02 ± 0.01	0.18 ± 0.02	1.70 ± 0.05

Note:
[a)] The commercial membrane was selected for DCMD test as benchmark in **Section 4.3.3**.

The impact of PTFE addition can also be reflected in the porosity and water permeability of the resultant membranes, which are commonly used to indicate the interconnectivity of the pore structure. Generally, the interconnectivity of spherulitic structure is mainly determined by the tradeoff between the size and amount of cavities among the spherulites (Teipel 2006, Ehrenstein 2012). **Figure 4.6** shows that, the porosity of the prepared membranes initially reached the highest value at the loading of 1 wt% and then decreased with PTFE addition. As discussed in previously, the presence of an appropriate amount of PTFE could enhance the nucleation process, resulting in spherulites with smaller size but larger number. The size and density of spherulites normally have a positive relationship with those of cavities (Gu *et al.* 2006). Therefore, when the PTFE loading exceeded 1 wt%, the impact from decreased cavity sizes might surpass that from increased cavity numbers, leading to the reduction in the porosity. This trend is in accordance with the results of water permeability presented in **Figure 4.6**. Pure water permeability was observed to be directly related to both pore size distribution and porosity, and the membrane with 1 wt% of PTFE loading possessed the highest water permeability due to its relatively high overall and surface porosities.

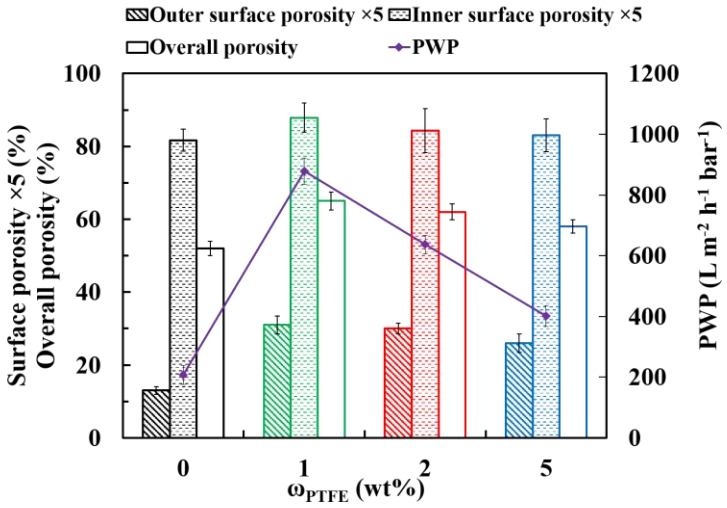

Figure 4.6. Porosity and pure water permeability of membranes obtained with different PTFE loadings

Instinctively, the mechanical strength of TIPS membranes can be improved by increasing the polymer concentration. However, as discussed previously, a high polymer concentration could make it possible for the occurrence of phase separation at the region beyond the monotectic point, which results in the formation of spherulitic structure. This structure is considered relatively weaker than the bicontinous structure owing to the low interconnectivity between the spherulites (Gu *et al.* 2006). Nevertheless, the formation of bicontinuous structure often requires a low polymer concentration in most dope systems, resulting in membranes with a low mechanical strength. Therefore, improving the mechanical strength by adjusting the polymer concentration remains a dilemma. The effect of PTFE addition on the tensile strength and elongation at break is depicted in **Figure 4.7**. The tensile strength and elongation could reach the maximum values of 9.4 ± 0.3 MPa and 235 ± 36%, respectively, showing outstanding durability and ductility. It can be seen clearly that the tensile strength, representing the toughness, was improved as the loading of PTFE particles varied from 0 to 5 wt%. However, the elongation, which indicates the elasticity, experienced ups and downs along with the addition of PTFE particles. This may be due to two factors: (1) the nucleation effect of PTFE; and (2) the formation of lamellae structure which contained more amorphous regions with higher loadings PTFE. Generally, the spherulites in the PVDF-based membranes contain semi-crystalline structure where lamellae crystallites with orderly polymer alignment are embedded between amorphous regions (Ehrenstein 2012). It is widely accepted that the toughness is mainly contributed by the intermolecular interactions within the crystallites, while the elasticity is dependent more on the amorphous regions between the lamellae (Teipel 2006, Ehrenstein 2012, Cui *et al.* 2015). As PTFE loading increased, the nucleation of PVDF was probably promoted as discussed before, suggesting stronger intermolecular interactions within spherulites and tighter impingement between spherulites. This could be responsible for the increase in the tensile strength. On the other hand, it was also found that the planar formation of lamellae structure might be enhanced as discussed previously. In addition, the crystallinity of membranes was also decreased with higher loadings of PTFE, indicating the increase in the amorphous region as shown in **Table 4.3**. The elasticity was therefore improved noticeably as the loading of PTFE was increased from 2 to 5

wt%. It should be pointed out that the toughness was supposed to be slightly compromised with increased amorphous regions. However, it was not obviously reflected in the trend of tensile strength probably due to a stronger impact from increased interconnectivity between spherulites.

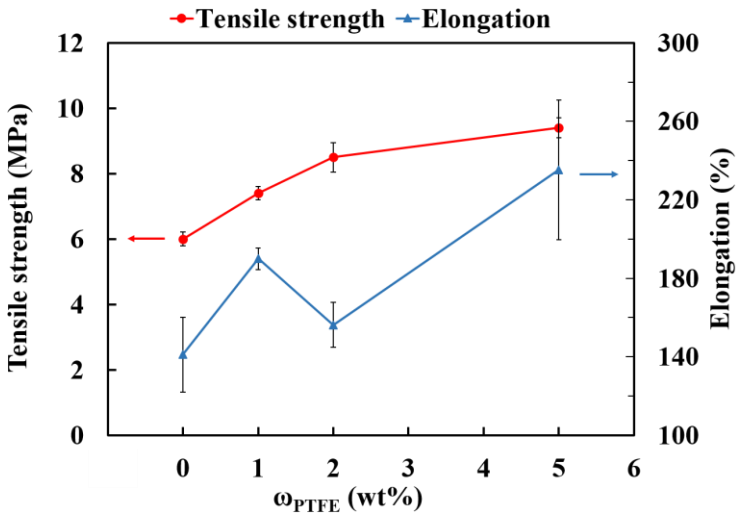

Figure 4.7. Mechanical properties of membranes obtained with different PTFE loadings

Water contact angle is an important indication to the surface hydrophobicity of hollow fiber membranes. The enhancement of hydrophobicity is a major concern on wetting control as this study aims at developing membranes suitable for MD process (Liao *et al.* 2014). The addition of PTFE particles is expected to serve dual functions: (1) to adjust the membrane pore structure, which has been verified in the prior sections; and (2) to improve the hydrophobicity of the PVDF membranes. The variations of dynamic contact angle of prepared membranes are shown in **Figure 4.8**. Compared with the virgin PVDF membrane with a contact angle of 95 ± 1º, all prepared membranes with PTFE addition exhibited a higher water contact angle of more than 105º, suggesting that the incorporation of PTFE particles is an effective way to enhance the surface hydrophobicity of membranes. In addition to the intrinsic hydrophobic nature of PTFE particles, the enhanced hydrophobicity could also be attributed to the surface topography of the membranes, which contains information

of the surface roughness. As presented in **Figure 4.9**, the outer surface of the membranes becomes more rugged with increasing loading of PTFE particles. Furthermore, it can be seen from **Table 4.5** that the roughness of both the internal and external surfaces of the PTFE-incorporated membranes are noticeably higher than those of virgin membranes. The mean roughness increased slightly as PTFE loading was further increased from 2 to 5 wt%. This result may be attributed to the intensified impingement among spherulites resulted from the addition of PTFE particles. Such spherulite-led rugged structures could be essential to improve the hydrophobicity of membranes.

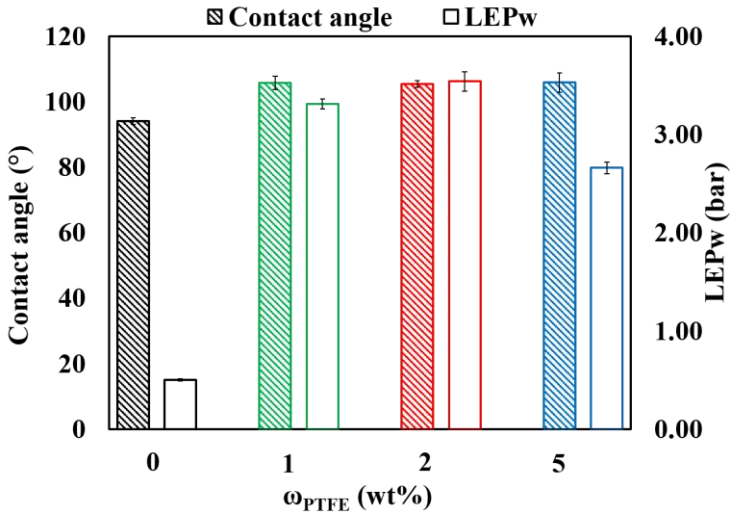

Figure 4.8. Dynamic contact angle and LEPw of membranes obtained with different PTFE loadings

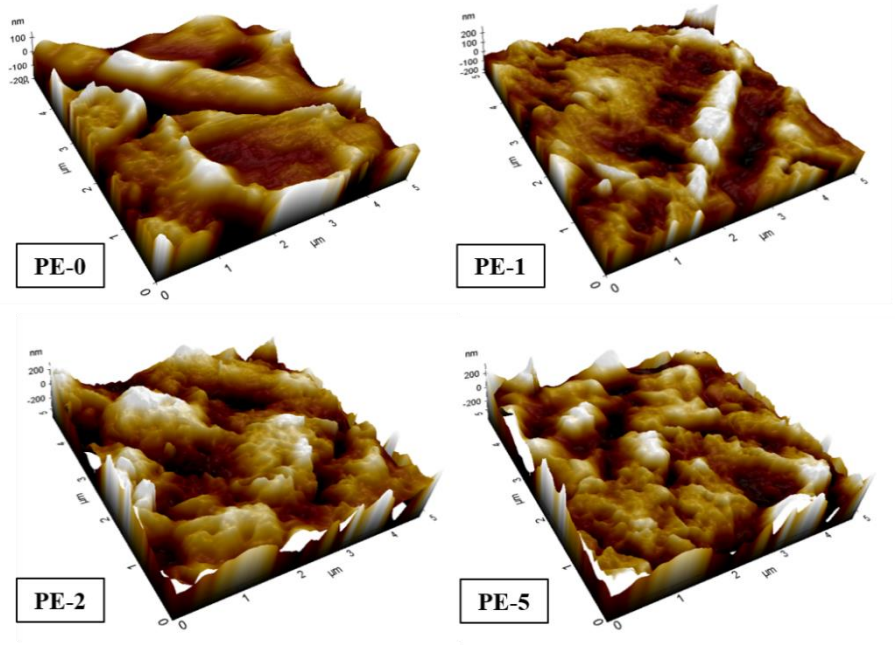

Figure 4.9. AFM images (3D) of the outer surface of membranes obtained with different PTFE loadings

Table 4.5. Surface properties of membranes with different PTFE loadings

Code	R_a of inner surface (nm)	R_a of outer surface (nm)
PE-0	69.2 ± 1.2	45.7 ± 0.6
PE-1	73.0 ± 1.3	55.8 ± 0.9
PE-2	74.2 ± 1.2	56.7 ± 1.3
PE-5	78.5 ± 1.5	58.9 ± 1.5

LEPw is one of the critical characteristics commonly used to select the suitable membranes for MD application as it indicates the anti-wetting properties of the membranes (García-Payo *et al.* 2010, Liao *et al.* 2014). It can be found from **Table 4.4** and **Figure 4.8** that the LEPw values of the PTFE-incorporated membranes are much higher than that of virgin membranes. This is possibly due to the reduced maximum pore size as well as the increased hydrophobicity. PE-2 exhibits the largest LEPw of 3.54 ± 0.10 bar given its smallest maximum pore size among all the in-house fabricated membranes.

4.3.3. Performance of PVDF/PTFE hollow fiber membranes in DCMD

DCMD tests were conducted to evaluate the MD performance of the PVDF hollow fiber membranes with and without PTFE addition. The permeation flux of each test was recorded after a 3-h stabilization. The effect of feed temperature on the permeation flux for the membranes with different PTFE loadings is plotted in **Figure 4.10**. It can be observed that all membranes with PTFE incorporation exhibited enhanced flux over the virgin membrane (PE-0). The membrane with 1 wt% PTFE addition (PE-1) achieved the best performance, which possessed a flux of 28.3 kg m^{-2} h^{-1} at a feed temperature of 60 ºC. Such results agree well with the tendency of pore size, porosity and water permeability presented in **Table 4.4** and **Figure 4.6**, which show that the PE-1 membrane possessed the largest porosity and water permeability. As discussed previously, an appropriate PTFE addition improved the interconnectivity and uniformity of the pore structure, so that it could greatly reduce the resistance for water vapor transport (Matsuyama *et al.* 1999, Yang *et al.* 2011, Chen *et al.* 2013, Song *et al.* 2016). To better assess the long-term performance, a continuous study was performed at a feed temperature of 60 ºC. One commercial hollow fiber membrane was selected for comparison with PE-0 and PE-1 membranes. The characteristics of the selected commercial membrane are summarized in **Table 4.4**.

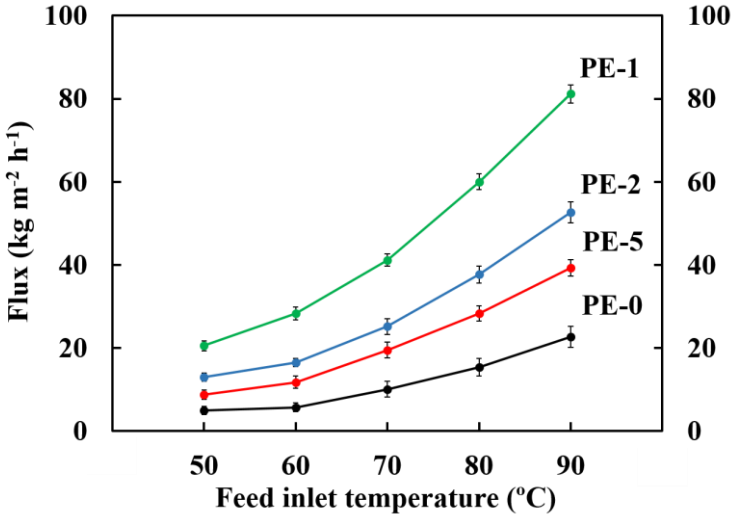

Figure 4.10. DCMD permeation flux of membranes with different PTFE loadings

Figure 4.11 shows that the PVDF/PTFE hollow fiber membranes achieved a relatively stable permeation flux throughout the entire testing period of 50 h, which was much better than the performance of the selected commercial membrane. In contrast, the virgin PVDF (PE-0) membranes was easily wetted within only 5 h, possibly due to its relatively low anti-wetting property which is closely linked with the LEPw of membrane (Liao *et al.* 2014). When PTFE particles were introduced, the reduced pore sizes and improved hydrophobicity resulted in a higher LEPw as presented in **Section 5.3.2**, and hence a better wetting resistance. A further benchmark comparison of the selected PE-1 membrane and other membranes reported in the literature is shown in **Table 4.6**. The PVDF/PTFE membrane showed comparable performance with others, while it exhibited better mechanical strength, indicating its good potential in MD application.

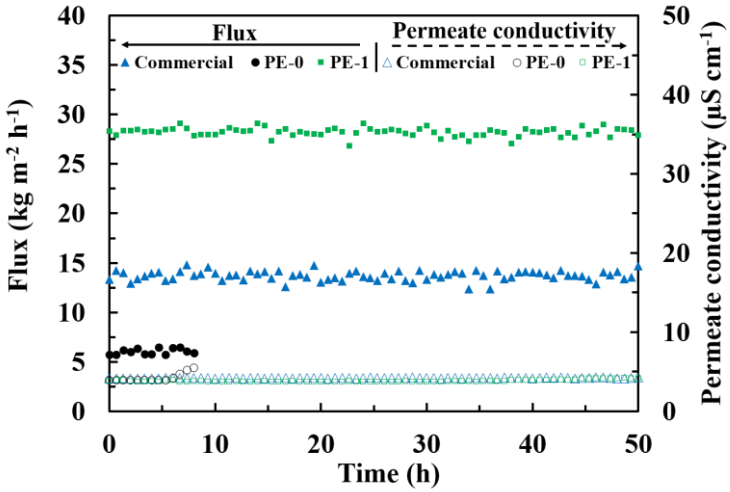

Figure 4.11. Effect of PTFE addition on PVDF membranes for DCMD application (3.5 wt% NaCl as feed, T_f = 60 °C, T_p = 20 ºC)

Table 4.6. Performance and properties of different PVDF hollow fiber membranes

				Feed solution			Permeate solution			
Membrane	Method	Mean pore size (μm)	Tensile strength (MPa)	NaCl conc. (wt%)	T_f (°C)	Flow velocity (m s^{-1})	T_p (°C)	Flow velocity (m s^{-1})	Permeate flux (kg m^{-2} h^{-1})	Ref.
PVDF hollow fiber	NIPS	0.25[a]	-[b]	3.5	60.0	0.50	20.0	0.15	19.5[a]	(Hou *et al.* 2009)
PVDF/$CaCO_3$ hollow fiber	NIPS	0.25	5.7	3.5	60.0	0.50	20.0	0.15	21.1[a]	(Hou *et al.* 2012)
PVDF hollow fiber	NIPS	0.16[a]	-[b]	3.5	60.0	1.60	17.5	0.80	19.6[a]	(Wang *et al.* 2008)
PVDF/PTFE hollow fiber	NIPS	0.25	-[b]	3.5	60.0	1.90	17.5	0.90	18.9[a]	(Teoh and Chung 2009)
PVDF dual-layer hollow fiber	NIPS	0.41	-[b]	3.5	60.0	1.60	16.5	0.80	18.7[a]	(Bonyadi and Chung 2007)
PVDF dual-layer hollow fiber	NIPS	0.41	-[b]	3.5	60.0	1.80	16.6	0.72	35.8[a]	(Su *et al.* 2010)
PVDF/clay hollow fiber	NIPS	-[b]	1.0	3.5	60.0	1.80	17.5	1.20	35.9[a]	(Wang *et al.* 2009)
PVDF/PTFE dual-layer hollow fiber	NIPS	-[b]	-[b]	3.5	60.0	1.90	17.5	0.90	22.1[a]	(Teoh *et al.* 2011)
PVDF hollow fiber	TIPS	0.28	-[b]	3.5	60.0	0.04	20.0	0.04	8.5[a]	(Song *et al.* 2012)
PVDF hollow fiber	TIPS	0.31	6.8	3.5	60.0	0.80	25.0	0.80	28.1[a]	(Wang *et al.* 2014)
PVDF/$CaCO_3$ hollow fiber	TIPS	0.28[a]	2.1	3.5	60.0	1.00	25.0	0.80	22.2[a]	(Song *et al.* 2016)
PVDF/PTFE hollow fiber (PE-1)	TIPS	0.10	7.4	3.5	60.0	1.04	20.0	0.20	28.3	This work

Notes: [a)] The data were collected from figures in the literature by using the Digitizer function in *Origin* 9.1; [b)] The data are not shown in the paper.

4.4. Conclusions

In the second part of work, hydrophobically enhanced PVDF/PTFE hollow fiber membranes with various PTFE loadings have been developed via TIPS method for DCMD. PTFE particles were found to play an important role in the crystallization of PVDF polymer matrix during the S-L phase separation. Acting as the nucleating agent, PTFE particles could significantly enhance the NG of PVDF.

The major findings and conclusions are summarized as follows:

- With addition of PTFE, more uniform and smaller spherulites in a greater number were generated, which further resulted in smaller cavities in between. As a result, narrower pore size distributions of the resultant membranes can be achieved with smaller mean pore sizes varying from 0.08 to 0.12 μm. The porosity and water permeability initially increased with PTFE content and then declined with the addition of PTFE particles above 1 wt%. The tensile strength and elongation were noticeably improved to as high as 9.4 ± 0.3 MPa and 235 ± 36 %, respectively. On the other hand, owing to PTFE's good intrinsic hydrophobicity, the water contact angle of resultant membranes increased from 94 ± 1 to 106 ± 3 º.
- With all these enhanced properties, the prepared PVDF/PTFE membranes achieved good performance in the MD process. The membranes with the optimum PTFE loading of 1 wt% exhibited a flux of 28.3 kg m^{-2} h^{-1} at the feed temperature of 60 ºC with 99.99 % NaCl rejection over a 50-h continuous test. Above all, the DCMD performance demonstrated that the newly developed PVDF/PTFE membranes had improved anti-wetting and mechanical properties over the virgin PVDF membranes, suggesting its good potential in DCMD applications.

The approach of fabricating PVDF/PTFE hollow fiber membranes in the present study provides the advantages of simple preparation for future scale-up production and promising properties for MD applications for long-term operation.

CHAPTER 5 Explorations of Combined TIPS and NIPS (N-TIPS) Method for Development of PVDF-based Hollow Fiber Membranes

This chapter has been published as **Zhao, J.**, Chong, J. Y., Shi, L., and Wang, R. (2019). "Explorations of combined nonsolvent and thermally induced phase separation (N-TIPS) method for fabricating novel PVDF hollow fiber membranes using mixed diluents." Journal of Membrane Science 572: 210-222. Permission has been granted by the licensed content publisher "Elsevier" to use the published content as a chapter in this thesis for non commercial purposes.

5.1. Introduction

The previous results have shown that the properties of PVDF membranes can be greatly altered by varying the TIPS spinning conditions and introducing functional additives into the system. However, the surface properties such as pore size and hydrophilicity cannot be effectively controlled using pore-formers with different functions in the same way as the NIPS method (Shi *et al.* 2007). This can be attributed to the weak mass transfer in the conventional TIPS process as a result of low mutual affinity between commonly used TIPS diluents and the nonsolvent (usually water). In comparison, the NIPS method involves three major components (polymer, solvent, and nonsolvent). The membrane formation starts at the interface between the polymer solution and the nonsolvent driven by the solvent-nonsolvent exchange (van de Witte *et al.* 1996, Setiawan *et al.* 2012, Feng *et al.* 2013). The NIPS technique can expediently adjust the pore size and other surface characteristics of membranes with the help of additives, which have been extensively studied (Shi *et al.* 2008, Wongchitphimon *et al.* 2011). Nevertheless, the NIPS membranes are frequently subjected to the macrovoids or defects formed during the exchange. There would be skinned macrovoids which can reduce the permeability of the membrane. Furthermore, the mass transfer has been found to be around two order slower than the heat transfer in the solution (Matsuyama *et al.* 2002), providing less evenly distributed driving force than that in the TIPS process. As a result, membranes

produced by the NIPS process often exhibit a wider pore size distribution and weaker mechanical properties than the TIPS membranes (Liu *et al.* 2011).

Researchers have been trying to bridge the gap between TIPS and NIPS. The study reported by Matsuyama and co-workers in 2002 has been recognized as the first attempt of the combined NIPS and TIPS (N-TIPS) method (Matsuyama *et al.* 2002). During the fabrication of poly(methyl methacrylate) (PMMA) membranes, they proposed to modify the conventional TIPS method by using cyclohexanol as the diluent, which possesses a high affinity with the nonsolvent. The diluent induced the NIPS process by facilitating the solvent-nonsolvent exchange at the dope-coagulant interface. Besides, a similar attempt to achieve the combination of NIPS and TIPS has also been made by adding an evaporative NIPS solvent to the polymer/diluent to induce the thermally assisted evaporative phase separation (TAEPS) (Hellman *et al.* 2004). As illustrated in **Figure 5.1**, we summarized the solvents/diluents commonly used in the N-TIPS process into four different categories based on their solubility with polymer and water. For the same chemical, the terms "diluent" (in TIPS) and "solvent" (in NIPS) are used interchangeably in this paper to emphasize its function in different processes. The solvents which can dissolve the polymer at the room temperature are defined as good solvents (Cui *et al.* 2013). The good solvents which are water-soluble are often used in the NIPS process (Shi *et al.* 2009, Chou *et al.* 2010, Wang *et al.* 2010). For instance, N-methyl-2-pyrrolidone (NMP) and dimethylacetamide (DMAc) are common NIPS solvents for PVDF (Loh *et al.* 2011). On the other hand, those water-insoluble poor solvents are normally used as diluents in the TIPS process. For PVDF, such diluents include dimethyl phthalate (DMP), diethyl phthalate (DEP), dibutyl phthalate (DBP), acetyl tributyl citrate (ATBC), etc. (Cui *et al.* 2014). Among various solvents, we found triethyl phosphate (TEP) is a special one that cannot be fitted into this figure (Bottino *et al.* 1991). TEP is a water-soluble solvent with a high boiling point (215 °C) and is able to completely dissolve PVDF only at a moderately high temperature (80 °C for PVDF at 20 wt%) (Lin *et al.* 2006). Thus, it can be considered as a neutral solvent for PVDF. It is able to induce both TIPS and NIPS processes under appropriate conditions (Liu *et al.* 2012). However, the membrane formation was found to be strongly hindered by the gelation induced possibly at high TEP concentration (Lin *et al.* 2006).

Herein, we proposed a modified N-TIPS approach using mixed diluents which contain a water-insoluble poor solvent and a water-soluble neutral solvent. This simple method is expected to allow us to tune the surface pore structure of membranes effectively without forming mechanically weak macrovoids, and to scale up membrane fabrication easily. Specifically, the water immiscible plasticizer, DMP, was used as the main diluent for PVDF since the hollow fiber membranes prepared from the PVDF/DMP dope mixtures exhibited an outstanding mechanical strength in our previous work (Zhao *et al.* 2018). TEP was used at a low concentration together with DMP for PVDF fabrication in an effort to control the solvent-nonsolvent concentration gradient and to avoid the occurrence of gelation. To further increase the membrane surface porosity, amphiphilic copolymer Pluronic F127 (abbreviated as F127 in the following paragraphs) was used as an additive. F127 has shown excellent surface-modifying and pore-forming abilities (Loh and Wang 2014), and its effects on N-TIPS PVDF membranes were also studied. This research aims at providing a facile approach for developing robust hollow fiber membranes with a tunable macrovoid-free surface pore structure, followed by studying the fundamental phenomena in the membrane formation during the N-TIPS process.

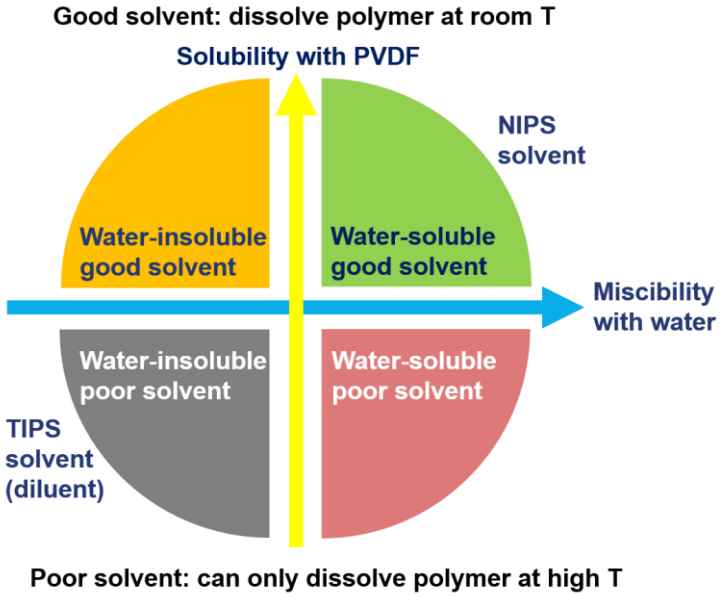

Figure 5.1. Four types of solvents categorized according to their solubility with polymer and water

5.2. Methodology and experiments

5.2.1. Materials

Polyvinylidene fluoride (PVDF Solef® 1015, M_w = 570,000–600,000, Solvay, Belgium) was purchased for the fabrication of hollow fiber membranes. Dimethyl phthalate (DMP, Merck KGaA, Germany) was used as the main diluent and bore fluid. Triethyl phosphate (TEP, Merck KGaA, Germany) was used as the second diluent. Pluronic® F127 (abbreviated as F127 in the following paragraphs, M_w = 12,600, PEO_{100}–PPO_{65}–PEO_{100}, Sigma Aldrich, Singapore) was used as an additive in hollow fiber fabrication. Ethanol (Merck KGaA, Germany) and n-hexane (Merck KGaA, Germany) were used successively in the post-treatment for resultant membranes. Bovine serum albumin (BSA, M_w = 67,000, Sigma-Aldrich) was used as a model protein foulant. Milli-Q ultra-pure water was used as the de-ionized (DI) water for all experiments. All the reagents were used as received.

5.2.2. Phase diagram determination

The phase diagram was determined by a method as described in **Section 3.2.2**.

5.2.3. Preparation of hollow fiber membranes

The hollow fiber membranes were fabricated using a TIPS machine as shown in

Figure 3.1. The detailed procedures of fabrication process have been described in **Section 3.2.3**. The samples with TEP weight fractions at 0, 5, 10 wt% were designated as T0, T5 and T10, accordingly. On top of T5, the samples with F127 weight fractions at 1 and 3 wt% were designated as T5F1 and T5F3. The corresponding characteristics of resultant membranes are summarized in **Table 5.1**. The spinning parameters are listed in **Table 5.2**.

Table 5.1. Dope compositions and characteristics of membranes

Code[a]	PVDF (wt%)	DMP (wt%)	TEP (wt%)	Pluronic F127 (wt%)
T0		70	0	0
T5		65	5	0
T10	30	60	10	0
T5F1		64	5	1
T5F3		62	5	3

Note:
[a)] Bore fluid composition (wt%): DMP (100).

Table 5.2. Spinning parameters for hollow fiber membranes

Extrusion rate (g min^{-1})	5.3
Extrusion temperature (°C)	200
Bore fluid flow rate (mL min^{-1})	2.0
Coagulation temperature (°C)	30
Air gap (cm)	1
OD/ID of spinneret (mm)	1.84/0.92

5.2.4. Characterization of hollow fiber membranes

Attenuated total reflectance Fourier transform infrared spectroscopy (ATR-FTIR, IRPrestige-21, Shimadzu, Japan) was used to assess the chemistry information of the membranes by. Short fibers were cut out and compressed to increase the surface area for scanning. The surface of dried membranes was directly analyzed and the IR spectra were obtained by 45 scans at a resolution of 4 cm^{-1} (Loh and Wang 2014). Other characterizations have been illustrated in **Section 3.2.5** and **4.3.2**.

5.3. Results and discussion

5.3.1. Thermodynamic properties of PVDF/DMP/TEP ternary system

Determining the thermodynamic properties of the polymer-diluent mixture is important for the understanding of N-TIPS membrane formation mechanism. The interactions between polymer and the mixed diluents are discussed in two scenarios: (a) between PVDF and individual diluent, and (b) between PVDF and the diluent mixture. The mutual affinity of a polymer and a solvent/diluent can be estimated by the Hansen's solubility parameter (δ_t) which comprises of three dimensional components: polar (δ_p), dispersion force (δ_d), and hydrogen bonding (δ_h) (Hansen 2012). In scenario (a), the individual relative affinity of PVDF with DMP and TEP can be examined by the following equation (Wongchitphimon *et al.* 2011):

$$\Delta\delta_{ps} = ((\delta_{ps} - \delta_{pp})^2 + (\delta_{ds} - \delta_{dp})^2 + (\delta_{hs} - \delta_{hp})^2)^{1/2} \quad (5.1)$$

where *p* and *s* represent the polymer and the solvent, respectively. Normally, a smaller value indicates a better interaction between the polymer and the solvent.

The solubility parameters are listed in **Table 5.3**. It can be seen that the value of $\Delta\delta_{ps}$ for PVDF and DMP is greater than that of PVDF and TEP, which suggests that the interaction of PVDF polymer chains with DMP is weaker than that with TEP. Besides, TEP also possesses a stronger affinity with PVDF than some of common NIPS solvents such as DMAc and NMP, and PVDF can be completely dissolved in TEP at a moderately high temperature (80 °C for PVDF at 20 wt%) (Lin *et al.* 2006). In addition, TEP has a high boiling point and miscibility with water. Such features render TEP a promising solvent to induce the low-temperature TIPS and high-temperature NIPS (Liu *et al.* 2012). The versatility of TEP was expected to play a key role in inducing the N-TIPS process.

Table 5.3. Solubility parameters of PVDF and some common solvents

Chemicals	δ_d	δ_p	δ_h	$\Delta\delta_{ps}$	Boiling point (°C)	Miscibility with H_2O	Ref.
		(MPa)$^{1/2}$					
PVDF	17.2	12.5	9.2	\	\	Low	(Xiao *et al.* 2015)
DMP	18.6	10.8	4.9	4.8	283.0	Low	(Yang *et al.* 2008)
TEP	16.8	11.5	9.2	1.1	215.0	High	(Liu *et al.* 2011)
DMAc	16.8	11.5	10.2	1.5	165.0	High	(Liu *et al.* 2011)
NMP	18.4	12.3	7.2	2.3	202.0	High	(Liu *et al.* 2011)

We also examined the interaction between PVDF and the mixture of DMP and TEP in scenario (b) based upon the Flory-Huggins solution theory (Lindvig *et al.* 2002, Fried 2003). The estimation of the interaction parameter (χ^*) can be expressed by the difference of the solubility parameters between polymer and the diluent in the following equation (Liu *et al.* 2000, Ji *et al.* 2008):

$$\chi^* = \frac{V_m}{RT}((\delta_{d1}-\delta_{d2})^2+(\delta_{p1}-\delta_{p1})^2+(\delta_{h1}-\delta_{h1})^2) \tag{5.2}$$

where V_m is a reference volume which equivalents to the molar volume of the specific repeating unit size of the polymer; R is the gas constant; T is the temperature; for δ_d, δ_p and δ_h, 1 and 2 denote the polymer and diluent, respectively. Assuming that V_m is identical for all systems, the interaction between PVDF and diluents for dope mixtures at a certain temperature and polymer concentration could be expressed by molar excess free energy of mixing (ΔG^E) (Ji *et al.* 2008):

$$\Delta G^E = (\delta_{d1}-\delta_{d2})^2+(\delta_{p1}-\delta_{p1})^2+(\delta_{h1}-\delta_{h1})^2 \tag{5.3}$$

where small values of χ^* or ΔG^E indicates better interaction between polymer and the diluent.

As listed in **Table 5.4**, five combinations of polymer and diluent mixtures were used to assess the interaction between PVDF and the mixtures of DMP and TEP. The value of each solubility parameter for the diluent mixtures was calculated as follows (Ji *et al.* 2007, Ji *et al.* 2008):

$$\delta_i = \delta_{i1}\varphi_1 + \delta_{i2}\varphi_2 \tag{5.4}$$

where φ is the volume fraction of the diluent, *1* and *2* refer to DMP and TEP, respectively; *i* represents *d*, *p* and *h*. By solving Eq. (7) and (8), ΔG^E can be determined accordingly. The value of ΔG^E decreased with increasing the weight fraction of TEP in the diluent mixture, which indicates that the increase of TEP in diluent mixtures enhanced the interaction between polymer and diluent mixture.

Table 5.4. Solubility parameters of diluent mixtures containing 30 wt% PVDF

Diluent mixture (TEP/DMP, wt%/wt%)	δ_d	δ_p	δ_h	ΔG^E
		$(MPa)^{1/2}$		$(J\ m^{-3})$
0/70	18.6	10.8	4.9	23.3
5/65	18.5	10.9	5.2	20.3
10/60	18.3	10.9	5.5	17.5
15/55	18.2	11.0	5.8	14.8
20/50	18.1	11.0	6.1	12.5

In order to determine suitable membrane synthesis conditions, the phase diagrams of the PVDF/DMP/TEP ternary system were determined, as shown in **Figure 5.2**. The illustration of a ternary system in TIPS process is usually difficult and error-prone due to its complexity which involves four dimensions, i.e., three concentrations (1 polymer, 2 diluents) and temperature (Ji *et al.* 2007). In this study, we projected these four dimensions onto two two-dimensional figures to help describe the interrelations among them clearly. Firstly, to discuss the effect of mixed diluents on the system, the

depiction was based on variations of TEP ratios where the PVDF concentrations were fixed at 30 wt%, as shown in **Figure 5.2(a)**. The crystallization temperature decreased significantly with increasing TEP content in the diluent mixture. It agrees with the finding that the affinity of the diluent mixture with PVDF can be enhanced by adding TEP as a second diluent as shown in **Table 5.5**. Therefore, the mixtures of DMP and TEP with different fractions of TEP could be prepared to enhance the interaction between PVDF and the mixed diluents. However, gelation took place when the concentration of TEP was higher than 40 wt%. It suggests that a relatively low weight fraction of TEP in the system is preferred to avoid the possible formation of a dense gel layer due to the gelation (Zhang *et al.* 2013, Zhang *et al.* 2014). Thus, we selected 5 and 10 wt% TEP in this study. When TEP fractions were fixed at 0, 5 and 10 wt%, we obtained the crystallization and cloud point curves by varying the weight fractions of PVDF as shown in **Figure 5.2(b-d)**. The monotectic points of the systems with 0, 5, 10 wt% TEP additions appeared to be about 29, 27, 26 wt%, respectively. In this study, we selected 30 wt% as the polymer concentration to ensure that there was adequate viscosity for continuous processing based on our previous study (Zhao *et al.* 2018). At the selected polymer concentration, the TIPS process is more likely to develop along the route of solid-liquid (S-L) phase separation instead of the liquid-liquid (L-L) phase separation (Lloyd *et al.* 1990, Zhao *et al.* 2018). In addition, it also shows that 200 °C is high enough to guarantee the homogeneity of dope solutions at all polymer concentrations.

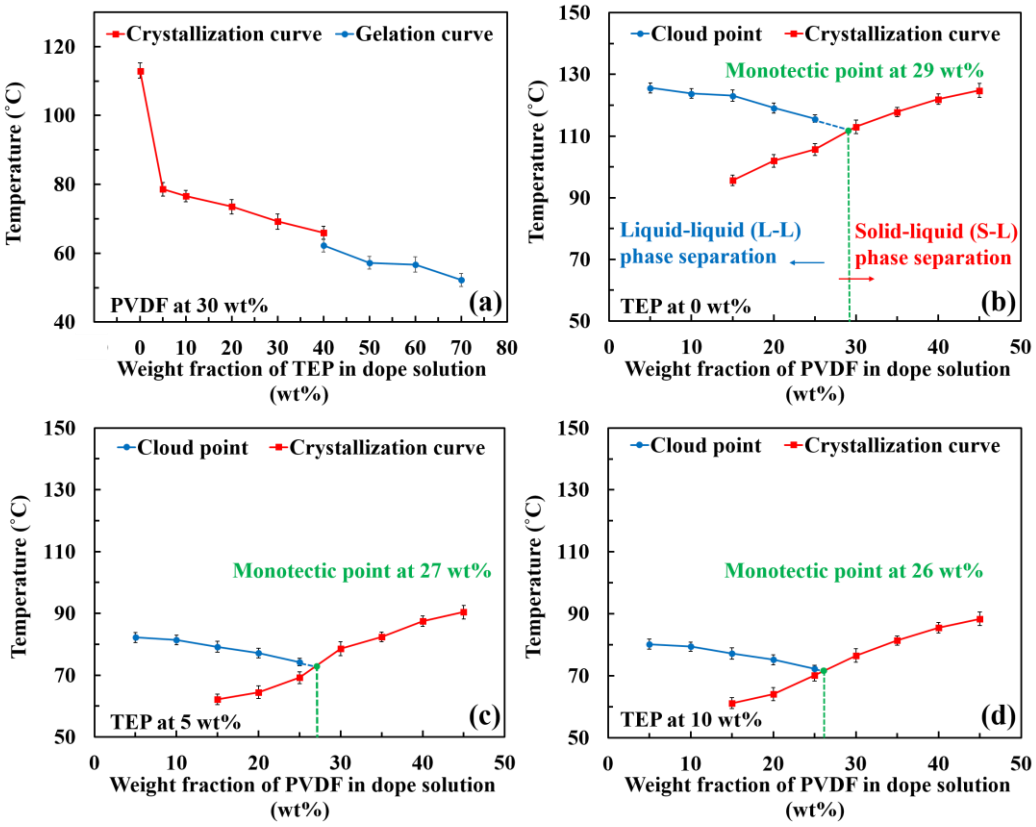

Figure 5.2. Phase diagrams for PVDF/DMP/TEP system based on different weight fractions of (a) TEP, where the PVDF concentration is fixed at 30 wt% and an increase in TEP weight fraction was compensated by a decrease in DMP weight fraction; (b-d) PVDF, where TEP concentrations are fixed at 0, 5, 10 wt%, respectively

5.3.2. Morphological properties of membranes and possible mechanism for the formation of membrane structure

In the study, the addition of the water-miscible TEP and F127 was expected to induce the NIPS process near the membrane surface along with the TIPS process throughout the bulk of membrane structure. **Figure 5.3** displays the SEM images of the cross-sections and the surfaces of prepared hollow fiber membranes. In the cross-sectional images as shown in **Figure 5.3(a)**, the general spherulite-like structures can be found in all membranes. However, the morphologies vary from one to another in terms of the shape, size and density of the spherulites and cavities among them. For the virgin membrane (T0), a non-typical spherulitic structure was obtained, which comprised loosely packed spherulites with large cavities in between. The boundaries of spherulites could hardly be spotted, while some regions appeared similar to the

bicontinuous structure. Meanwhile, a relatively dense layer was observed at the outer surface. A relatively smooth outer surface was formed in the virgin membrane (T0) by tightly connected spherical crystalline structure, suggesting a low outer surface porosity. With 5 wt% of TEP added (T5), stronger impingements can be found among the spherulites with larger sizes and more discernable peripheries. The spherulites became smaller and more compact when the fraction of TEP was augmented to 10 wt% (T10). The morphology turned into a rugged surface with protuberant spherulites and ravines in between. The protruding structure then grew thicker but smoother on the surface with clear canyons at the bottom with a further addition of TEP (T10). However, the borders of the spherulites gradually disappeared with the addition of F127 from 1 to 3 wt% (T5F1 to T5F3). The plausible bicontinuous structure dominated the bulk cross-sectional morphology of T5F3, leaving only a minor portion of spherulitic-like structure. From the cross-sectional view, the outer surfaces of membranes with F127 addition appeared to be more porous than those without F127. A porous sponge-like surface layer in a shape of valley can be seen in T5F3. In regard to the inner surface as presented in **Figure 5.3(c)**, without TEP addition (T0), the membranes exhibited moderate pore sizes among others. The membranes with TEP added (T5 and T10) exhibited slightly fewer pores on the inner surface than the virgin one (T0). However, it can be seen that a more porous structure was obtained with the addition of F127 (T5F1 to T5F3).

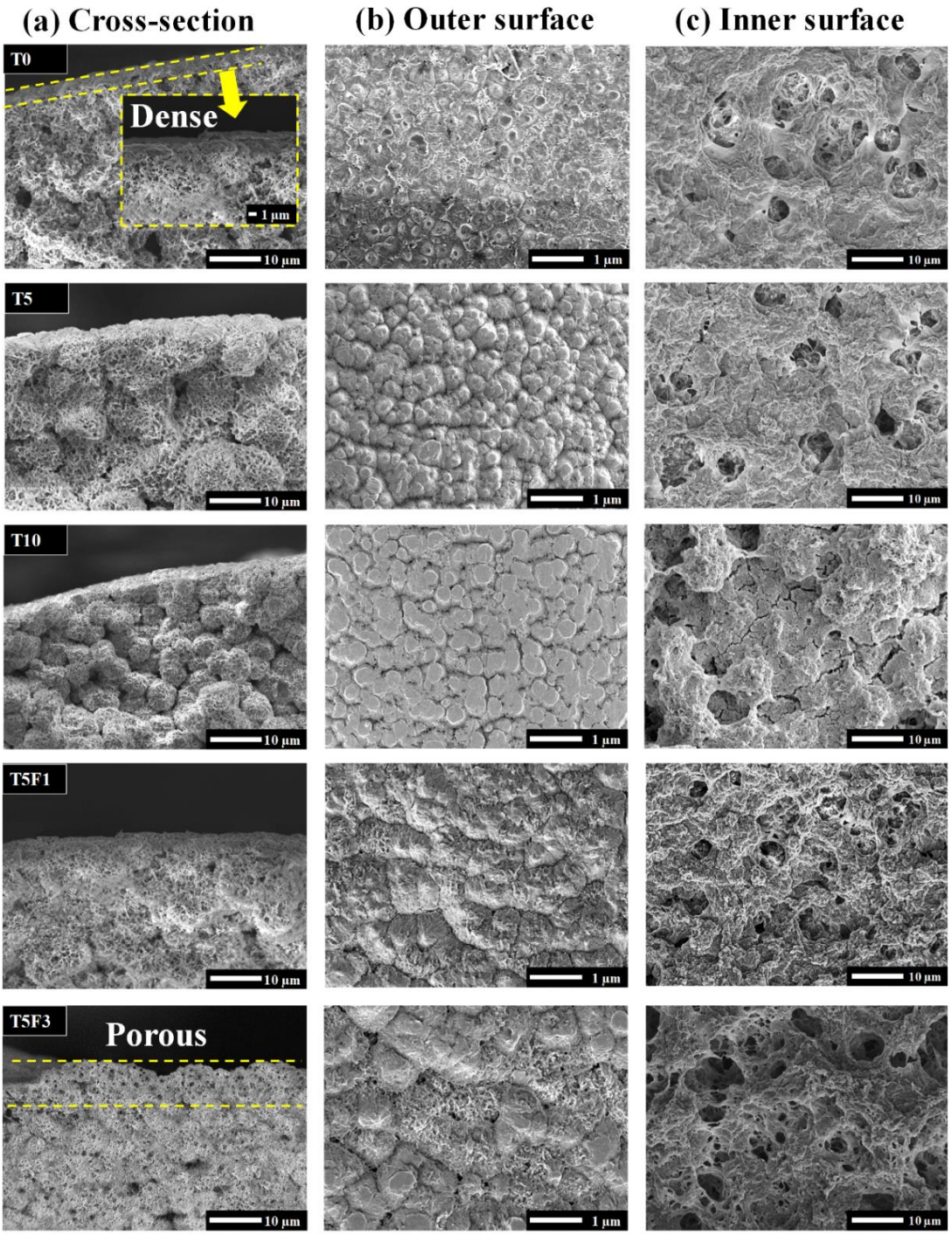

Figure 5.3. SEM images of hollow fiber membranes obtained with different mixed diluents and Pluronic F127 fractions: (a) cross-section near outer surface; (b) outer surface; (c) inner surface

In order to provide clear explanations for the membrane morphology obtained, we proposed a conceptual schematic drawing to visualize our understanding of the membrane formation mechanism, as shown in **Figure 5.4**. When DMP was used as a single diluent, the presence of spherulitic structures indicates that the S-L phase separation in the TIPS process (C1 in **Figure 5.4**) was dominant in the formation of the bulk structure of membranes. The indistinct boundaries of spherulites suggest a weak impingement of spherulites during the coarsening and perfection of crystallization (Ji *et al.* 2007). Apart from the S-L phase separation, the L-L phase separation (C2) might also have taken place in certain areas where the local PVDF concentration was below the monotectic point (29 wt%, close to 30 wt% as used) as bicontinuous-like structure was found in some regions. Besides that, a dense layer was also observed near the membrane outer surface when only DMP was used as the diluent. This could be ascribed to the low affinity between DMP and the nonsolvent (water), resulting nearly no inflow of nonsolvent. In this scenario, the composition near the outer surface might shift to the polymer-rich region possibly due to the outflow of diluents during the solidification of polymer matrix. Consequently, a relatively dense layer with small pores was formed owing to the high polymer concentration generated by the outflow of diluent (O1).

When mixed diluents containing TEP as a bridging agent (diluent in TIPS, solvent in NIPS) were used, the formation of spherulites in smaller sizes and a higher density could be attributed to the enhanced polymer-diluent interaction as discussed in **Section 5.3.1**. An enhanced interaction could postpone the phase separation and subsequent crystallization, allowing less time for spherulite growth (Lloyd *et al.* 1990). In addition, the mutual affinity between the diluent mixture and nonsolvent (water) was also enhanced with the presence of TEP. This allowed the N-TIPS process to happen, and an increase inflow of nonsolvent produced was likely to rebalance the ratio of outflow to inflow. Though the NIPS process might be limited with the small amount of TEP, it still helped open up the pore structure near the membrane surface. The effect of NIPS became more significant with the addition of F127 in the polymer dope solution especially at concentration 3 wt% where a porous sponge-like surface layer can be seen clearly from the SEM image. At a moderate coagulation temperature, solvent-nonsolvent (TEP/water) exchange may happen at a

relatively low rate (O2). The formation of sponge-like structure provides strong evidence for the occurrence of NIPS processes at the outer surface but can also be ascribed to the pore-forming effect of the amphiphilic F127 as it could participate in the pore formation upon contact with the water inflow (Loh and Wang 2014). This study did not reveal the case when a high rate of solvent-nonsolvent exchange was achieved. It is possible that the typical macroviod structure could be obtained if sufficient amount of TEP was added into the external coagulation tank to increase the exchange rate at the outer surface of membranes (Zhang *et al.* 2013, Zhang *et al.* 2014). Matsuyama and co-workers have demonstrated that the macrovoid structure can be observed from a PMMA/cyclohexanol system, which is likely to involve the exchange between cyclohexanol and water (nonsolvent) (Matsuyama *et al.* 2002). Similar morphology with finger-like macrovoid structure has also been reported by Jung and co-workers using water-soluble PolarClean as the diluent for PVDF (Jung *et al.* 2016) (O3).

Different from the situation on the shell side, the bore fluid used on the lumen side was DMP. The contact between the polymer solution and the bore fluid took place in the stainless spinneret, which was kept at 200 °C. Thus, the temperature gradient on the lumen side was lower than that on the shell side, contributing to a dampened heat transfer rate. Without TEP addition (T0), the polymer concentration near the interface was hardly changed, leading to moderate pore sizes as compared with others (I1). As the out diffusion of TEP occurred at the interface, the polymer concentration was increased and thus the structure became less porous (I2). When F127 was added from 0 to 3 wt%, the inner pore structure was probably opened up by the aggregated instable F127 particles which might diffused out along with the diluent outflow(Vasilescu and Bandula 2011). Above all, the pore formation at the inner surface could be mainly influenced by the diluent diffusion driven by the concentration gradient of TEP during the TIPS process.

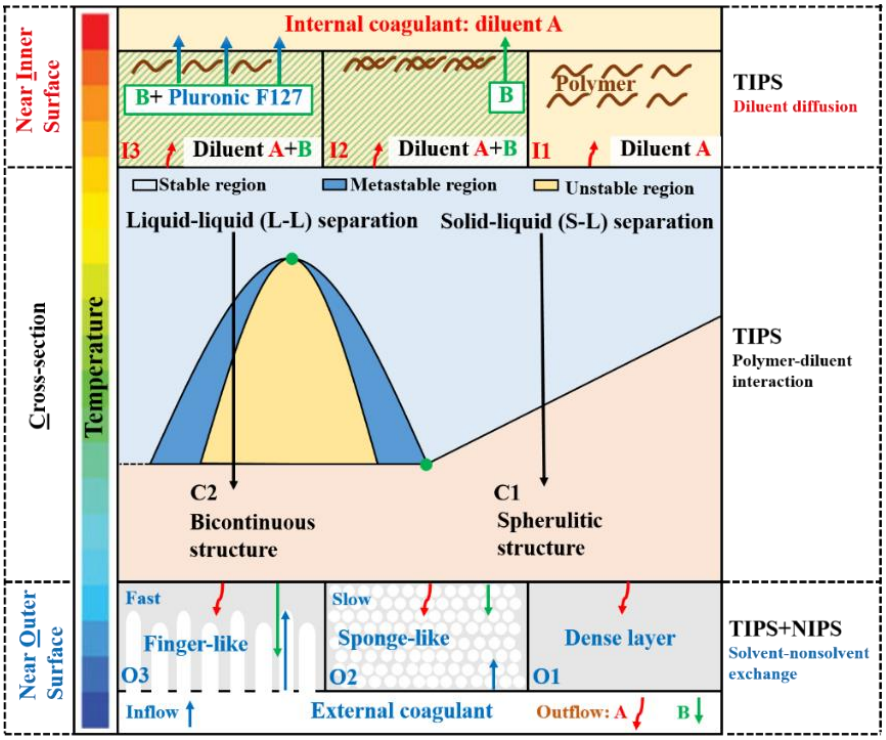

Figure 5.4. Proposed conceptual illustration of N-TIPS process

5.3.3. Characteristics of hollow fiber membranes

Figure 5.5(a) depicts the pore size and pore size distribution curves of the produced PVDF membranes. The results of porosity are presented in **Figure 5.5(b)**. It can be seen that both mean and maximum pore sizes of membranes increased with the addition of TEP (T5 and T10) and F127 (T5F1 and T5F3) as compared to the virgin membrane (T0). Meanwhile, the curves of pore size distribution were maintained similar shapes with the increase in the pore size and porosity as shown in **Figure 5.5(a)** and **(b)**. From the SEM images shown in **Figure 5.3**, we can find that the pores on the inner surface are far larger than those on the outer surface. Thus, the mass transfer resistance is expected to be mostly determined by the pores in the bulk structure or on the outer surface. The formation of these pores can be mainly explained by two major factors. Firstly, with the addition of TEP, smaller spherulites in a higher density were formed due to enhanced polymer-diluent interaction during the TIPS process, which can reduce the pore size. Similar reductions in the pore size due to a higher density of spherulites were reported in our previous study (Zhao *et al.* 2018). Secondly, the pores were opened up in a large amount as a result of solvent-

nonsolvent (TEP/water) exchange, which can be supported by the increase in the pore size and porosity as shown in **Figure 5.5(b)**. It should be pointed out that the pore size and porosity of T10 appeared to be smaller than that of T5. This could be ascribed to the stronger impact of the increase in the polymer-diluent interaction over the solvent-nonsolvent (TEP/water) exchange, which probably fixed the pore structure before the NIPS process came into effect. The effect of these two factors was likely to be rebalanced with the addition of F127. Dual functions might be provided by F127 in this process, i.e., (a) hindering the polymer-diluent interaction; (b) participating in the pore formation due to its affinity with the external coagulant (water) at the outer surface or aggregation-led mobility at the inner surface (Xiong *et al.* 2003). Therefore, the pore size and porosity could be tuned by inducing N-TIPS effect using the combination of mixed diluents and F127. The overall porosity of membranes was improved from 50 ± 2 to 69 ± 3 % without widening the pore size distribution. From **Figure 5.5(b)** and **Figure 5.6**, it can be found that the PWP results are strongly correlated with the pore size and porosity of tested membranes. The water permeability of membranes was increased from 389 ± 30.3 (T0) to 1060 ± 29 (T5F3) L m^{-2} h^{-1} bar^{-1}. When TEP and F127 was added to induce the N-TIPS effect, the enlarged pore size and porosity significantly contributed to the enhancement in PWP.

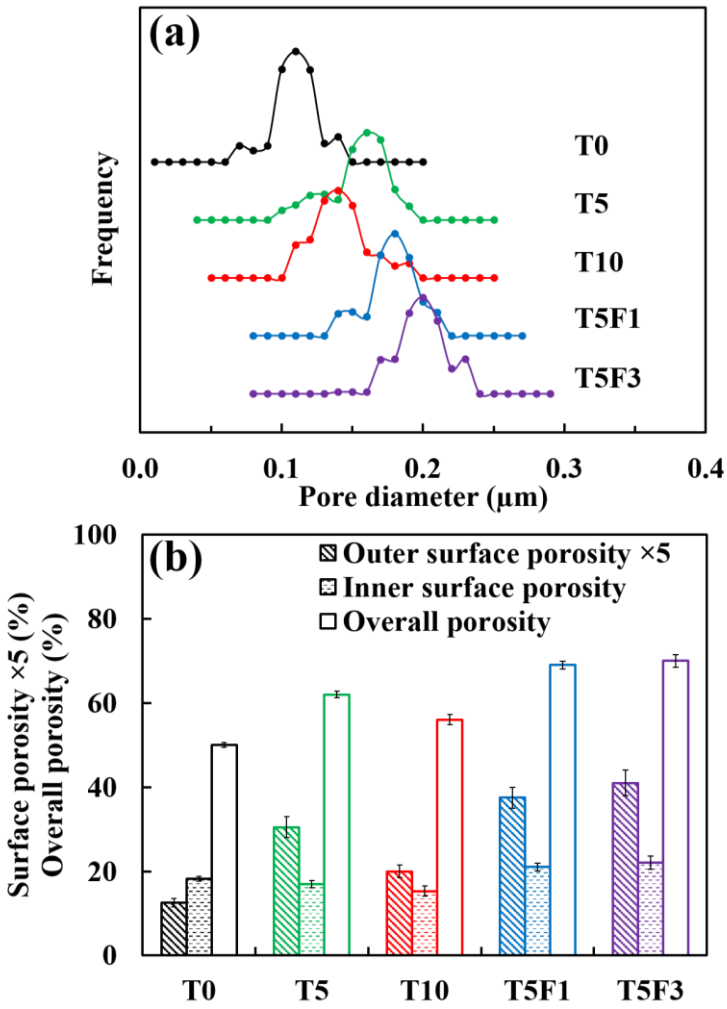

Figure 5.5. Pore size distribution (a), and porosity (b) of membranes obtained with different mixed diluents and Pluronic F127 fractions

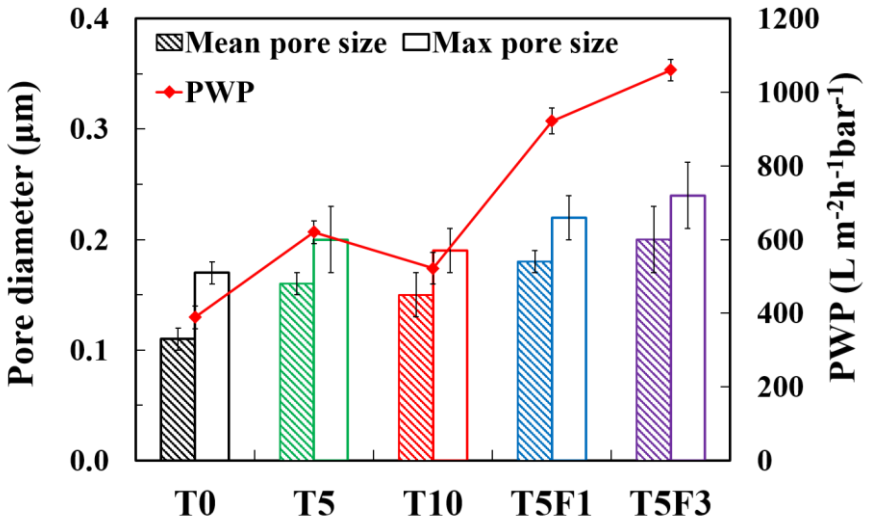

Figure 5.6. Pure water permeability and corresponding pore size of membranes obtained with different mixed diluents and Pluronic F127 fractions

The surface hydrophobicity can normally be indicated by the water contact angle and the surface roughness of membranes as presented in **Table 5.5** and **Figure 5.7**. In general (except for T5F1), the contact angle of membranes increased when mixed diluents were used, which indicates the formation of hydrophobic outer surfaces. This is probably due to the hydrophobic nature of PVDF and the increased surface roughness. As suggested by SEM images in **Figure 5.3**, the embossment of spherulitic structure on the outer surface became more evident with protruding spherulites when mixed diluents were used. With further addition of F127, the exposed spherulites were similar to the lotus structure, which could enhance the surface roughness and consequently enhance the hydrophobicity (Shi *et al.* 2012). However, the contact angle of T5F1 dropped to 89 ± 3 °, and then increased to 105 ± 6 ° at 3 wt% F127 fraction (T5F3). As an amphiphilic block copolymer, F127 comprises of hydrophilic polyethylene oxide (PEO) and hydrophobic polypropylene oxide (PPO) units. During the N-TIPS process, the hydrophobic PPO units can adsorb onto the PVDF matrix, anchoring itself in the membranes. The hydrophilic PEO units can thus protruding exteriorly, equipping the membrane surface with better hydrophilicity (Zhao *et al.* 2008). Therefore, the decrease in contact angle with 1 wt% of F127 addition can be ascribed to the exposed hydrophilic units on the outer surface. For membranes with a higher concentration of F127, the stability was found to be subjected to the possible aggregation behavior (Loh and Wang 2012, Loh and Wang 2013, Loh and Wang 2014). This could be responsible for the increase in contact angle of T5F3 as the surface roughness might dominantly affect the hydrophobicity if the F127 was washed out. The presence of F127 will be further analyzed based on the FTIR results in the next section.

Table 5.5. Surface properties of membranes obtained with different mixed diluents and Pluronic F127 fractions

Code	R_a of inner surface (nm)	R_a of outer surface (nm)	Dynamic contact angle (°)
T0	70.7 ± 1.1	49.4 ± 0.5	96 ± 6
T5	85.0 ± 1.2	68.5 ± 0.6	101 ± 4
T10	90.2 ± 1.5	53.2 ± 0.9	103 ± 5
T5F1	96.1 ± 1.3	62.5 ± 0.7	89 ± 3
T5F3	95.2 ± 1.5	75.0 ± 1.2	105 ± 6

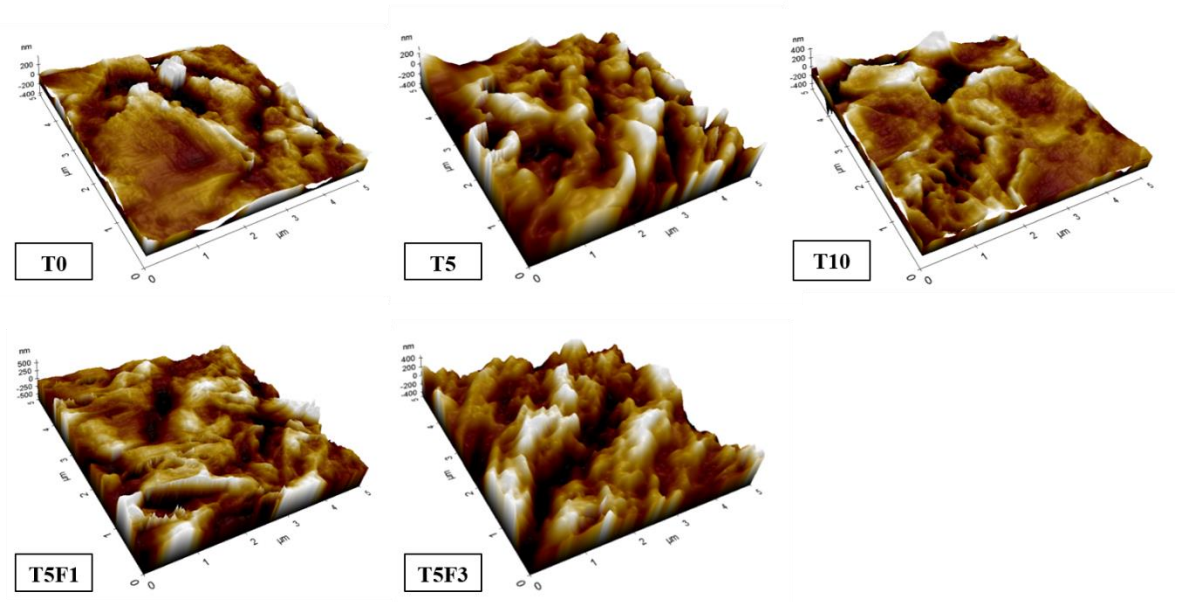

Figure 5.7. AFM images (3D) of the outer surface of membranes obtained with different mixed diluents and Pluronic F127 fractions

In previous sections, it was found that the TIPS effect mainly contributed to the formation of the bulk structure by controlling the phase inversion and the subsequent crystallization of PVDF. The intrinsic properties of the semi-crystalline PVDF are greatly dependent on its crystal structure, which can consequently affect the durability and other important properties of the membranes. Therefore, it is necessary to investigate the crystalline characteristics of prepared membranes to further understand the effects of mixed diluents and F127 on the TIPS process.

As shown in **Figure 5.8(a)**, the peak crystallization temperature of the dope mixtures decreased drastically after introducing TEP into the mixture (T0 to T5), and then continued to drop slightly with a further increase in the TEP fraction from 5 wt% to 10 wt% (T5 to T10). The result was also presented in the phase diagram in **Figure 5.2(a)**. However, the crystallization temperature bounced back when the F127 was added to the mixture (T5 to T5F1 and T5F3), which suggests that the PVDF-diluent interaction was probably weakened.

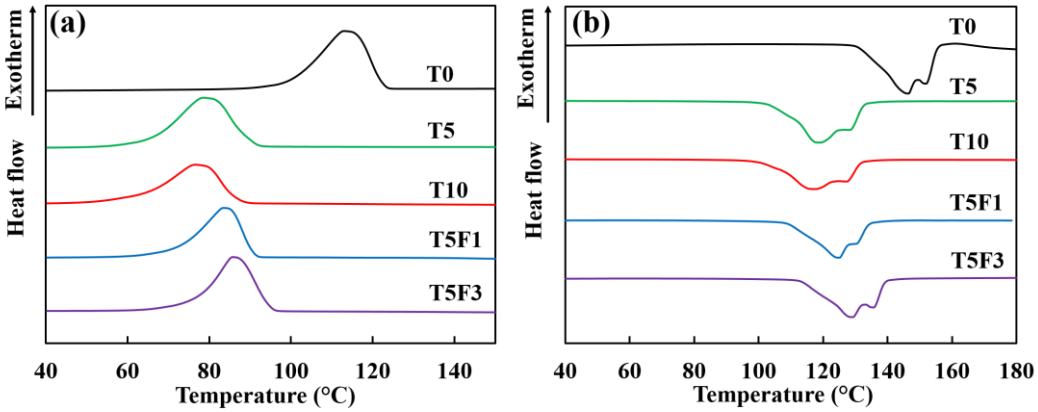

Figure 5.8. Crystallization and thermal behaviors of dope mixtures with different mixed diluents fractions: (a) crystallization curves; (b) melting curves

The melting curves of dope mixtures are shown in **Figure 5.8(b)**. All the curves exhibit the phenomenon of "double melting endotherms", which involves a low melting endotherm and a high melting endotherm (Ji *et al.* 2007). It can be seen that the high melting endotherm was dampened with the addition of TEP from 5 wt% to 10 wt% (T0 to T5 and T10). However, the peak of the low melting endotherm grew back into a similar shape when F127 was added into the dope mixtures (T5 to T5F1 and T5F3). The occurrence of "double melting endotherms" can normally be attributed to: (a) the presence of polymorphism (F. 1960), (b) a secondary crystallization during the heating process (Ji *et al.* 2007). As shown in **Figure 5.9(a)**, the peaks at $2\theta = 17.66\ °$, $18.30\ °$ and $19.90\ °$ in the WAXD patterns for both virgin and TEP-added membranes relate to the diffractions in planes (100), (020), and (110), respectively, which indicates the presence of α-phase crystals of PVDF (Cui *et al.*

2014). However, the β-phase crystals of PVDF were only found in the TEP-added membranes as confirmed by the peaks at 2θ = 20.26 °, 41.22 ° (in planes (200) and (201)) (Chun‐Hui *et al.* 2012, Cui *et al.* 2014). The addition of TEP was shown to be responsible for the formation of β-phase in the surface layer of PVDF membranes previously (Tao *et al.* 2013). It was possible that the mass transfer induced by TEP at the interface might have resulted in a high polymer concentration near the surface. That could facilitate the oriented packing of CH_2-CH_2 dipoles and the conformation of consequential trans-trans-trans (TTT) which are correlated to the formation of β-phase (Zhang *et al.* 2008). Possessing a good piezoelectricity, the β-phase is normally preferred in the fabrication of membranes for electrochemical purposes such as the polymer electrolyte in the lithium-ion batteries. The antifouling properties of PVDF membrane can also be enhanced by applying AC signals to generate the vibration (Cui *et al.* 2015). Owing to the absence of β-phase crystals in the virgin membrane, the prevalent appearance of "double melting endotherms" could not be fully explained by the existence of polymorphism. Previous studies have revealed the correlation of the spherulitic structure with the secondary crystallization in different polymer-diluent systems including PVDF with DBP and di(2-ethylhexyl) phthalate (DEHP) (Ji *et al.* 2008). It has also been reported that the secondary crystallization of PVDF could be induced by the entanglement of polymer chains and impingement of spherulites, as well as the perfection of the internal spherulite crystallization (Ji *et al.* 2007). The evidence points to the occurrence of a secondary crystallization of PVDF at a later stage of the crystallization process, which can be ascribed to the enhanced PVDF-diluent interaction along with the addition of TEP (from T0 to T5 and T10). With further addition of F127, the possible weakening of the PVDF-diluent interaction might result in the restoration of the high melting endotherm. In this study, the crystallinity of membranes followed the same tendency with the variation of high melting endotherms as shown in **Table 5.6**. This indicates that the variation of the amorphous portion in PVDF can be controlled by the addition of TEP and F127, which are considered as the N-TIPS inducers in this study. Besides, it can also be noticed that the peak melting temperatures shadowed the similar down-up trend in **Figure 5.8(b)**. The peak melting temperature has been suggested to be related with the degree of the long-range order in the crystalline structure, which normally has a

positive correlation with the crystal size (Raimo 2011, Ehrenstein 2012, Zhao *et al.* 2018). The results of crystal sizes summarized in **Table 5.6** conform well to the previous findings and the morphology variations discussed in **Section 5.3.2**.

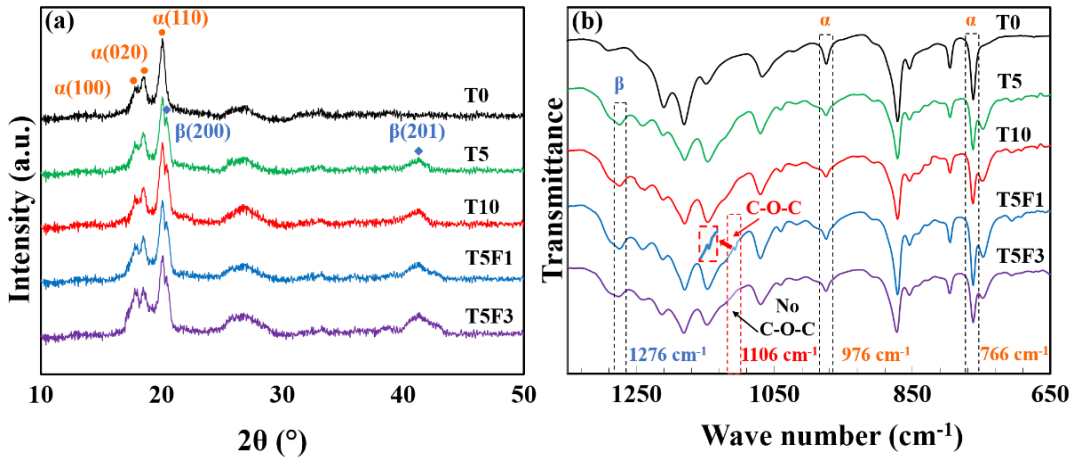

Figure 5.9. X-ray diffraction patterns (a) and ATR-FTIR spectra (b) of membranes obtained with different mixed diluents and Pluronic F127 fractions

Table 5.6. Crystalline properties of membranes obtained with different TEP and Pluronic F127 fractions

Code	ΔH_m (J g^{-1})	χ_c (%)	D (nm)
T0	51.6 ± 2.1	49.4 ± 2.0	6.33 ± 0.24
T5	50.1 ± 3.3	47.9 ± 3.2	6.01 ± 0.19
T10	46.2 ± 1.9	44.2 ± 2.3	5.71 ± 0.16
T5F1	49.0 ± 2.0	46.9 ± 1.9	6.09 ± 0.12
T5F3	48.5 ± 1.1	46.4 ± 1.6	6.11 ± 0.20

ATR-FTIR analysis was conducted to further investigate the variation of crystalline phases and the presence of F127 in the membrane matrix. **Figure 5.9(b)** depicts the ATR-FTIR spectra for as-spun hollow fiber membranes with different mixed diluents and F127 weight fractions. The presence of peaks at 766 and 976 cm^{-1} confirms the existence of the α-phase for all membranes, while the β-phase was found in the matrix of all TEP-added membranes (T5, T10, T5F1 and T5F3) except for the virgin ones

(T0) as suggested by the peaks at 1276 cm^{-1} (Cui *et al.* 2014). This result accords with the findings from WAXD analysis, which implies that the addition of TEP could have a strong effect on the crystallization of PVDF during the membrane formation process.

With regard to F127, it is necessary to validate its presence in the resultant PVDF matrix since F127 is soluble in both the nonsolvent (water) and solvents for the post-treatment (n-hexane and ethanol). It can be seen that the peak at 1106 cm^{-1} only presents in the spectrum of the membranes with 1 wt% addition of F127 (T5F1). The absorbance peak around 1105 to 1115 cm^{-1} normally represents the characteristic band for the C-O-C stretching related to the ether group, which indicates the presence of F127 in the PVDF matrix. It has been found that an anchorage can be provided by the PPO block in F127 molecules, which is likely to help immobilize F127 particles in the PVDF against the elution (Wang *et al.* 2005). However, the absence of the C-O-C peak in the spectrum of membranes with 3 wt% of F127 (T5F3) suggests that a major amount of F127 particles was eluted by either the nonsolvent solvents when the dosing concentration was high. The instability of F127 in the PVDF matrix has also been reported by Loh and co-workers (Loh *et al.* 2011, Loh and Wang 2012, Loh and Wang 2014). This phenomenon could be ascribed to the aggregation behaviors of F127 at a high concentration, which possibly turn the F127 particles into spheres in larger sizes and diminish the surface contact of F127 with PVDF (Vasilescu and Bandula 2011). As a result, it became easier for the nonsolvent or solvents to wash out the F127 particles. This is in accord with the variations of contact angle as discussed previously. The instability of F127 was more severe when the addition was as high as 3 wt% due to possible agglomeration and poor anchorage in the PVDF matrix (Dmitrenko *et al.* 2019).

The effect of mixed diluents and F127 addition on the tensile strength and elongation at break is presented in **Figure 5.10**. The sequence of tensile strength is T10 ≈ T5 > T5F1 > T5F3 > T0, while the ranking of elongation is listed as follows: T10 > T5F3 > T5F1 > T5 > T0. In the structure of a semi-crystalline polymer-based membrane, the lamellae crystallites with orderly polymer alignment are embedded between

amorphous regions. When spherulites exist in the PVDF-based membranes, the toughness is primarily provided by the intermolecular interactions within the crystallites, while the elasticity is reliant more on the amorphous regions between the lamellae (Ehrenstein 2012). The former was found to be affected by the polymer-diluent interaction in this study, while the latter can be suggested from the crystallinity as shown in **Table 5.6**. Summarizing the previous results, the strength of polymer-diluent interaction might follow the sequence: T10 > T5 > T5F1 > T5F3 > T0. The ranking of crystallinity is placed as follows: T10 < T5F3 < T5F1 < T5 < T0. By and large, the data conform with this trend with a few exceptions. T10 exhibited lower toughness but higher ductility as compared to T5. This could be attributed to the decreased size of spherulites, which was likely to contain crystalline structure with shorter PVDF chains. Above all, the inducing of N-TIPS effect by addition of TEP and F127 did not weaken the mechanical properties. Instead, the membranes were slightly reinforced as a result of the enhancement in polymer-diluent interaction, showing a tensile strength which ranges from 5.6 ± 0.1 to 6.5 ± 0.2 MPa.

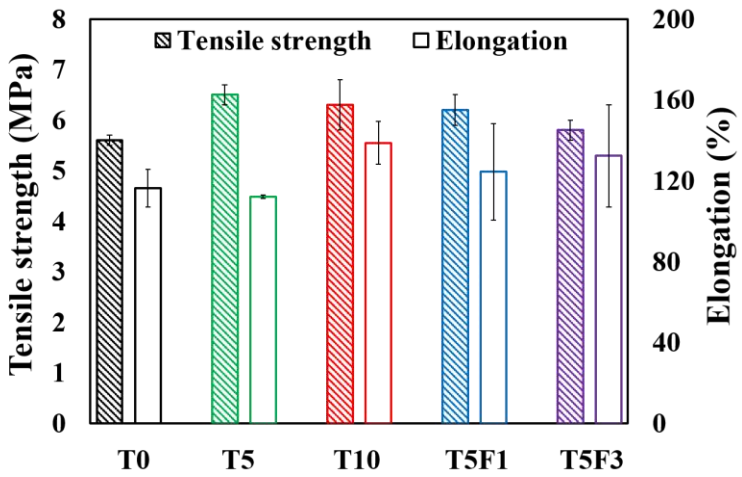

Figure 5.10. Mechanical properties of PVDF hollow fiber membranes obtained with different mixed diluents and Pluronic F127 fractions

5.3.4. Potential applications of prepared hollow fiber membranes

This work has demonstrated that the use of mixed diluents could help induce the occurrence of N-TIPS process, and consequently affect the membrane properties in

three major aspects: membrane pore structure, surface roughness and hydrophobicity, as well as polymorphism of PVDF crystals. To further understand the distinct effect of N-TIPS on membrane properties, various PVDF hollow fiber membranes fabricated via NIPS and TIPS are listed together with the T5F1 and T5F3 membranes as shown in **Table 5.7**. It can be seen that membranes developed by the N-TIPS method possess improved porosity and water permeability than TIPS membranes without significantly enlarged pore sizes. It is worth noting that the drawback of dense gel layer formation induced by high-concentration TEP, which results in nearly no flux, can be circumvented by using the mixed diluent. Meanwhile, the N-TIPS membranes have much higher mechanical strength than those prepared via the NIPS method, reaching a level comparable to the TIPS membranes. In addition, the outer surface of prepared N-TIPS membranes are considered relatively hydrophobic due to the intrinsic hydrophobic nature of PVDF and increased roughness contributed by exposed lotus-like spherulitic structure. Such features indicate that the N-TIPS membranes can be used for applications of (1) membrane distillation (requiring hydrophobicity) with further constrained pore size (below 0.1 μm), or (2) microfiltration (requiring hydrophilicity) with further hydrophilic modified outer surface. Besides, the formation of piezoelectric β-phase crystal of PVDF in N-TIPS membranes suggests their potential roles as antifouling piezoelectric membranes or polymer electrolytes for lithium-ion batteries (Cui *et al.* 2015).

Table 5.7. Comparison of various PVDF hollow fiber membranes prepared via phase inversion method

Solvent (diluent)	Method	Tensile stress (MPa)	Mean pore size (μm)	Overall porosity (%)	PWP (L m^{-2} h^{-1} bar^{-1})	Ref.
DMAc	NIPS	2.5	-[b]	-[b]	116	(Moghareh Abed *et al.* 2013)
DMAc	NIPS	~1.2[a]	-[b]	~90[a]	~190[a]	(Zhang *et al.* 2013)
NMP	NIPS	3.3	-[b]	74	974	(Zhang *et al.* 2013)
DEP	TIPS	~4.0[a]	-[b]	-[b]	~500[a]	(Rajabzadeh *et al.* 2012)
DMP	TIPS	9.3[a]	0.12[a]	~65[a]	~71[a]	(Shi *et al.* 2012)
TEP	TIPS	6.3	~0.05	~41	0[c]	(Zhang *et al.* 2014)
ATBC	TIPS	2.2	0.18	61	740	(Cui *et al.* 2013)
DMP/TEP (T5F1)	N-TIPS	6.2	0.18	69	922	This work
DMP/TEP (T5F3)	N-TIPS	5.8	0.20	70	1060	This work

Notes:
[a)] The data were collected from figures in the literature by using the Digitizer function in *Origin* 9.1;
[b)] The data were not shown in the paper;
[c)] The membrane did show any flux probably due to the formation of dense skin layer (Zhang *et al.* 2014).

5.4. Conclusions

In this part of study, PVDF hollow fiber membranes have been developed via a modified N-TIPS method using the TEP as a second diluent and Pluronic F127 particles as additives. The advantages of this approach include simple fabrication steps, mild coagulation conditions, tailorable membrane structure and promising water permeability.

The following conclusions can be drawn from this study:

- The addition of TEP and F127 might together initiate the occurrence of the NIPS process on the outer surface before the solidification of membrane structure. Furthermore, the existence of TEP also helped establish a concentration difference on the two sides of inner interface, providing more control over the pore formation. On top of the TEP addition, F127 particles introduced at 1wt% were demonstrated to play an important role in the pore formation process.
- The prepared membranes possess a narrow pore size distribution with enhanced surface and overall porosity. The pure water permeability was correspondingly improved from 389 to above 900 L m^{-2} h^{-1} bar^{-1} with a mean pore size of 0.18 μm. The tensile strength of membranes was well-maintained, ranging from 5.6 ± 0.1 to 6.5 ± 0.2 MPa.
- Furthermore, the addition of TEP as N-TIPS inducer was found to be correlated to the formation of piezoelectric β-phase crystals of PVDF.

This study provides a new perspective of the interrelations between TIPS and NIPS process with an effort in harvesting their features altogether. This approach exhibited promising versatility in tailoring the surface pore structure of PVDF hollow fiber membranes without formation of mechanically weak macrovoids. Upon specific modification, the preparing PVDF hollow fiber membranes have potential for a wide range of applications, which includes but are not limited to membrane distillation, microfiltration as well as electrochemical-related processes.

CHAPTER 6 Fabrication of Hydrophilic PVDF-based Hollow Fiber Membranes with Improved Antifouling Property through N-TIPS Method

6.1. Introduction

As demonstrated in **Chapter 5**, Pluronic F127 (abbreviated as F127 in the following paragraphs) exhibited outstanding pore-forming ability in enhancing the porosity of PVDF membranes (Cui *et al.* 2008, Loh and Wang 2012, Loh and Wang 2013, Loh and Wang 2014). As one of the commercially available amphiphilic block copolymers, F127 comprises of hydrophilic polyethylene oxide (PEO) and hydrophobic polypropylene oxide (PPO) units, which can be approximately represented by the molecular formula of PEO_{106}–PPO_{70}–PEO_{106} (Vadnere *et al.* 1984, Kabanov *et al.* 2002, Escobar-Chávez *et al.* 2006, Bercea *et al.* 2011, Pitto-Barry and Barry 2014). The main feature of F127 different from other pore-formers is its potential in acting as an antifouling surface modifier for hydrophobic membranes such as polyethersulfone (PES) and PVDF (Wang *et al.* 2005, Zhao *et al.* 2008, Chen *et al.* 2009, Loh *et al.* 2011, Li *et al.* 2014). However, our previous studies have shown that the presence of F127 in PVDF-based membranes applied in water treatment were unstable probably due to relatively weak anchorage of F127 in the PVDF matrix and its strong solubility in aqueous solutions (Loh and Wang 2012, Loh and Wang 2013, Loh and Wang 2014). Loh *et al*. suggested that the F127 particles were largely eluted by water or 2-propanol and they could only act as pore-formers but not surface modifiers under the experimental conditions used in their study (Loh and Wang 2013, Loh and Wang 2014). Compared with PVDF, PTFE is a fluoropolymer with even higher hydrophobicity in nature (Schneider *et al.* 2001, Ma *et al.* 2013, Cui *et al.* 2014). It was found that the amphiphilic F127 could surround the PTFE particle with its hydrophobic PPO segments adsorbed firmly onto PTFE (Mirko *et al.* 2000). The exteriorly protruding hydrophilic PEO segments could enhance the wetting of PTFE through in the aqueous solutions (Shah *et al.* 2015, Shah *et al.* 2018). This feature was believed to indicate good interactions between F127 and PTFE in the aqueous environment (Sharma *et al.* 2014, Shah *et al.* 2015, Shah *et al.* 2018). Besides, we have demonstrated that PTFE could act as a nucleating agent

to enhance the nucleation process of PVDF and subsequently produce membranes with smaller pore sizes but higher overall porosity in our previous work (Zhao *et al.* 2018). These results mentioned above provide the possibility of using PTFE as a mediating agent to connect F127 with PVDF owing to its good affinity to both F127 and PVDF.

In this part of work, we report a novel approach for development of PVDF hollow fiber membranes with tunable pore structure and improved antifouling properties by using PTFE and F127 as additives through N-TIPS method. The strategy is to utilize PTFE as a binding agent to immobilize F127 in the PVDF matrix during the membrane preparation and subsequent post-treatment processes, which take place in both the nonaqueous and aqueous environment. In this way, we are able to combine the nucleating effect of PTFE with the pore-forming and hydrophilization ability of F127 via the N-TIPS method. Therefore, the addition of F127 particles are anticipated to dual functions: (1) pore former and (2) hydrophilic modifier for PVDF membranes. The individual and combined effects of PTFE and F127 on the PVDF membrane formation were investigated. The presence and stability of F127 were examined by comparing the characteristics of membranes with different combination of additives. Furthermore, comparative filtration tests using bovine serum albumin (BSA) were conducted to evaluate the organic antifouling property of the prepared membranes. To the best of our knowledge, there is no report on the immobilization of F127 in the polymer matrix by using PTFE in the preparation of PVDF membranes. This study aims to explore the potential of the N-TIPS process to provide a simple method with promising scalability for tailoring the pore structure and surface hydrophilicity of PVDF membranes.

6.2. Methodology and experiments

6.2.1. Materials

Polyvinylidene fluoride (PVDF Solef® 1015, M_w = 570,000–600,000, Solvay, Belgium) was used to develop porous hollow fiber membranes. Dimethyl phthalate (DMP, Merck KGaA, Germany) was used as the main diluent and bore fluid. Triethyl phosphate (TEP, Merck KGaA, Germany) was used as a second diluent.

Polytetrafluoroethylene (PTFE microparticles, Microdispers-200, M_w ~ 80,000, Size ~ 200–300 nm, Polysciences) and Pluronic® F127 (abbreviated as F127 in the following paragraphs, M_w = 12,600, PEO_{100}–PPO_{65}–PEO_{100}, Sigma Aldrich, Singapore) was used as an additive in the hollow fiber fabrication. Ethanol (Merck KGaA, Germany) and n-hexane (Merck KGaA, Germany) were used to conduct the post-treatment for the produced hollow fiber membranes. Bovine serum albumin (BSA, M_w = 67,000, Sigma-Aldrich) was used as a model protein foulant. Immediately upon receiving, the powder-form BSA was stored in a cold room at 4–5 °C. All the reagents were used as received (Kabanov *et al.* 2002, She *et al.* 2009, Loh and Wang 2013, Li *et al.* 2014, Loh and Wang 2014, Pitto-Barry and Barry 2014).

6.2.2. Surface tensiometry and liquid penetration test

To find out whether pluronic forms micelles in NMP, an attempt was made to determine the critical micelle concentration from the surface tension–concentration curve as described by Lin et al. (Lin *et al.* 1999). The surface tension of pluronic/DMP/TEP solutions with different pluronic concentrations was measured by the Wilhelmy plate method using a tensiometer (DCAT11, Dataphysics) at 24.0 ± 0.5 °C. Surface tension measurement was carried out and repeated at an interval of 10 min until the readings within an hour were stable. This was to ensure that the equilibrium value was obtained. An average of the last 5 readings was used in the plotting of surface tension–log(concentration) curve. The critical micelle concentration of pluronic in the diluent mixture can be obtained from the graph if there is an abrupt change in gradient (Lin *et al.* 1999, Desai *et al.* 2001, Bercea *et al.* 2011, Vasilescu and Bandula 2011).

The wetting of PTFE powder using surfactant solutions was achieved by a liquid penetration method with tensiometer (DCAT11, Dataphysics). The PTFE powder was used to fill a metal cylinder hanging on a sensor that measures the change in weight with time. The end of the cylinder was allowed to dip into the solution with different additives for 5 min at a constant depth of 3 mm, and the resultant weight gain due to the adsorption of water was noted. The measurements were repeated three

times in order to ensure reproducibility (Sharma *et al.* 2014, Shah *et al.* 2015, Shah *et al.* 2018).

6.2.3. Phase diagram determination

The phase diagram was determined by a method as described in **Section 3.2.2**.

6.2.4. Preparation of hollow fiber membranes

The hollow fiber membranes were fabricated using a TIPS machine as shown in **Figure 3.1**. The detailed procedures of fabrication process have been described in **Section 3.2.3**. The corresponding compositions of dope mixtures are summarized in **Table 6.1**. The spinning parameters are listed in **Table 6.2**.

Table 6.1. Dope compositions and characteristics of membranes

Code[a]	Dope compositions				
	PVDF (wt%)	DMP (wt%)	TEP (wt%)	PTFE (wt%)	Pluronic F127 (wt%)
TP0F0	30	65	5	0	0
TP1F0		64		1	0
TP0F1		64		0	1
TP1F1		63		1	1

Note:
[a)] Bore fluid composition (wt%): DMP (100).

Table 6.2. Spinning parameters for hollow fiber membranes

Extrusion rate (g min^{-1})	5.3
Extrusion temperature (°C)	200
Bore fluid flow rate (mL min^{-1})	2.0
Coagulation temperature (°C)	30
Air gap (cm)	1
OD/ID of spinneret (mm)	1.84/0.92

6.2.5. Characterization of hollow fiber membranes

The characterizations have been illustrated in **Section 3.2.5**, **4.2.4** and **5.2.4**.

6.2.6. Filtration test of hollow fiber membranes

The PWP was measured by a method illustrated in **Section 3.2.5**.

The compacted hollow fiber membranes were subsequently used for filtration test using a 1 g L^{-1} BSA aqueous solution in phosphate buffer solution (PBS, pH = 7.0) (Xu *et al.* 2014). The permeation device mentioned above was used again and the one cycle of filtration lasted for 120 min. After the permeation experiments with BSA aqueous solution, the fouled membranes were immediately washed for 30 min with a 500 ppm NaClO aqueous solution at 25 °C (Xu *et al.* 2014). After washing, the membrane module was rinsed with DI water, and then the PWPs were tested again. Each membrane was conducted by fouling thrice and washing twice. In order to evaluate the fouling-resistant ability of membranes, flux recovery ratio (FRR) was calculated using the following expression (Zhao *et al.* 2008):

$$FRR = (\frac{J_{wn}}{J_{w0}}) \times 100\% \quad (6.1)$$

where J_{w0} is the PWP; J_{wn} is the pure water flux after cleaning at each cycle, n is the number of cycle.

To analyze the fouling process in details, we defined the total flux reduction ratio (R_t) in the following equation (Li *et al.* 2014):

$$R_t = (1 - \frac{J_{pn}}{J_{w0}}) \times 100\% \quad (6.2)$$

where J_{pn} is the permeate flux at each cycle.

6.3. Results and discussion

6.3.1. Interaction between PTFE and Pluronic F127 in nonaqueous solutions

The interaction between PTFE and F127 was firstly investigated by examining the wetting ability of F127 on PTFE as a surfactant. In this study, both PTFE and F127

were used in nonaqueous mixed diluents comprising of two polar solvents (DMP and TEP) during the membrane preparation (Reichardt and Welton 2011). As amphiphilic block copolymers, Pluronics are commonly known for their micellization behaviors in water and some polar organic solvents in an effort to minimize the free energy in polymer solutions (Liu *et al.* 2000). Therefore, we conducted the surface tensiometry measurement for F127 to find out whether micellization occurs or not in the mixed diluents prior to the wetting test. The plot in **Figure 6.1** shows the correlation of the surface tension and F127 concentration in mixed diluents. It can been seen that there is no abrupt change in gradient within the range of 0.01 to 20 wt%. This indicates that the polar-solvent mixture did not possess a significantly stronger selectivity for one kind of block over the other one. Different from the amphiphilic behavior of F127 in aqueous environment, the solubility of PEO and PPO blocks in the mixed diluents turned out to be similar. As a result, the possibility of the micelle formation is considered substantially low in this study.

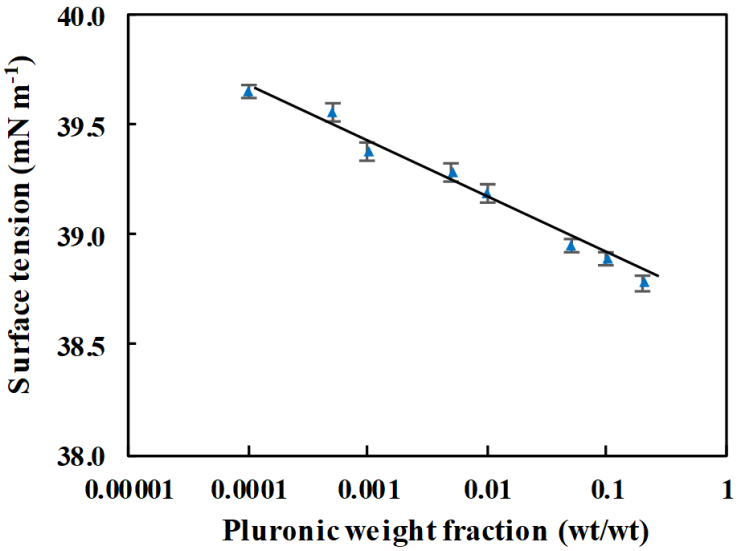

Figure 6.1. Surface tension versus log (concentration) curve of Pluronic F127 in mixed diluents

Subsequently, we performed the liquid penetration test using the mixtures of DMP and TEP with compositions proportional to those in the real preparation process (Sharma *et al.* 2014, Shah *et al.* 2015, Shah *et al.* 2018). Apart from F127, PEG with

comparable molecular weight to F127 was selected for comparison since it has a similar chemical structure to F127 except for the hydrophobic PPO block. The samples were designated as P1, TP1, TP1F1 and TP1G1 corresponding to solutions containing DMP/PTFE, DMP/TEP/PTFE, DMP/TEP/PTFE/F127 and DMP/TEP/PTFE/PEG, respectively. **Figure 6.2** and **Figure 6.3** present the liquid penetration results for PTFE powders in different nonaqueous solutions. It can be seen from **Figure 6.2** that the PTFE particles were suggested to be quickly wetted in the presence of 1 wt% F127, while they were hardly penetrated in other solutions. This is in agreement with images of dispersions in showing floating powders of PTFE in all nonaqueous solutions except the one with F127 as shown in **Figure 6.3**. Shah and co-workers have found out that the hydrophobic PPO units of F127 can possibly adsorb onto the hydrophobic surface of PTFE. This absorption is likely to pave the way for the formation of polar channels with hydrophilic PEO units extending into polar solvents, and consequently favor the penetration of solvents via a mechanism analogous to the capillary effect (Shah *et al.* 2015). This possible interaction between PTFE and hydrophobic PPO units in F127 could correspondingly provide anchorage for F127 when using PTFE and F127 jointly in the selected mixed diluents.

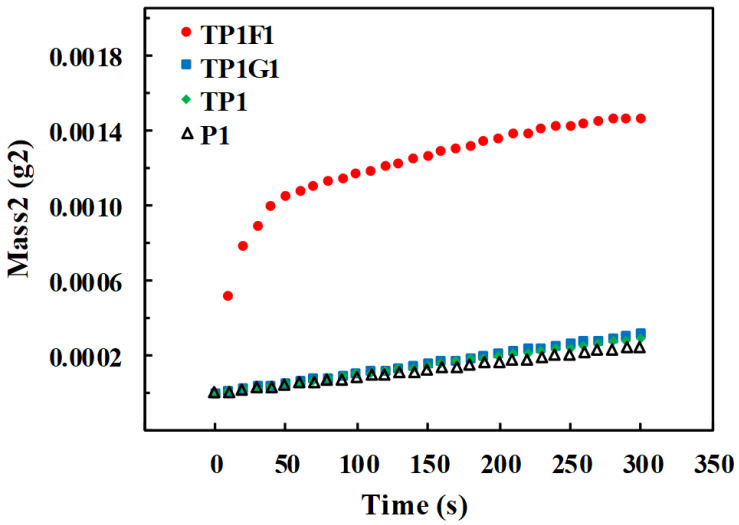

Figure 6.2. Liquid penetration profile for PTFE powder in different nonaqueous solutions

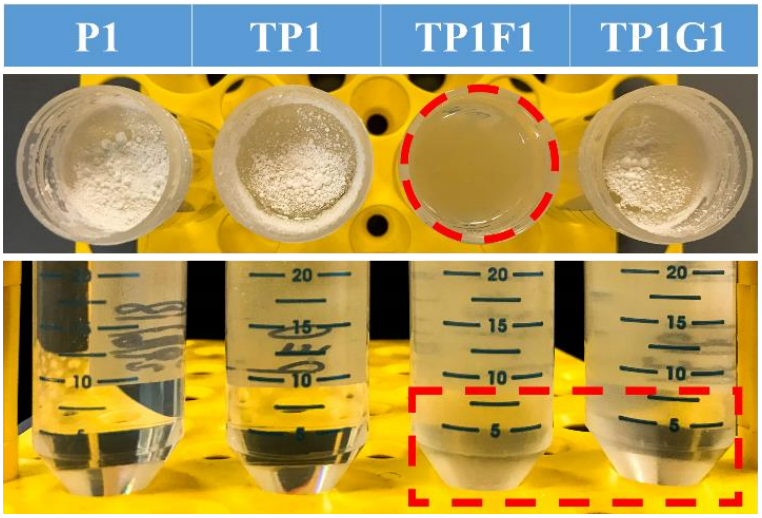

Figure 6.3. Wetting of PTFE powder in different nonaqueous solutions

6.3.2. Effect of PTFE and Pluronic F127 on the formation of membrane pore structure

Having demonstrated the possible interaction between PTFE and F127, we further investigated their individual and combined effect on the pore structure formation of PVDF hollow fiber membranes based on the thermodynamic studies of polymer solutions. In order to analyze the fundamentals from a thermodynamic perspective, we firstly obtained the phase diagrams for the PVDF/DMP/TEP ternary system with the addition of different additives as shown in **Figure 6.4**. When PTFE or F127 was individually introduced into the dope solution with 30 wt% of PVDF, the crystallization temperatures increased gradually while no cloud points were observed as shown in **Figure 6.4(a)**. This suggests that (1) the addition of PTFE or F127 can induce an earlier occurrence of crystallization; (2) the solid-liquid (S-L) phase separation was dominant rather than the liquid-liquid (L-L) phase separation when the weight fraction of PVDF or F127 was increased from 1 to 5 wt%. In our previous studies, 1 wt% of PVDF or F127 addition was found to be sufficiently effective in PVDF hollow fiber membrane preparation while they were both susceptible to the aggregation phenomenon at a higher concentration (Loh and Wang 2013, Zhao *et al.* 2018). Therefore, 1 wt% was selected for both F127 and PTFE as joint amount of additions in this work. When varying the PVDF weight fraction with fixed addition of PTFE and F127, we obtained the monotectic point of this system at 27 wt% as

depicted in **Figure 6.4(b)**. It supports the abovementioned finding of the dominant occurrence of S-L phase separation when PVDF was added at 30 wt% in this system (Lloyd *et al.* 1990, Zhao *et al.* 2018).

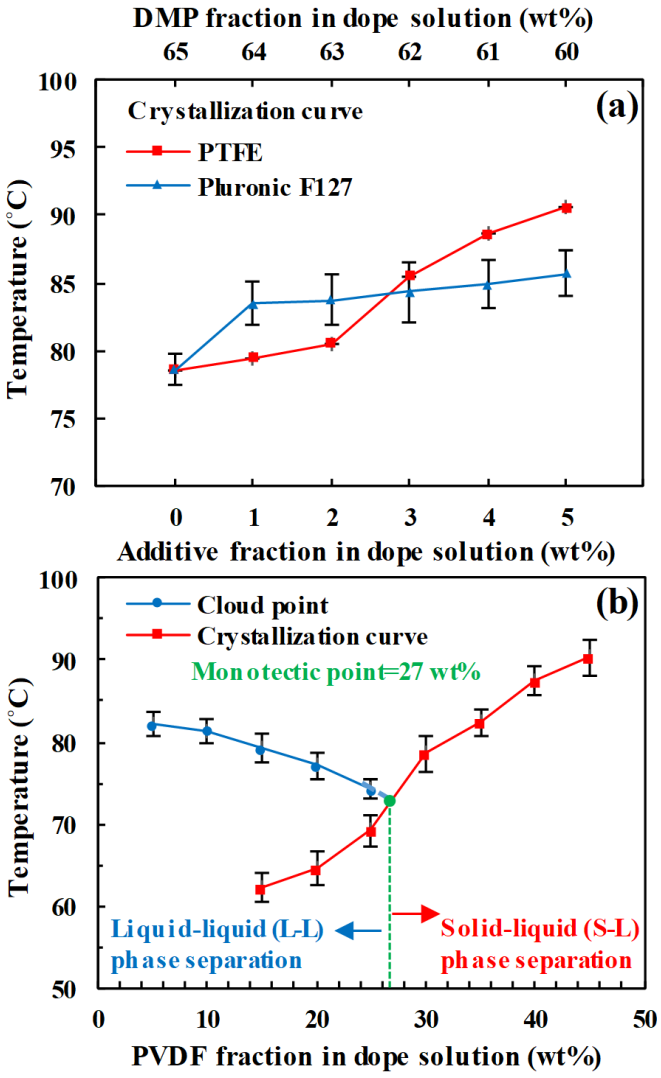

Figure 6.4. Phase diagrams for PVDF/DMP/TEP system based on different weight fractions of (a) PTFE or Pluronic F127, where PVDF concentration is fixed at 30 wt%; (b) PVDF, where PTFE and Pluronic F127 concentrations are both fixed at 1 wt% and an increase in the additive weight fraction is compensated by a decrease in DMP weight fraction

Secondly, we further looked into the SEM images of the microstructure of resultant membranes as shown in **Figure 6.5**. The corresponding results of the pore size and pore size distribution of membranes are presented in **Figure 6.6** and **Figure 6.7**, respectively. It can be seen from **Figure 6.5(a)** that the cross-sectional images of all membranes display a spherulitic structure, which is a typical indication of S-L phase separation (Lloyd *et al.* 1990, Lloyd *et al.* 1991). This is consistent the relative position of the monotectic point and actual dosage of PVDF as depicted in **Figure 6.4**, confirming that the system mainly underwent the S-L phase separation with subsequent crystallization (Lloyd *et al.* 1990, Kim and Lloyd 1991). Compared to the virgin membrane (TP0F0), smaller spherulites in greater amount can be found in the cross-sectional morphology of membranes with only 1 wt% of PTFE addition (TP1F0), while spherulites in similar sizes but more uniform shape can be obtained when only 1 wt% of F127 was added (TP0F1). The features observed in membranes with both PTFE and F127 additions will be discussed in the last paragraph of this section. The formation of spherulites originates from the aggregation of crystals in spherical crystallographic orientation during the crystallization (Teipel 2006). As shown in **Figure 6.4(a)**, the crystallization temperature (T_c) of dope mixtures increased when PTFE or F127 was introduced into the system individually. It seems that the addition of these two additives could both bring down the threshold of activation energy for crystallization of nuclei (Ma *et al.* 2013, Zhao *et al.* 2018).

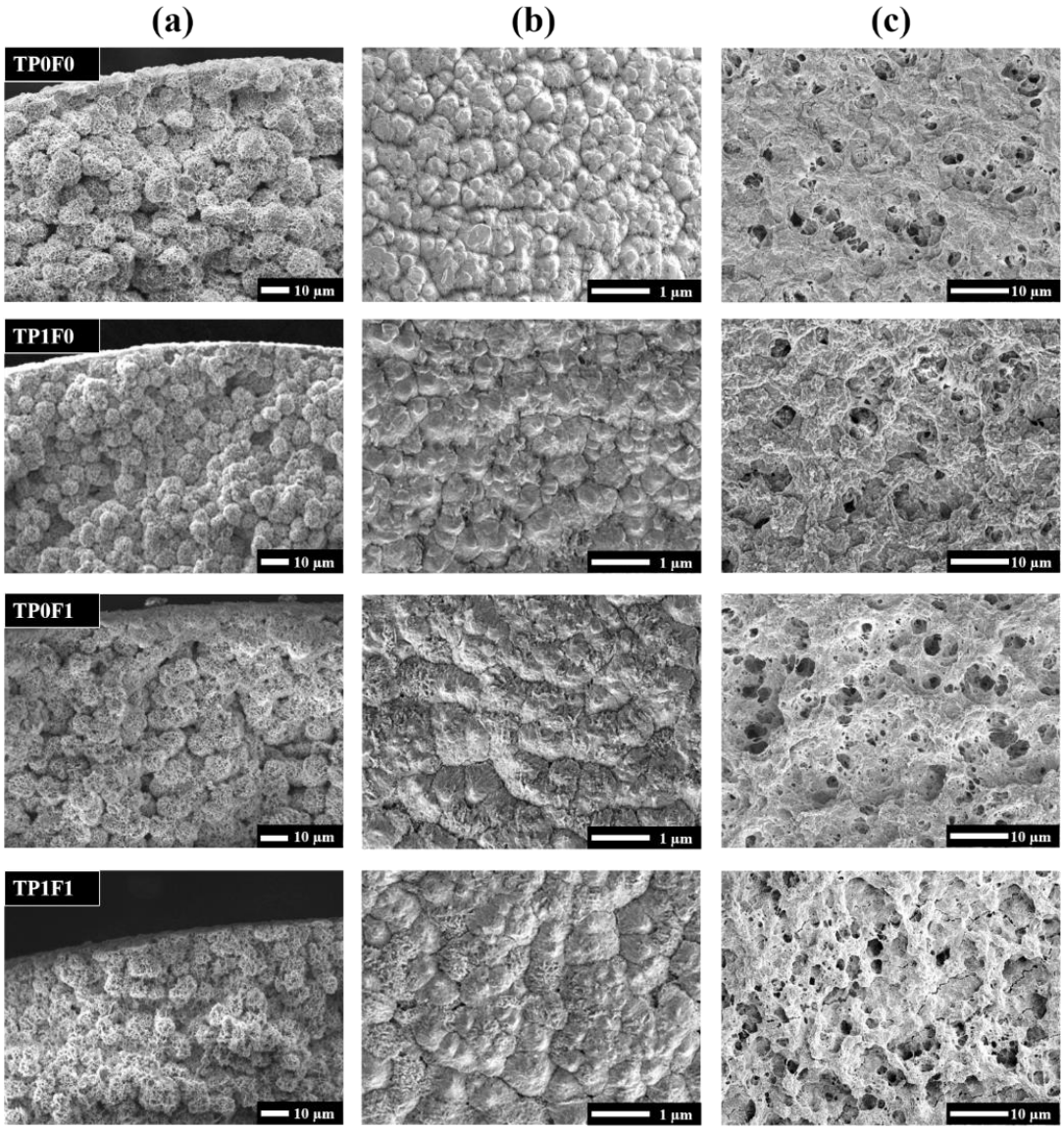

Figure 6.5. SEM images of hollow fiber membranes spun from the dopes with different combinations of additives: (a) cross-section near outer surface; (b) outer surface; (c) inner surface

However, significant differences can be found between TP1F0 and TP0F1 in terms of outer surface structure (**Figure 6.5(b)**), pore size (**Figure 6.6**) and pore size distribution (**Figure 6.7**), indicating that the effect of PTFE and F127 may result from different mechanisms. It can be clearly seen from **Figure 6.5(b)** that the membrane with only PTFE addition (TP1F0) possesses an evidently less porous outer surface structure compared to the membrane with only F127 addition (TP0F1). This can be also reflected in the pore size and pore size distribution properties. Taking the TP0F0

membrane as reference, we can see that the TP1F0 membrane has a smaller mean pore size while the TP0F1 membrane possesses a larger one as shown in **Figure 6.6(a)** and **Figure 6.7**. It is worth noting that the addition of PTFE and F127 both improved the overall porosity as presented in **Figure 6.6(b)**. Nevertheless, it can be seen from **Figure 6.6(c)** and **(d)** that their effects differed remarkably on the surface porosity. The addition of PTFE exerted merely no change while that of F127 strongly enhanced both outer and inner surface porosity. Theoretically, the size, number and shape of spherulites have a strong correlation with the nucleation and growth (NG) of the polymer-rich phase during the phase separation (Teipel 2006, Ehrenstein 2012). In our previous study, the addition of PTFE at 1 wt% was found to be effective in enhancing the NG process by transforming the homogeneous PVDF nucleation into heterogeneous PVDF-PTFE nucleation as nucleating agents in the TIPS process (Zhao *et al.* 2018). With more nucleation sites supplied, a greater number of crystals growing simultaneously might facilitate the formation of more spherulites in similarly smaller sizes with correspondingly increased amount of cavities in between. This could be responsible for the reduction in the pore size and improvement mainly in the bulk pore porosity when PTFE was added at 1wt%. In regard to F127, no evidence has been found that F127 can induce a similar nucleating effect on the crystallization of PVDF in the literature to our best knowledge. Most previous studies focused on the pore-forming ability of F127 when it was used as an additive in the membrane preparation via NIPS process (Loh *et al.* 2011, Loh and Wang 2012, Loh and Wang 2013, Li *et al.* 2014, Loh and Wang 2014). In this work, it was found that the addition of F127 could result in enlarged pore sizes as well as surface porosity. Therefore, it is possible that the pore-forming mechanism of F127 can also be applied in this study. The porous outer surface structure of F127-incorporated membrane implies that the NIPS process might be induced by the exchange between TEP and further facilitated by F127 acting as pore-forming agents.

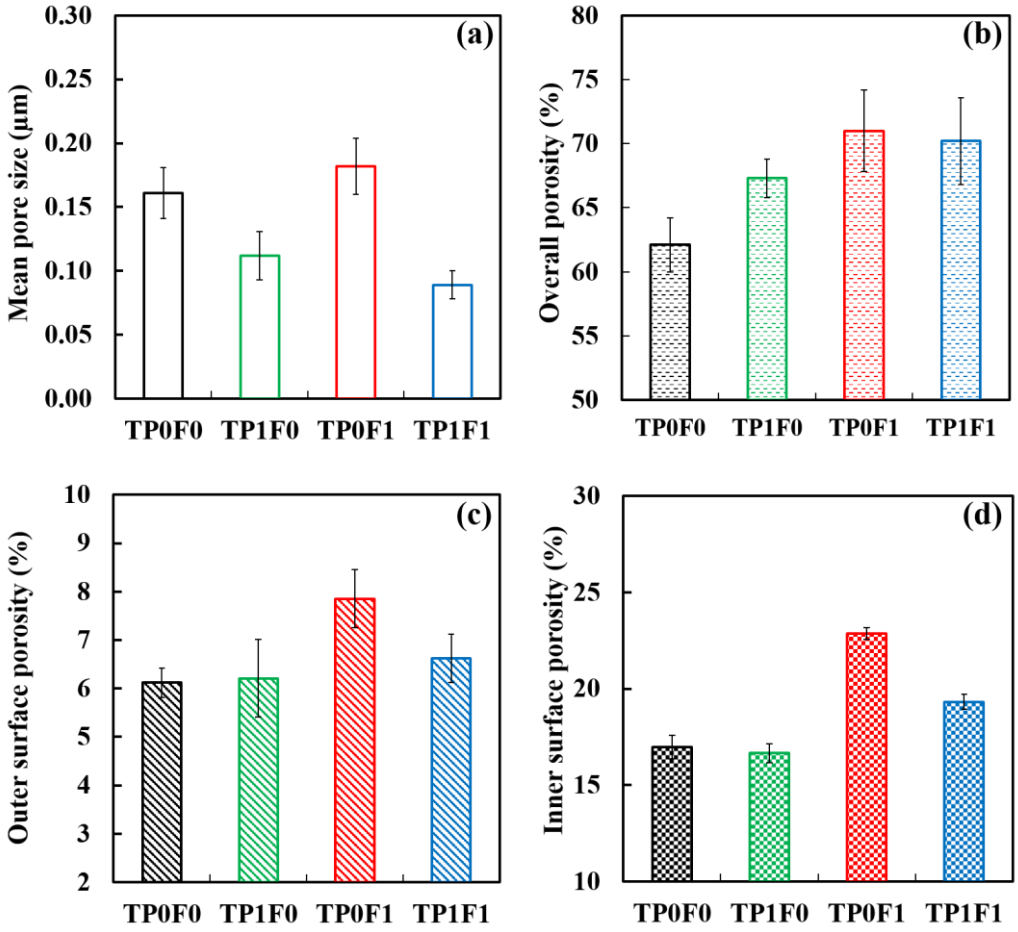

Figure 6.6. Effect of different combinations of additives on the membrane properties: (a) mean pore size; (b) overall, (c) outer surface, (d) inner surface porosity

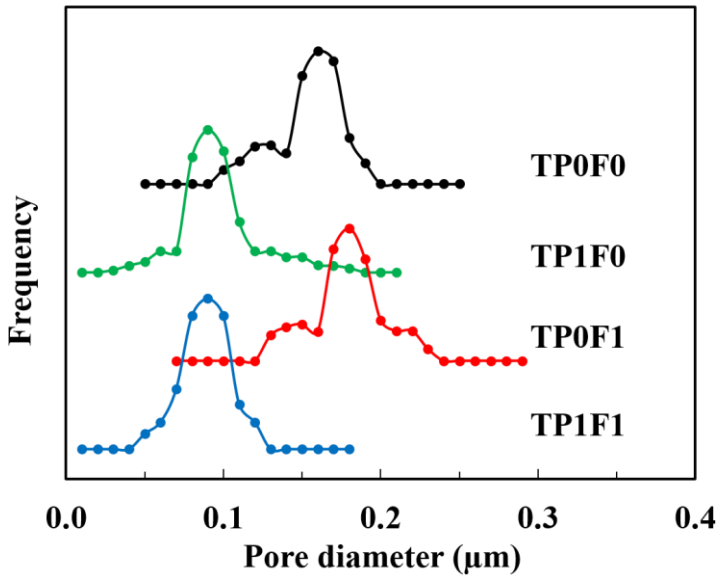

Figure 6.7. Pore size distribution of membranes obtained with different combinations of additives

Based on the above findings, we took one step further to analyze whether there was a combined effect of PTFE-F127 on the PVDF membrane formation via N-TIPS process. From the SEM images in **Figure 6.5**, we can see that the surface and bulk structure of the TP1F1 membrane inherited features from both TP1F0 and TP0F1, suggesting a combined effect of PTFE and F127 on the membrane formation. More importantly, it can be found that the pore structure properties of TP1F1 are closer to those of TP1F0 in terms of mean pore size, porosity and pore size distribution as shown in **Figure 6.6** and **Figure 6.7**. This implies that PTFE might have a more significant impact than F127 on the pore formation in the current dope system. Above all, it can be concluded that (1) PTFE was mainly responsible for enhancing the nucleation process as a nucleating agent in the TIPS process, generating membranes with smaller pore sizes and a greater bulk porosity; (2) F127 could facilitate the NIPS process acting as a pore-forming agent, producing membranes with larger pore sizes and a greater surface porosity; (3) PTFE can be used in conjunction with F127 to exert a combined effect during the N-TIPS process, resulting in membranes with combined features.

6.3.3. Effect of PTFE and Pluronic F127 on the crystalline and mechanical properties of membranes

In **Section 3.2**, we have discussed the possibility that PTFE and F127 can work conjunctively to affect the pore formation of membranes during the N-TIPS process. In order to reveal the mechanisms for this finding, we conducted DSC, WAXD analyses to reveal the crystalline properties of the dope mixtures and membranes from both thermodynamic and kinetic perspectives. The corresponding results are shown in **Table 6.3**, **Figure 6.8** and **Figure 6.9**, respectively. Furthermore, the mechanical properties, which are normally regarded as the manifestation of crystalline characteristics in the studies of semi-crystalline polymers, were also measured with results presented in **Figure 6.10** (Rajabzadeh *et al.* 2008, Rajabzadeh *et al.* 2009).

Table 6.3 presents the crystallization results for different dope mixtures and membranes obtained from the DSC analysis. It can be seen from **Table 6.3** that all the additive-introduced dope mixtures possess higher peak crystallization

temperatures (T_c^p) compared with the virgin one (TP0F0). We have mentioned this phenomenon in **Section 3.2** with the implication that the addition of PTFE and F127 could both induce an earlier crystallization by reducing the threshold of activation energy for crystallization of nuclei (Zhao *et al.* 2018). As shown in **Figure 6.4(a)** and **Table 6.3**, F127 showed a stronger impact on the increase of T_c^p than PTFE. However, the dope mixtures with PTFE additions exhibit a smaller ΔT_c than that of F127-added dope mixtures. The ΔT_c indicates the kinetic characteristics of the crystallization process (Raimo 2011, Ma *et al.* 2013). This suggests that the PVDF crystallization haft-time ($t_{1/2}$) of PTFE-added dope mixtures was shorter than that of F127-added dope mixtures under the same cooling conditions. Therefore, PTFE exhibited a more significant effect on accelerating the nucleation process of PVDF compared to F127 in this study.

Table 6.3. Crystallization and melting results and crystalline properties of dope mixtures and membranes with different combinations of additives

	Crystallization and melting results of dope mixtures				Crystalline properties of corresponding membranes		
Code	T_c^p (°C)	ΔT_c (°C)	T_m^p (°C)	ΔT_m (°C)	ΔH_m (J g^{-1})	χ_c (%)	D (nm)
TP0F0	78.6 ± 2.2	14.9 ± 0.2	119.1 ± 2.5	29.8 ± 1.2	50.1 ± 3.3	47.9 ± 3.2	6.01 ± 0.19
TP1F0	79.4 ± 1.9	8.1 ± 0.5	117.7 ± 3.7	27.5 ± 0.9	52.5 ± 3.4	50.2 ± 2.8	5.65 ± 0.15
TP0F1	83.5 ± 3.1	9.6 ± 0.3	124.7 ± 4.2	25.6 ± 1.1	49.0 ± 2.0	46.9 ± 1.9	6.09 ± 0.12
TP1F1	83.9 ± 2.6	7.3 ± 0.2	118.3 ± 2.9	24.2 ± 0.6	51.2 ± 3.0	49.0 ± 3.5	5.78 ± 0.11

Notes:
T_c^p, peak crystallization temperature of PVDF; ΔT_c = T_c^{on} - T_c^p; T_c^{on}, onset crystallization temperature of PVDF; T_m^p: peak melting temperature of PVDF; ΔT_m= T_m^f-T_m^{on}; T_m^{on}: onset melting temperature of PVDF; T_m^f: final melting temperature of PVDF; ΔH_m: melting enthalpy; χ_c: crystallinity of PVDF; D: crystal size.

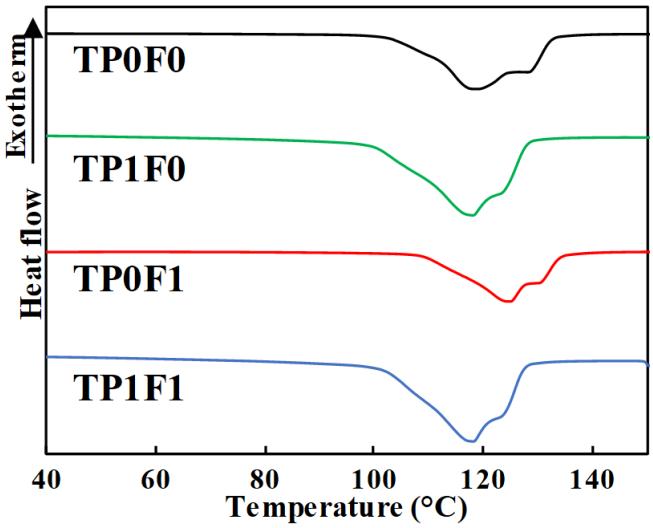

Figure 6.8. DSC melting curves of dope mixtures with different combinations of additives: (a) low temperature range; (b) high temperature range

The influence on the nucleation could be extended to the growth of crystals and subsequent formation of spherulites, which are correlated with the variation of the melting curves in **Figure 6.8** (Ma *et al.* 2008, Ma *et al.* 2013). As shown in **Figure 6.8(a)**, the "double melting endotherms" phenomenon can be found in all the curves including the ones with or without additives (Ji *et al.* 2007). There are several possible explanations for the occurrence of "double melting endotherms": (a) the presence of polymorphism of PVDF (F. 1960), (b) a secondary crystallization followed by remelting during the DSC heating process (Ji *et al.* 2007, Ji *et al.* 2008, Wang *et al.* 2015). To understand the reasons behind, we verified the explanation (a) based on the WAXD results as shown in **Figure 6.9**. It can be found that the peaks at $2\theta = 17.66°$, 18.30 ° and 19.90 ° (in planes (100), (020), and (110)) and the peaks at $2\theta = 20.26°$, 41.22 ° (in planes (200) and (201)) suggest the co-existence of α and β-phase crystals of PVDF, respectively (Chun‐Hui *et al.* 2012, Cui *et al.* 2014). However, the presence of polymorphism seems not sufficient to explain the shifts and variations of the double peaks. Compared to the virgin one (TP0F0), the melting endotherms of PTFE-added ones (TP1F0 and TP1F1) shifted to a lower temperature region with larger low melting peaks. Marega and co-workers have pointed out that the low melting peak is a signal for the original crystals formed during the phase separation and subsequent crystallization process, while the high peak can be ascribed

to the secondary crystallization during the heating process (Marega and Marigo 2003, Ma *et al.* 2008, Ma *et al.* 2013). The promoted low melting peaks of the PTFE-added ones indicate that the addition of PTFE could enhance the original crystallization of PVDF, resulting in membranes with a higher degree of crystallinity as presented in **Table 6.3**. With the possible help of accelerated nucleation process by PTFE, much smaller crystals were found in the membranes of TP1F0 and TP1F1. This is consistent with the corresponding cross-sectional SEM images displaying more compact membrane structure with smaller spherulites as presented in **Figure 6.5(a)**. On the contrary, the melting endotherm of only F127 added one (TP0F1) shifted to a higher temperature region with no significant change on the low melting peaks. The cross-sectional SEM images suggest no obvious effect of F127 on the size of spherulites. This is supported by the slightly increased crystal size as listed in **Table 6.3**. It is worth noting that when PTFE and F127 were both added, the resultant dope mixtures and membranes exhibited features with a high similarity to the ones with only PTFE addition. This suggest that the addition of PTFE played a major role in affecting the crystallization process of PVDF compared with that of F127. On the other hand, the addition of PTFE and F127 were both found to be able to reducing the difference of final and onset melting temperatures (ΔT_m). The melting temperature can be used to indicate the size of PVDF crystals since it signals the degree of the long-range order in the crystalline structure by describing the rate of heat absorption (Marega and Marigo 2003, Ma *et al.* 2008, Raimo 2011, Ehrenstein 2012, Ma *et al.* 2013). A lower ΔT_m normally suggests a higher degree of homogeneity of PVDF crystals (Ma *et al.* 2013). This agrees well with the finding from the SEM images in **Figure 6.5(a)** that membranes with additives possess a structure with enhanced uniformity of spherulites.

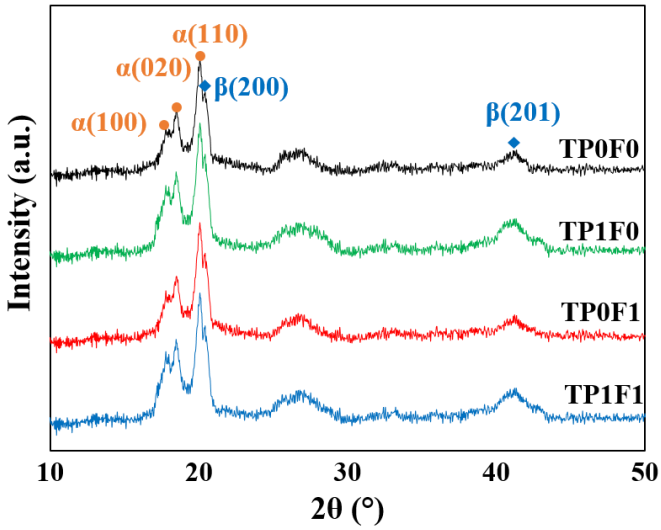

Figure 6.9. X-ray diffraction patterns of membranes obtained with different combinations of additives

As presented in **Figure 6.10**, the results of tensile strength and elongation can be used to respectively indicate the effect of PTFE and F127 addition on the toughness and elasticity of membranes. Theoretically, the orderly aligned lamellae crystallites of a semi-crystalline polymer are embedded by the amorphous regions (Ehrenstein 2012). With the existence of spherulites, the intermolecular interactions within the crystallites mainly determines the toughness of PVDF-based membranes, while the amorphous regions between the lamellae have a major impact on the elasticity (Teipel 2006, Ehrenstein 2012, Cui *et al.* 2015). Compared to the pristine membrane (TP0F0), the mechanical properties of the membranes with PTFE addition (TP1F0 and TP1F1) increased significantly. Among them, the TP1F0 membrane possesses the maximum tensile strength and elongation values of 7.5 ± 0.1 MPa and 170 ± 5 %, respectively, followed by the TP1F1 membrane with corresponding values of 7.1 ± 0.2 MPa and 156 ± 7 %. On the contrary, it can be seen that the mechanical properties decreased when F127 was introduced into the system from the comparisons of TP0F0/TP0F1 and TP1F0/TP1F1. In addition, these counteractive effects of PTFE and F127 can also be found in **Table 6.3**, showing that the PTFE-added membranes have a higher crystallinity while the F127-added ones possess a lower crystallinity compared with the pristine membranes. This suggests their different impact on the growth of crystalline and amorphous regions in the PVDF matrix. In our previous study, we have demonstrated that the toughness and elasticity of PVDF membranes

can be both strengthened by adding the PTFE possibly due to the enhanced interconnectivity between spherulites as a result of the facilitated nucleation and formation of lamellae crystallites (Zhao *et al.* 2018). This is consistent with the effect of PTFE addition found in this study. On the other hand, the interconnectivity might be impaired by the addition of F127 but this impairment can be largely compensated when the PTFE was added jointly with F127.

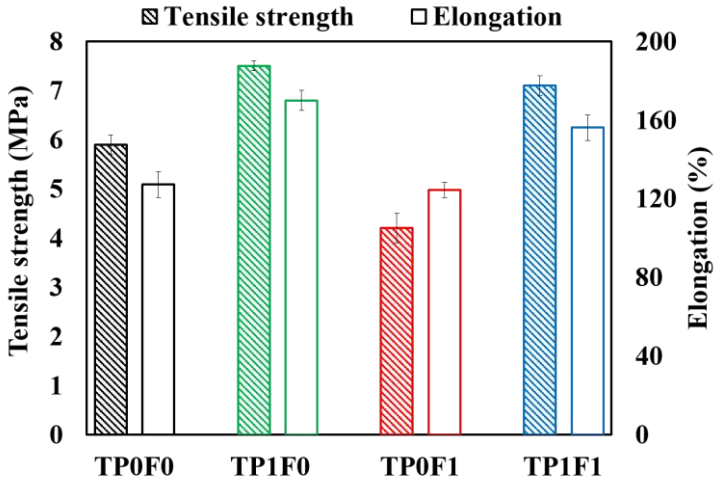

Figure 6.10. Mechanical properties of membranes obtained with different combinations of additives

6.3.4. Stability of Pluronic F127 in the PVDF matrix with or without the presence of PTFE

Previously, we have demonstrated the individual and combined effect of PTFE and F127 addition on the structure formation and corresponding properties of PVDF hollow fiber membranes prepared via N-TIPS process. However, the stability of F127 in the PVDF matrix remained unclear. Thus, we conducted DSC, FTIR and weight variation analyses to investigate whether the addition of PTFE can help immobilize the F127 during the N-TIPS process. In an effort to examine the effect of F127 stability on the surface hydrophilicity of PVDF membranes, the measurement of dynamic contact angle was performed with results presented in **Figure 6.13**.

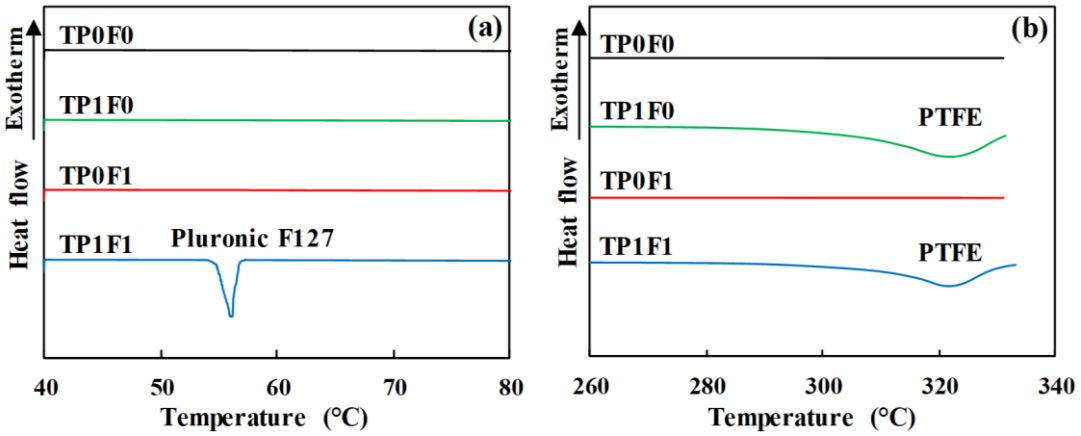

Figure 6.11. Thermal behaviors of membranes with different combinations of additives

As shown in **Figure 6.11(b)**, the melting peaks at about 327 °C from the curves of TP1F0 and TP1F1 indicate the presence of PTFE in both PTFE-added membranes after the prolonged post-treatment (Wang *et al.* 2002). Conversely, the absence of the melting peak at about 56 °C in **Figure 6.11(a)**, which suggests the nonexistence of F127 in TP0F1, implies the instability of F127 when it was used solely as an additive for the membrane preparation (Cui *et al.* 2008). However, the melting peak of F127 can be spotted from the curves of TP1F1, which suggests the possibility that the F127 was largely protected from being eluted with the presence of PTFE. To further understand this phenomenon, we specifically compared the FTIR spectra of membranes with normal (24 h) and prolonged (5 day) post-treatment as shown in **Figure 6.12**. It is worth noting that the peak at 1106 cm^{-1} can be found in both TP0F1 and TP1F1 after the normal post-treatment. Nevertheless, this peak disappeared in the spectrum of TP0F1 but persisted in that of TP1F1 after the prolonged post-treatment. The presence of F127 can normally be indicated by the adsorbance peak around 1105 to 1115 cm^{-1}, which represents the characteristic band for the C-O-C stretching related to the ether group. Some studies have shown that the interaction of PPO block and PVDF can exert an anchorage effect to stabilize the F127 in the PVDF matrix (Wang *et al.* 2005, Cui *et al.* 2008). However, this anchorage was demonstrated to be insufficiently robust against the elution in our previous studies (Loh *et al.* 2011, Loh and Wang 2012, Loh and Wang 2014). To quantitatively investigate the elution process, the weight variation of membranes after the normal

and prolonged post-treatment was measured using a gravimetric method. It can be seen from **Table 6.4** that, there was obvious weight loss detected in the membranes with only F127 addition (TP0F1). On the contrary, the membrane with both PTFE and F127 additions (TP1F1) exhibited similar trace amount of weight loss to that of membranes without F127 addition (TP0F0 and TP1F0), which can be ascribed to the extraction of trace amount of diluents left in the membrane pore structure. According to the results mentioned above, it can be inferred that (1) the F127 was partially stable in the PVDF matrix due to the relatively weaker interaction between PPO block and PVDF; (2) the immobilization of F127 in the PVDF matrix can be further strengthened against the elution with the presence of PTFE.

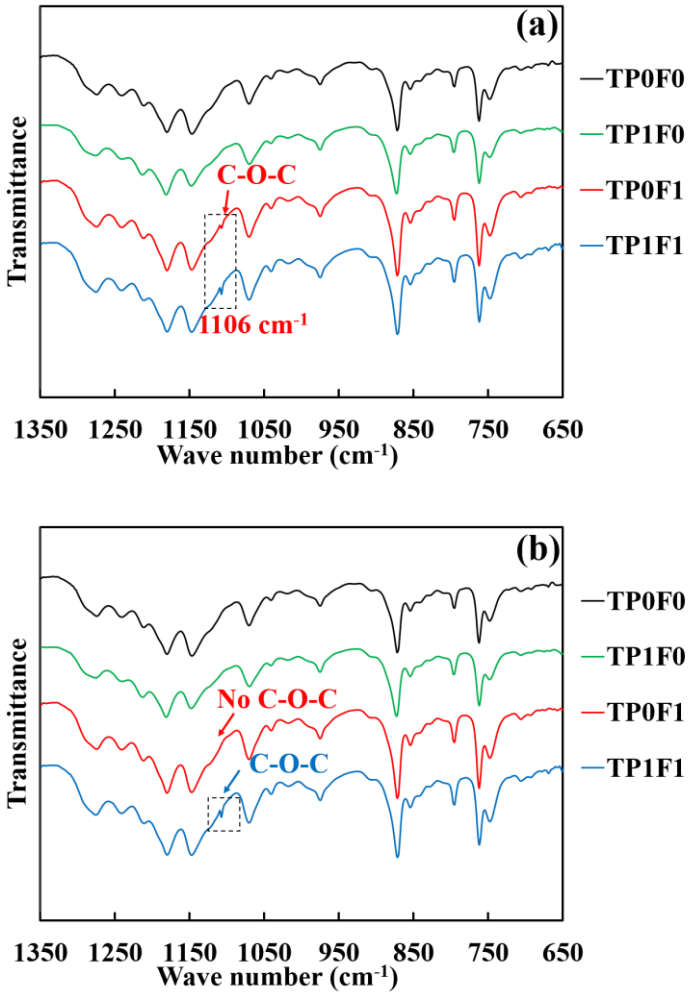

Figure 6.12. FTIR spectra of membranes spun with different combinations of additives: (a) normal post-treatment; (b) prolonged post-treatment

Table 6.4. Weight variations of membranes after prolonged post-treatment

Code	m_n (mg)	m_p (mg)	ω (wt%)	$\Delta m/m_n$ (wt%)
TP0F0	150.6 ± 0.6	150.3 ± 0.3	0.0	0.2
TP1F0	154.6 ± 0.3	154.1 ± 0.4	0.0	0.3
TP0F1	151.9 ± 0.5	146.9 ± 0.6	3.2	3.3
TP1F1	153.3 ± 0.7	152.9 ± 0.5	3.1	0.3

Notes:
m_n, weight of dried hollow fiber after normal post-treatment; m_p, weight of dried hollow fiber after prolonged post-treatment; ω, weight fraction of Pluronic F127 in the hollow fiber; $\Delta m = m_n - m_p$, weight loss after prolonged post-treatment.

The effect of F127 stability in the PVDF matrix can be further reflected by the surface hydrophilicity, which is normally indicated based on the water contact angle of hollow fiber membranes (Loh and Wang 2013). In addition, the surface hydrophilicity is also a major concern in the fouling control (Loh and Wang 2014). As shown in **Figure 6.13**, the post-treatment condition did not show a significant impact on the membranes except for TP0F1. For the membranes after the normal post-treatment, the contact angle of the pristine membrane (TP0F0) is 101 ± 4 °, indicating the intrinsic hydrophobicity of the PVDF membranes prepared via N-TIPS process in this study. With only PTFE addition (TP1F0), the contact angle slightly increased to 105 ± 6 °. This is consistent with the results from our previous study on PVDF/PTFE membranes, which revealed that the addition of PTFE has a strong correlation with the enhancement in the surface hydrophobicity of PVDF membranes (Zhao *et al.* 2018). When only the F127 was added (TP0F1), the contact angle decreased to 89 ± 3 ° but bounced back to 102 ± 4 ° after the prolonged post-treatment. However, this phenomenon was not observed in the membranes with both PTFE and F127 additions (TP1F1). Different from other properties discussed previously, the TP1F1 membranes do not possess a similar surface hydrophilicity to that of TP1F0. Conversely, the contact angle of TP1F1 is even lower than that of TP0F1, reaching 69 ± 3 ° and 70 ± 6 ° after normal and prolonged post-treatment, respectively. It can be inferred that the F127 might exert a shielding effect around the PTFE when they were added conjunctively into the PVDF matrix (Sharma *et al.* 2014, Shah *et al.*

2015). With the hydrophobic blocks attached to the surface of PTFE, the hydrophilic PEO blocks of the F127 were able to extend outwards to establish contact with water (Li *et al.* 2009, Liu *et al.* 2009, Li *et al.* 2014). On the other hand, the presence of PTFE could play an important role in immobilize the F127 in the PVDF matrix. Therefore, the conjunctive addition of PTFE and F127 could result in a better hydrophilicity of PVDF membranes.

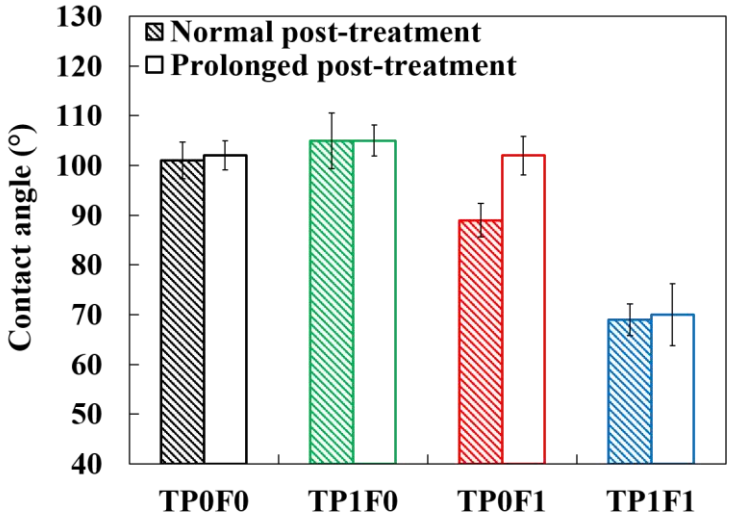

Figure 6.13. Dynamic contact angle of membranes with different combinations of additives after normal post-treatment and prolonged post-treatment

6.3.5. Filtration performance of hollow fiber membranes

Membrane fouling is a major concern during the entire life cycle of membrane used in water or wastewater treatment (She *et al.* 2009, Wang and Tang 2011, Fane *et al.* 2015). To elucidate the antifouling property of PVDF membranes with different combination of additives, we conducted a filtration test with three cycles using BSA as model protein in the test solution. The variation and recovery of flux as well as corresponding data are presented in **Figure 6.14** and **Table 6.5**. The fluxes of membranes decreased drastically compared to the initial PWP (J_{w0}) values at each cycle. During general microfiltration or ultrafiltration tests, progressive drop in the permeation flux under constant pressure can be ascribed to two factors, namely, the concentration polarization and membrane fouling (Zhao *et al.* 2008, Li *et al.* 2014).

In this study, the concentration polarization was thought to be negligible due to the high molecular weight of protein used and sufficient scouring by crossflow solutions (Zhao *et al.* 2008). Hence, the substantial flux decline was mainly contributed by the deposition and adsorption of protein onto the membrane surface or in the surface pores (Li *et al.* 2014). The flux reduction (R_t) and lower flux recovery ratio (FRR) values were calculated to evaluate the antifouling performance. A higher FRR value normally implies a better antifouling property (Zhao *et al.* 2008, Xu *et al.* 2014). Compared to the control membrane (TP0F0), the membrane with only PTFE addition (TP0F1) showed even faster R_t and lower FRR values probably due to its smaller pore size and higher hydrophobicity. For the membranes with F127 additions, TP0F1 and TP1F1 membranes behaved similarly during the first cycle with significantly higher fluxes than the ones without F127 addition. This could be ascribed to their higher levels of surface porosity. However, TP0F1 membrane exhibited much higher R_t and lower FRR values compared with TP1F1 membrane during the second and third cycles. On the contrary, the membrane with both PTFE and F127 additions (TP1F1) exhibited excellent flux recovery property after cleaning. This implies that the protein fouling was reversible possible due to the PEO segments protruding exteriorly. Therefore, the co-addition of PTFE and F127 could obtain PVDF membranes with promising permeability and antifouling property.

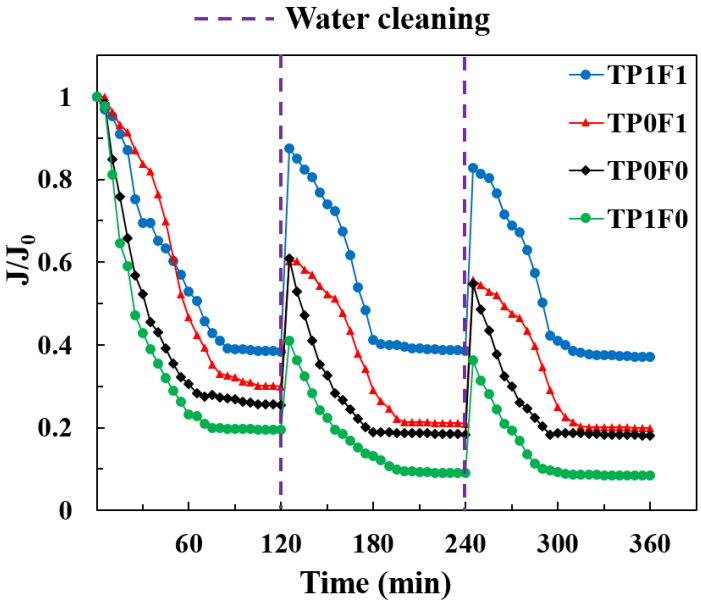

Figure 6.14. Normalized flux variation during filtration test of 1g/L BSA solution at 0.1 MPa for membranes obtained with different combinations of additives

Table 6.5. The filtration and fouling properties of PVDF membranes in BSA filtration

Code	J_{w0}	1st cycle		2nd cycle		3rd cycle	
		FRR	R_t	FRR	R_t	FRR	R_t
	(L m^{-2} h^{-1} bar^{-1})	(%)	(%)	(%)	(%)	(%)	(%)
TP0F0	620 ± 31	64.2	74.4	60.0	81.1	56.6	81.7
TP1F0	852 ± 39	59.3	77.1	53.2	84.5	50.9	85.4
TP0F1	922 ± 36	75.4	69.9	70.6	75.0	66.1	76.1
TP1F1	876 ± 32	81.7	60.9	77.4	65.0	71.2	66.3

6.3.6. Possible mechanism for PTFE-Pluronic F127 interactions in PVDF matrix

The stabilization of F127 in the PVDF-based membranes has remained unsolved due to (1) relatively weak interactions between the hydrophobic PPO units of F127 and PVDF, and (2) its high solubility in water and common solvents used for the PVDF membrane preparation (Loh and Wang 2012, Loh and Wang 2013, Loh and Wang

2014). On the other hand, we have demonstrated that PTFE can act as a nucleating agent during the crystallization process of PVDF in our previous study (Zhao *et al.* 2018). Thanks to its outstanding hydrophobic surface characteristics, good interactions between PTFE and PPO units of 127 have also been found in the aqueous environment (Sharma *et al.* 2014, Shah *et al.* 2015, Shah *et al.* 2018). Therefore, we proposed to use PTFE as a mediating agent in an effort to establish a stronger connection between F127 and PVDF during the phase inversion in nonaqueous-aqueous environment in this study.

In the liquid penetration test using nonaqueous polar solvents in **Section 3.1**, F127 played a unique role in wetting the PTFE powders, indicating good interactions between PTFE and F127 in the nonaqueous environment. Previous studies suggested that the adsorption of PEO-PPO-PEO Pluronic block copolymers onto the hydrophobic PTFE surface could lead to hydrophilization of PTFE (Sharma *et al.* 2014, Shah *et al.* 2015, Shah *et al.* 2018). Without sufficient dispersion in the nonaqueous solutions, the packed PTFE powder may encompass a number of hydrophobic microcapillaries (Shah *et al.* 2015, Shah *et al.* 2018). Due to the hydrophobic interactions, the PPO units of F127 could adsorb onto the surface of PTFE with hydrophilic PEO units protruding outwards to the surrounding nonaqueous polar solvents. Based on the surface tensiometry measurement, we found out that the PEO and PPO blocks exhibited similar levels of solubility in the selected polar solvent mixtures. Thus, the hydrophilization of PTFE microcapillaries by polar solvents were able to occur through the exterior PEO blocks. Shah and co-workers believed that the wetting of PTFE could be explained by the negatively enhanced surface free energy of PTFE in the presence of F127 (Shah *et al.* 2018).

Furthermore, we analyzed the effects of PTFE and F127 on the PVDF membranes in terms of microstructure, pore size, crystalline, surface chemistry and hydrophilicity characteristics as well as antifouling property in **Sections 3.2–3.5**. It was found that PTFE and F127 imposed different individual effects on the membrane properties. Scheinder *et al.* observed that PVDF could epitaxially crystallize on PTFE due to fluorine-fluorine interactions (Schneider *et al.* 2001). PTFE was demonstrated to be nucleating agents to enhance the heterogeneous nucleation and subsequently facilitate the crystallization of PVDF, generating smaller crystals in a larger amount.

On the other hand, F127 acted more as pore-forming agents in enhancing the pore structure, which resulted in membranes with larger pore sizes and higher porosity (Loh and Wang 2012, Loh and Wang 2013, Loh and Wang 2014). In this case, it was reasonable to anticipate that the membranes obtained with conjunctive addition of PTFE and F127 would inherit features similarly from both membranes. However, we found that the resultant membranes (TP1F1) possess structural and crystalline properties closer to those of PTFE-solely-added membranes (TP1F0), while they (TP1F1) have the surface hydrophilicity more similar to those of F127-solely-added membranes (TP0F1). From the stability test, the presence of PTFE in the PVDF matrix remained unchanged under different post-treatment conditions. On the contrary, the stability of F127 was discovered to be significantly improved in the presence of PTFE. These phenomena suggest that PTFE could interact with PVDF directly, while the interactions between F127 and PVDF were largely dependent on PTFE. Through the bridging force provided by PTFE, F127 could be further immobilized in the PVDF matrix. Therefore, we conclusively proposed a schematic illustration of the interactions between PTFE and F127 in the PVDF membrane as shown in **Figure 6.15**. Through this method, the prepared hybrid membrane (TP1F1) exhibited an outstanding tensile strength, hydrophilicity, porosity as well as PWP with a mean pore size of 0.09 ± 0.01 μm among other PVDF hollow fiber membranes reported previously which were produced by TIPS or N-TIPS method as shown in **Table 6.6**.

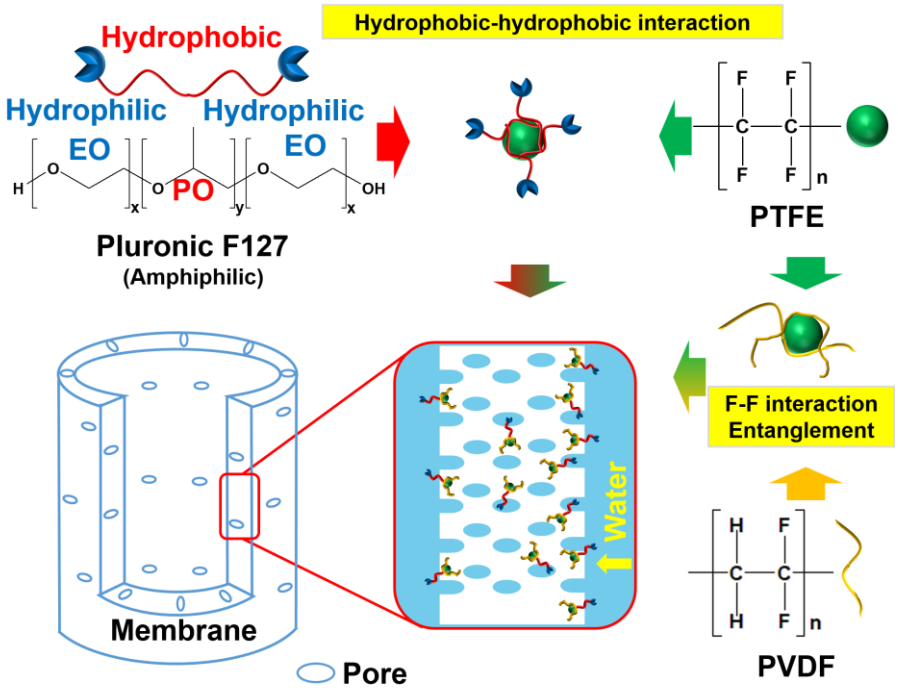

Figure 6.15. Proposed conceptual illustration of PTFE-Pluronic interactions in PVDF matrix

Table 6.6. Comparison of various PVDF hollow fiber membranes prepared via TIPS or N-TIPS method

Additive	Method	Tensile strength (MPa)	Contact angle (°)	Mean pore diameter (μm)	Porosity (%)	PWP (L m^{-2} h^{-1} bar^{-1})	Ref.
$CaCO_3$	TIPS	~2.1[a]	94	0.28	70	~1250[a]	(Song *et al.* 2016)
PMMA	TIPS	~3.2[a]	98	-[b]	-[b]	~350[a]	(Rajabzadeh *et al.* 2012)
PVP	TIPS	~5.2[a]	89	-[b]	-[b]	~190[a]	(Rajabzadeh *et al.* 2012)
PTFE	TIPS	7.4	106	0.10	65	878	(Zhao *et al.* 2018)
PVP1300	N-TIPS	0.8	-[b]	-[b]	80	1153	(Hassankiadeh *et al.* 2015)
LiCl/glycerol	N-TIPS	4.9	-[b]	0.68	63	912	(Lee *et al.* 2015)
F127/PTFE (TP1F1)	N-TIPS	7.1	69	0.09	70	876	This work

Notes:
[a)] The data were collected from figures in the literature by using the Digitizer function in *Origin* 9.1;
[b)] The data were not shown in the paper.

6.4. Conclusions

In the final part of study, novel hydrophilic PVDF hollow fiber membranes have been prepared via N-TIPS method using PTFE and Pluronic F127 particles as additives. Good interactions between PTFE and F127 in the nonaqueous environment were demonstrated. The addition of PTFE and F127 during the membrane fabrication exerted significantly different effect on the resultant properties of PVDF membranes.

The following conclusions can be drawn from this study:

- The individual addition of PTFE was found to be effective in facilitating the nucleation and growth of PVDF crystals during the crystallization, resulting in membranes with smaller pore sizes, larger bulk porosity and better mechanical strength. Different from PTFE, the individually used F127 could enhance the pore formation, generating membranes with larger pore sizes and surface porosity.
- Without the presence of PTFE, F127 was largely eluted from the membranes during the prolonged post-treatment using ethanol. On the contrary, we demonstrated that the stability of F127 in PVDF membranes could be improved in the presence of PTFE possibly due to the mediating effect of PTFE, which possesses good interactions with both PVDF and F127. The immobilized F127 could thus serve dual functions by acting as a pore-former and surface hydrophilic modifier for PVDF membranes.
- These features endowed the prepared membranes with a narrower pore size distribution, improved porosity and strengthened tensile strength as high as 7.1 ± 0.2 MPa. Compared with the pristine PVDF membranes, the water contact angle decreased from 101 ± 4 to 69 ± 3 °. The hybrid membranes exhibited a PWP value of 876 ± 32 L m^{-2} h^{-1} bar^{-1} with a mean pore size of 0.09 ± 0.01 μm and a remarkably enhanced antifouling property during a three-cycle continuous test.

This study indicates the promising versatility of N-TIPS method in tailoring the surface and bulk properties of polymeric membranes by combining the merits of functional additives originated from pure NIPS and TIPS processes.

CHAPTER 7 Conclusions and Future Work

7.1. Overall conclusions

This thesis presents the development of PVDF hollow fiber membranes prepared via novel TIPS method. The PVDF hollow fiber membranes fabricated from the conventional NIPS process are subjected to a lower mechanical strength resulted from the macrovoids formation. Meanwhile, the development of TIPS process are also hindered by toxic solvents used, inconvenience in the control over surface pore structure as well as limited choices of additives compared to NIPS process. In practice, a porous and narrow distributed pore structure with high permeability and tailorable surface hydrophobicity is desirable for common separation applications such as membrane distillation and membrane contactor. Therefore, a series of PVDF-based hollow fiber membranes were prepared via either novel TIPS process by using mild diluents with different dope compositions and spinning conditions (**Chapter 3**) and further incorporating hydrophobic additives (**Chapter 4**) or N-TIPS process using mixed diluents (**Chapter 5**) and further immobilizing multifunctional amphiphilic additives (**Chapter 6**).

The basic understanding of TIPS process has been built by fabricating and characterizing the PVDF hollow fiber membranes prepared using mild diluents with different spinning conditions. Subsequently, hydrophobically enhanced PVDF-based hollow fiber membranes with various PTFE loadings have been developed via TIPS method for direct contact membrane distillation (DCMD). Acting as the nucleating agent, PTFE particles were found to play an important role in the crystallization of PVDF polymer matrix during the solid-liquid (S-L) phase separation. On the other hand, a novel hybrid method involving NIPS and TIPS (N-TIPS) has been successfully explored. By using a modified N-TIPS method, PVDF hollow fiber membranes have been developed using the TEP as a second diluent and Pluronic F127 particles as additives. Based on this development, hydrophilic PVDF hollow fiber membranes have been prepared via N-TIPS method using PTFE and Pluronic F127 particles as additives. The immobilization of Pluronic F127 in PVDF membranes by PTFE has been demonstrated to be feasible.

The major findings and conclusions are summarized as follows:

- The conventional TIPS spinning process can be sustainably enhanced by using greener solvents and post-treatment method. The mild solvents with a lower toxicity such as DMP can also be used to replace the conventional toxic solvents to obtain comparable properties and performance of membranes.
- The packing density of spherulites increased when increasing PVDF molecular weight (MW) or initial polymer concentration, resulting in membranes with smaller sizes and better tensile strength. The TIPS process can be controlled thermodynamically and kinetically by adjusting the air gap and coagulation temperature. Robust hollow fiber membranes with a small pore size and high pure water permeability (PWP) can be achieved with a moderate air gap and coagulation temperature.
- The prepared PVDF hollow fiber membranes possess promising pure water permeability values from 663 ± 33 to 878 ± 5 L m^{-2} h^{-1} bar^{-1} with reinforced tensile strength values from 3.8 ± 1.1 to 5.6 ± 0.3 MPa and a mean pore size below 0.2 µm which are comparable other membranes reported previously.
- The fabricated PVDF/PTFE hollow fiber membranes possess a narrower pore size distribution with smaller mean pore sizes varying from 0.08 to 0.12 µm. The tensile strength and elongation were noticeably improved to as high as 9.4 ± 0.3 MPa and 235 ± 36 %, respectively. The water contact angle of resultant membranes increased from 94 ± 1 to 106 ± 3 º.
- The hybrid PVDF/PTFE membranes achieved good performance in the DCMD process. The membranes with the optimum PTFE loading of 1 wt% exhibited a flux of 28.3 kg m^{-2} h^{-1} at the feed temperature of 60 ºC with 99.99 % NaCl rejection over a 50-h continuous test. The DCMD performance demonstrated that the newly developed PVDF/PTFE membranes had improved anti-wetting and mechanical properties over the virgin PVDF membranes.
- This study on N-TIPS process provides a new perspective of the interrelations between TIPS and NIPS process with an effort in harvesting their features altogether. The addition of TEP and F127 might together initiate the occurrence of the NIPS process on the outer surface before the solidification of membrane structure.

- The pore size and surface porosity were improved with enhanced mechanical properties, producing membranes with a narrow pore size distribution and water permeability as high as 922 ± 36 L m^{-2} h^{-1} bar^{-1}, suggesting the possibility of applying the membranes in water production or water reclamation processes with further modification.
- The transformation from the α-phase to the piezoelectric β-phase crystals of PVDF was found in membranes with TEP addition, endowing prepared membranes great potential in electrochemical-related applications.
- The F127 could act as a competitor against PVDF for the diluent at a relatively high dosing concentration (3 wt%), which was found to possibly hinder the polymer-diluent interaction. Besides, the instability of F127 in the PVDF matrix resulted in a low antifouling resistance of produced membranes.
- Good interactions between PTFE and F127 in the nonaqueous environment were demonstrated. The individual addition of PTFE was found to be effective in facilitating the nucleation and growth of PVDF crystals during the crystallization, resulting in membranes with smaller pore sizes, larger bulk porosity and better mechanical strength. Different from PTFE, the individually used F127 could enhance the pore formation, generating membranes with larger pore sizes and surface porosity.
- The stability of F127 in PVDF membranes could be improved in the presence of PTFE possibly due to the mediating effect of PTFE, which possesses good interactions with both PVDF and F127. The immobilized F127 could thus serve dual functions by acting as a pore-former and surface hydrophilic modifier for PVDF membranes. The prepared membranes have a narrower pore size distribution, improved porosity and strengthened tensile strength as high as 7.1 ± 0.2 MPa. Compared with the pristine PVDF membranes, the water contact angle decreased from 101 ± 4 ° to 69 ± 3 °. The hybrid membranes possess a PWP value of 876 ± 32 L m^{-2} h^{-1} bar^{-1} with mean pore size of 0.09 ± 0.01 μm and a remarkably enhanced antifouling property during a three-cycle continuous test.

7.2. Recommendations for future work

TIPS method has exhibited its potential in fabricating membranes suitable for different applications when equipped with NIPS features as suggested above. To further explore its versatility, three main directions of research are recommended, which include engineering the N-TIPS process, modeling the N-TIPS process, and applying the N-TIPS membranes to emerging separation situations in the environment-energy-health nexus.

Firstly, the current technique of fabrication should be further engineered from micro-, meso- and macro-perspectives. Rooted from the phase inversion, both TIPS and NIPS process can be substantively affected by factors on a molecular level. It is highly anticipated that the thermodynamics and kinetics of involved molecules can be observed, analyzed and engineered. Multi-dimensional carbon-based materials are recommended to be utilized as an engineering tool owing to their transformable structure, elasticity and thermal conductivity on a micro scale. From the meso-perspective, inorganic-organic composite membranes can be synthesized through surface deposition, sintering or direct blending with inorganic. On a macro scale, a new triple orifice spinneret with one more channel has been recently designed and manufactured to introduce the additional NIPS coating solution on the shell side (outer surface). The spinneret has three separate channels, namely a bore fluid channel on the inner side, a NIPS coating solution channel on the outer side and a polymer solution channel in between. This will be beneficial to the integrated fabrication of TIPS substrate and NIPS coating layer in one step, which has great potential to be scaled up in the future. Besides, it is also probable to equip the current hollow fiber spinning apparatus with co-axial 3D printing features to improve the precision of production.

Secondly, the N-TIPS process can be investigated through the modeling and simulation using tools from computational material science. A research work can be eventually regarded as a complete work only when the science meets enegineering. Substantial experimental work on TIPS and N-TIPS have been done in this study, which indicates the possibility of builing a theoretical model. The parameters involved in the fabrication can be used to develop the three-dimensional phase-field

simulation based on the Flory-Huggins theory described in **Section 2.2.2** and **5.3.1**. Testing experiments will be conducted to verify the coherence of the developed model with practical data. In this way, the knowledge acquired from the experiments can be summarized and re-structured to provide a systematic guide on the future work.

Thirdly, the membranes produced by the novel TIPS and N-TIPS methods are expected to meet the demand of emerging applications in the nexus of environment, energy and human health. With respect to the environmental needs, clean water production and wastewater purification are still two major tasks. In addition, prepared inorganic-organic membranes integrated with metal–organic frameworks (MOFs), multi-walled carbon nanotubes (MWCNTs) and graphene oxide (GO) nanosheets can also be applied to filtration of organic solvents and acid/alkali concentration with proper modifications. Other than the environmental applications, the piezoelectricity of PVDF membranes can be utilized to achieve the separation and extraction of lithium from seawater or directly used as the polyelectrolyte in the lithium-ion batteries. It can contribute to industries such as electric automobile and personal electronic device manufacturing. Last but not least, with improved anti-fouling property, membranes based on biocompatible materials can be used for diafiltration during blood purification and other medical applications.

Above all, the efforts made by researchers in the field have been pushing the boundary of TIPS and NIPS forward to an unprecedented level that makes it possible to produce membranes ranging from nonporous to microporous with various functions. It is expected that this work and its following studies can contribute to the membrane community and address the challenges in the environmental science and engineering.

Future plans for publications:

1. Fabrication of PVDF hollow fiber membranes using mild diluents via TIPS method
2. Development of dual-layer PVDF hollow fiber membranes using a triple-orifice spinneret via N-TIPS method
3. Modeling of N-TIPS process using three-dimensional phase-field simulation

References

Akshaya Jena, K. G. (2002). "Flow Porometry: What Can Flow Porometry Do For Us?".

Alwattari, A. A. and Lloyd, D. R. (1991). "Microporous membrane formation via thermally-induced phase separation. VI. Effect of diluent morphology and relative crystallization kinetics on polypropylene membrane structure." Journal of Membrane Science **64**(1–2): 55-67.

Atchariyawut, S., Feng, C., Wang, R., Jiraratananon, R. and Liang, D. T. (2006). "Effect of membrane structure on mass-transfer in the membrane gas–liquid contacting process using microporous PVDF hollow fibers." Journal of Membrane Science **285**(1–2): 272-281.

Aubert, J. H. (1990). "Structural coarsening of demixed polymer-solutions." Macromolecules **23**(5): 1446-1452.

Barton, B. and McHugh, A. (2000). "Modeling the dynamics of membrane structure formation in quenched polymer solutions." Journal of Membrane Science **166**(1): 119-125.

Bercea, M., Darie, R. N., Niţă, L. E. and Morariu, S. (2011). "Temperature Responsive Gels Based on Pluronic F127 and Poly(vinyl alcohol)." Industrial & Engineering Chemistry Research **50**(7): 4199-4206.

Bonyadi, S. and Chung, T. S. (2007). "Flux enhancement in membrane distillation by fabrication of dual layer hydrophilic–hydrophobic hollow fiber membranes." Journal of Membrane Science **306**(1–2): 134-146.

Boributh, S., Chanachai, A. and Jiraratananon, R. (2009). "Modification of PVDF membrane by chitosan solution for reducing protein fouling." Journal of Membrane Science **342**(1–2): 97-104.

Bottino, A., Camera-Roda, G., Capannelli, G. and Munari, S. (1991). "The formation of microporous polyvinylidene difluoride membranes by phase separation." Journal of Membrane Science **57**(1): 1-20.

Bottino, A., Capannelli, G. and Comite, A. (2002). "Preparation and characterization of novel porous PVDF-ZrO2 composite membranes." Desalination **146**(1): 35-40.

Bottino, A., Capannelli, G. and Comite, A. (2005). "Novel porous poly (vinylidene fluoride) membranes for membrane distillation." Desalination **183**(1–3): 375-382.

Bottino, A., Capannelli, G., D'asti, V. and Piaggio, P. (2001). "Preparation and properties of novel organic–inorganic porous membranes." Separation and purification technology **22**: 269-275.

Bottino, A., Capannelli, G., Monticelli, O. and Piaggio, P. (2000). "Poly(vinylidene fluoride) with improved functionalization for membrane production." Journal of Membrane Science **166**(1): 23-29.

Burton, A. W., Ong, K., Rea, T. and Chan, I. Y. (2009). "On the estimation of average crystallite size of zeolites from the Scherrer equation: A critical evaluation of its

application to zeolites with one-dimensional pore systems." Microporous and Mesoporous Materials **117**(1): 75-90.

Cao, X., Ma, J., Shi, X. and Ren, Z. (2006). "Effect of TiO< sub> 2</sub> nanoparticle size on the performance of PVDF membrane." Applied Surface Science **253**(4): 2003-2010.

Cha, B. J. and Yang, J. M. (2006). "Effect of high-temperature spinning and PVP additive on the properties of PVDF hollow fiber membranes for microfiltration." Macromolecular Research **14**(6): 596-602.

Chang, J., Zuo, J., Zhang, L., O'Brien, G. S. and Chung, T.-S. (2017). "Using green solvent, triethyl phosphate (TEP), to fabricate highly porous PVDF hollow fiber membranes for membrane distillation." Journal of Membrane Science **539**: 295-304.

Chen, G., Yang, X., Lu, Y., Wang, R. and Fane, A. G. (2014). "Heat transfer intensification and scaling mitigation in bubbling-enhanced membrane distillation for brine concentration." Journal of Membrane Science **470**(0): 60-69.

Chen, G., Yang, X., Wang, R. and Fane, A. G. (2013). "Performance enhancement and scaling control with gas bubbling in direct contact membrane distillation." Desalination **308**(0): 47-55.

Chen, W., Peng, J., Su, Y., Zheng, L., Wang, L. and Jiang, Z. (2009). "Separation of oil/water emulsion using Pluronic F127 modified polyethersulfone ultrafiltration membranes." Separation and Purification Technology **66**(3): 591-597.

Chou, S., Shi, L., Wang, R., Tang, C. Y., Qiu, C. and Fane, A. G. (2010). "Characteristics and potential applications of a novel forward osmosis hollow fiber membrane." Desalination **261**(3): 365-372.

Chun‐Hui, D., Chun‐Jin, W. and Li‐Guang, W. (2012). "Effects of pluronic F127 on the polymorphism and thermoresponsive properties of PVDF blend membranes via immersion precipitation process." Journal of Applied Polymer Science **124**(S1): E330-E337.

Chung, T.-S. (1997). "A critical review of polybenzimidazoles: Historical development and future r&d." Journal of Macromolecular Science, Part C: Polymer Reviews **37**(2): 277-301.

Cui, A., Liu, Z., Xiao, C. and Zhang, Y. (2010). "Effect of micro-sized SiO2-particle on the performance of PVDF blend membranes via TIPS." Journal of Membrane Science **360**(1–2): 259-264.

Cui, Z.-Y., Xu, Y.-Y., Zhu, L.-P., Wang, J.-Y., Xi, Z.-Y. and Zhu, B.-K. (2008). "Preparation of PVDF/peo-ppo-peo blend microporous membranes for lithium ion batteries via thermally induced phase separation process." Journal of Membrane Science **325**(2): 957-963.

Cui, Z.-Y., Xu, Y.-Y., Zhu, L.-P., Wei, X.-Z., Zhang, C.-F. and Zhu, B.-K. (2008). "Preparation of PVDF/PMMA blend microporous membranes for lithium ion batteries via thermally induced phase separation process." Materials Letters **62**(23): 3809-3811.

Cui, Z., Drioli, E. and Lee, Y. M. (2014). "Recent progress in fluoropolymers for membranes." Progress in Polymer Science **39**(1): 164-198.

Cui, Z., Hassankiadeh, N. T., Lee, S. Y., Lee, J. M., Woo, K. T., Sanguineti, A., Arcella, V., Lee, Y. M. and Drioli, E. (2013). "Poly(vinylidene fluoride) membrane preparation with an environmental diluent via thermally induced phase separation." Journal of Membrane Science **444**(0): 223-236.

Cui, Z., Hassankiadeh, N. T., Lee, S. Y., Woo, K. T., Lee, J. M., Sanguineti, A., Arcella, V., Lee, Y. M. and Drioli, E. (2015). "Tailoring novel fibrillar morphologies in poly(vinylidene fluoride) membranes using a low toxic triethylene glycol diacetate (TEGDA) diluent." Journal of Membrane Science **473**(0): 128-136.

Cui, Z., Hassankiadeh, N. T., Zhuang, Y., Drioli, E. and Lee, Y. M. (2015). "Crystalline polymorphism in poly(vinylidenefluoride) membranes." Progress in Polymer Science **51**: 94-126.

Cui, Z. Y., Du, C. H., Xu, Y. Y., Ji, G. L. and Zhu, B. K. (2008). "Preparation of porous PVDF membrane via thermally induced phase separation using sulfolane." Journal of Applied Polymer Science **108**(1): 272-280.

Damodar, R. A., You, S.-J. and Chou, H.-H. (2009). "Study the self cleaning, antibacterial and photocatalytic properties of tio2 entrapped PVDF membranes." Journal of Hazardous Materials **172**(2–3): 1321-1328.

Desai, P. R., Jain, N. J., Sharma, R. K. and Bahadur, P. (2001). "Effect of additives on the micellization of PEO/PPO/PEO block copolymer F127 in aqueous solution." Colloids and Surfaces A: Physicochemical and Engineering Aspects **178**(1): 57-69.

Dmitrenko, M. E., Penkova, A. V., Atta, R. R., Zolotarev, A. A., Plisko, T. V., Mazur, A. S., Solovyev, N. D. and Ermakov, S. S. (2019). "The development and study of novel membrane materials based on polyphenylene isophthalamide - Pluronic F127 composite." Materials & Design **165**: 107596.

Dohany, J. E. (2000). Fluorine-containing polymers, poly(vinylidene fluoride). Kirk-Othmer Encyclopedia of Chemical Technology, John Wiley & Sons, Inc.

Dong, C., He, G., Li, H., Zhao, R., Han, Y. and Deng, Y. (2012). "Antifouling enhancement of poly (vinylidene fluoride) microfiltration membrane by adding Mg (OH)< sub> 2</sub> nanoparticles." Journal of Membrane Science **387**: 40-47.

Drioli, E., Curcio, E. and di Profio, G. (2005). "State of the Art and Recent Progresses in Membrane Contactors." Chemical Engineering Research and Design **83**(3): 223-233.

Du, C. H., Zhu, B. K. and Xu, Y. Y. (2007). "Effects of stretching on crystalline phase structure and morphology of hard elastic PVDF fibers." Journal of Applied Polymer Science **104**(4): 2254-2259.

Ehrenstein, G. W. (2012). Polymeric Materials: Structure, Properties, Applications, Carl Hanser Verlag GmbH & Company KG.

Escobar-Chávez, J. J., López-Cervantes, M., Naik, A., Kalia, Y., Quintanar-Guerrero, D. and Ganem-Quintanar, A. (2006). "Applications of thermo-reversible pluronic F-127 gels in pharmaceutical formulations." Journal of Pharmacy & Pharmaceutical Sciences **9**(3): 339-358.

F., R. (1960). "Secondary crystallization of polymers." Journal of Polymer Science **44**(144): 517-522.

Fan, H. and Peng, Y. (2012). "Application of PVDF membranes in desalination and comparison of the VMD and DCMD processes." Chemical Engineering Science **79**(0): 94-102.

Fane, A. G., Tang, C. and Wang, R. Membrane Technology for Water: Microfiltration, Ultrafiltration, Nanofiltration and Reverse Osmosis.

Fane, A. G., Wang, R. and Hu, M. X. (2015). "Synthetic Membranes for Water Purification: Status and Future." Angewandte Chemie International Edition **54**(11): 3368-3386.

Feng, C. Y., Khulbe, K. C., Matsuura, T. and Ismail, A. F. (2013). "Recent progresses in polymeric hollow fiber membrane preparation, characterization and applications." Separation and Purification Technology **111**(0): 43-71.

Figoli, A., Marino, T., Simone, S., Di Nicolò, E., Li, X. M., He, T., Tornaghi, S. and Drioli, E. (2014). "Towards non-toxic solvents for membrane preparation: A review." Green Chemistry **16**(9): 4034-4059.

Flory, P. J. (1953). Principles of polymer chemistry. Ithaca, NY, Cornell University Press

Fried, J. R. (2003). Conformations, solutions and molecular weight. Polymer Science and Technology, Prentice Hall Professional Technical Reference.

Furusho, N., Komatsu, T. and Nakagawa, T. (1974). "A study of the thermal degradation of several halogen containing polymers by torsional braid analysis." Bulletin of the Chemical Society of Japan **47**(7): 1573-1577.

Gabelman, A. and Hwang, S.-T. (1999). "Hollow fiber membrane contactors." Journal of Membrane Science **159**(1–2): 61-106.

García-Payo, M. C., Essalhi, M. and Khayet, M. (2010). "Effects of PVDF-HFP concentration on membrane distillation performance and structural morphology of hollow fiber membranes." Journal of Membrane Science **347**(1): 209-219.

Ghasem, N., Al-Marzouqi, M. and Duaidar, A. (2011). "Effect of quenching temperature on the performance of poly(vinylidene fluoride) microporous hollow fiber membranes fabricated via thermally induced phase separation technique on the removal of CO2 from CO2-gas mixture." International Journal of Greenhouse Gas Control **5**(6): 1550-1558.

Gu, M., Zhang, J., Wang, X. and Ma, W. (2006). "Crystallization behavior of PVDF in PVDF-DMP system via thermally induced phase separation." Journal of Applied Polymer Science **102**(4): 3714-3719.

Gu, M., Zhang, J., Wang, X., Tao, H. and Ge, L. (2006). "Formation of poly(vinylidene fluoride) (PVDF) membranes via thermally induced phase separation." Desalination **192**(1–3): 160-167.

Güell, C. and Davis, R. H. (1996). "Membrane fouling during microfiltration of protein mixtures." Journal of Membrane Science **119**(2): 269-284.

Guenet, J.-M. (1992). Thermoreversible gelation of polymers and biopolymers, Academic Pr.

Hansen, C. M. (2012). Hansen solubility parameters: a user's handbook, CRC press.

Hassankiadeh, N. T., Cui, Z., Kim, J. H., Shin, D. W., Lee, S. Y., Sanguineti, A., Arcella, V., Lee, Y. M. and Drioli, E. (2015). "Microporous poly(vinylidene fluoride) hollow fiber membranes fabricated with PolarClean as water-soluble green diluent and additives." Journal of Membrane Science **479**: 204-212.

Hassankiadeh, N. T., Cui, Z., Kim, J. H., Shin, D. W., Sanguineti, A., Arcella, V., Lee, Y. M. and Drioli, E. (2014). "PVDF hollow fiber membranes prepared from green diluent via thermally induced phase separation: Effect of PVDF molecular weight." Journal of Membrane Science **471**(0): 237-246.

Hellman, D. J., Greenberg, A. R. and Krantz, W. B. (2004). "A novel process for membrane fabrication: thermally assisted evaporative phase separation (TAEPS)." Journal of Membrane Science **230**(1–2): 99-109.

Heo, C.-H., Lee, K.-M., Kim, J.-H. and Kim, S.-S. (2007). "Preparation of PVDF membrane by thermally-induced phase separation." Korean Membrane Journal **9**(1): 27-33.

Hirschinger, J., Schaefer, D., Spiess, H. W. and Lovinger, A. J. (1991). "Chain dynamics in the crystalline α-phase of poly(vinylidene fluoride) by two-dimensional exchange 2h nmr." Macromolecules **24**(9): 2428-2433.

Hou, D., Wang, J., Qu, D., Luan, Z. and Ren, X. (2009). "Fabrication and characterization of hydrophobic PVDF hollow fiber membranes for desalination through direct contact membrane distillation." Separation and Purification Technology **69**(1): 78-86.

Hou, D., Wang, J., Sun, X., Ji, Z. and Luan, Z. (2012). "Preparation and properties of PVDF composite hollow fiber membranes for desalination through direct contact membrane distillation." Journal of Membrane Science **405–406**(0): 185-200.

Ji, G.-L., Zhu, B.-K., Cui, Z.-Y., Zhang, C.-F. and Xu, Y.-Y. (2007). "PVDF porous matrix with controlled microstructure prepared by TIPS process as polymer electrolyte for lithium ion battery." Polymer **48**(21): 6415-6425.

Ji, G.-L., Zhu, L.-P., Zhu, B.-K., Zhang, C.-F. and Xu, Y.-Y. (2008). "Structure formation and characterization of PVDF hollow fiber membrane prepared via TIPS with diluent mixture." Journal of Membrane Science **319**(1–2): 264-270.

Ji, G. L., Du, C. H., Zhu, B. K. and Xu, Y. Y. (2007). "Preparation of porous PVDF membrane via thermally induced phase separation with diluent mixture of DBP and DEHP." Journal of Applied Polymer Science **105**(3): 1496-1502.

Ji, G. L., Zhu, L. P., Zhu, B. K. and Xu, Y. Y. (2008). "Effect of diluents on crystallization of poly(vinylidene fluoride) and phase separated structure in a ternary system via thermally induced phase separation." Chinese Journal of Polymer Science (English Edition) **26**(3): 291-298.

Jian, K. and Pintauro, P. N. (1997). "Asymmetric PVDF hollow-fiber membranes for organic/water pervaporation separations." Journal of Membrane Science **135**(1): 41-53.

Jung, J. T., Kim, J. F., Wang, H. H., di Nicolo, E., Drioli, E. and Lee, Y. M. (2016). "Understanding the non-solvent induced phase separation (NIPS) effect during the fabrication of microporous PVDF membranes via thermally induced phase separation (TIPS)." Journal of Membrane Science **514**: 250-263.

Jung, J. T., Wang, H. H., Kim, J. F., Lee, J., Kim, J. S., Drioli, E. and Lee, Y. M. (2018). "Tailoring nonsolvent-thermally induced phase separation (N-TIPS) effect using triple spinneret to fabricate high performance PVDF hollow fiber membranes." Journal of Membrane Science **559**: 117-126.

Kabanov, A. V., Batrakova, E. V. and Alakhov, V. Y. (2002). "Pluronic® block copolymers as novel polymer therapeutics for drug and gene delivery." Journal of Controlled Release **82**(2): 189-212.

Kang, G.-d. and Cao, Y.-m. (2014). "Application and modification of poly(vinylidene fluoride) (PVDF) membranes – a review." Journal of Membrane Science **463**(0): 145-165.

Khayet, M., Feng, C. Y., Khulbe, K. C. and Matsuura, T. (2002). "Preparation and characterization of polyvinylidene fluoride hollow fiber membranes for ultrafiltration." Polymer **43**(14): 3879-3890.

Khayet, M., Khulbe, K. C. and Matsuura, T. (2004). "Characterization of membranes for membrane distillation by atomic force microscopy and estimation of their water vapor transfer coefficients in vacuum membrane distillation process." Journal of Membrane Science **238**(1–2): 199-211.

Khayet, M. and Matsuura, T. (2011). Membrane Distillation: Principles and Applications. Amsterdam, Elsevier.

Kim, J.-H. and Lee, K.-H. (1998). "Effect of PEG additive on membrane formation by phase inversion." Journal of Membrane Science **138**(2): 153-163.

Kim, J. F., Kim, J. H., Lee, Y. M. and Drioli, E. (2016). "Thermally induced phase separation and electrospinning methods for emerging membrane applications: A review." AIChE Journal **62**(2): 461-490.

Kim, S. S., Lim, G. B. A., Alwattari, A. A., Wang, Y. F. and Lloyd, D. R. (1991). "Microporous membrane formation via thermally-induced phase separation. V. Effect of diluent mobility and crystallization on the structure of isotactic polypropylene membranes." Journal of Membrane Science **64**(1–2): 41-53.

Kim, S. S. and Lloyd, D. R. (1991). "Microporous membrane formation via thermally-induced phase separation. III. Effect of thermodynamic interactions on the structure of isotactic polypropylene membranes." Journal of Membrane Science **64**(1–2): 13-29.

Kim, S. S. and Lloyd, D. R. (1992). "Thermodynamics of polymer/diluent systems for thermally induced phase separation: 3. Liquid-liquid phase separation systems." Polymer **33**(5): 1047-1057.

Komaki, Y. (1979). "Growth of fine holes by the chemical etching of fission tracks in polyvinylidene fluoride." Nuclear Tracks **3**(1-2): 33-44.

Lang, W.-Z., Xu, Z.-L., Yang, H. and Tong, W. (2007). "Preparation and characterization of PVDF–pfsa blend hollow fiber UF membrane." Journal of membrane science **288**(1): 123-131.

Larsen, S. T. L. (2009). Lack of freshwater throughout the world.

Lee, J., Park, B., Kim, J. and Park, S. B. (2015). "Effect of PVP, lithium chloride, and glycerol additives on PVDF dual-layer hollow fiber membranes fabricated using simultaneous spinning of TIPS and NIPS." Macromolecular Research **23**(3): 291-299.

Li, H. and Kim, H. (2008). "Thermal degradation and kinetic analysis of PVDF/modified mmt nanocomposite membranes." Desalination **234**(1): 9-15.

Li, J.-H., Xu, Y.-Y., Zhu, L.-P., Wang, J.-H. and Du, C.-H. (2009). "Fabrication and characterization of a novel TiO2 nanoparticle self-assembly membrane with improved fouling resistance." Journal of Membrane Science **326**(2): 659-666.

Li, K., Kong, J. F., Wang, D. and Teo, W. K. (1999). "Tailor-made asymmetric PVDF hollow fibers for soluble gas removal." AIChE Journal **45**(6): 1211-1219.

Li, N. N., Fane, A. G., Ho, W. S. W. and Matsuura, T. (2008). Advanced membrane technology and applications, Wiley-AIChE.

Li, X., Fang, X., Pang, R., Li, J., Sun, X., Shen, J., Han, W. and Wang, L. (2014). "Self-assembly of TiO2 nanoparticles around the pores of PES ultrafiltration membrane for mitigating organic fouling." Journal of Membrane Science **467**: 226-235.

Li, X. and Lu, X. (2006). "Morphology of polyvinylidene fluoride and its blend in thermally induced phase separation process." Journal of Applied Polymer Science **101**(5): 2944-2952.

Liao, Y., Loh, C.-H., Wang, R. and Fane, A. G. (2014). "Electrospun Superhydrophobic Membranes with Unique Structures for Membrane Distillation." ACS Applied Materials & Interfaces **6**(18): 16035-16048.

Liao, Y., Wang, R., Tian, M., Qiu, C. and Fane, A. G. (2013). "Fabrication of polyvinylidene fluoride (PVDF) nanofiber membranes by electro-spinning for direct contact membrane distillation." Journal of Membrane Science **425–426**(0): 30-39.

Lin, D.-J., Chang, H.-H., Chen, T.-C., Lee, Y.-C. and Cheng, L.-P. (2006). "Formation of porous poly(vinylidene fluoride) membranes with symmetric or asymmetric morphology by immersion precipitation in the water/TEP/PVDF system." European Polymer Journal **42**(7): 1581-1594.

Lin, S.-Y., Lin, Y.-Y., Chen, E.-M., Hsu, C.-T. and Kwan, C.-C. (1999). "A Study of the Equilibrium Surface Tension and the Critical Micelle Concentration of Mixed Surfactant Solutions." Langmuir **15**(13): 4370-4376.

Lindvig, T., Michelsen, M. L. and Kontogeorgis, G. M. (2002). "A flory–huggins model based on the hansen solubility parameters." Fluid phase equilibria **203**(1): 247-260.

Liu, B., Du, Q. and Yang, Y. (2000). "The phase diagrams of mixtures of EVAL and PEG in relation to membrane formation." Journal of Membrane Science **180**(1): 81-92.

Liu, F., Hashim, N. A., Liu, Y., Abed, M. R. M. and Li, K. (2011). "Progress in the production and modification of PVDF membranes." Journal of Membrane Science **375**(1-2): 1-27.

Liu, F., Tao, M.-m. and Xue, L.-x. (2012). "PVDF membranes with inter-connected pores prepared via a Nat-ips process." Desalination **298**: 99-105.

Liu, F., Xu, Y.-Y., Zhu, B.-K., Zhang, F. and Zhu, L.-P. (2009). "Preparation of hydrophilic and fouling resistant poly(vinylidene fluoride) hollow fiber membranes." Journal of Membrane Science **345**(1): 331-339.

Liu, T., Liu, L. and Chu, B. (2000). Formation of amphiphilic block copolymer micelles in nonaqueous solution. Amphiphilic Block Copolymers: Self-Assembly and Applications. P. Alexandridis and B. Lindman**:** 115-149.

Liu, Y., Koops, G. and Strathmann, H. (2003). "Characterization of morphology controlled polyethersulfone hollow fiber membranes by the addition of polyethylene glycol to the dope and bore liquid solution." Journal of membrane science **223**(1): 187-199.

Lloyd, D. R., Kim, S. S. and Kinzer, K. E. (1991). "Microporous membrane formation via thermally-induced phase separation. II. Liquid—liquid phase separation." Journal of Membrane Science **64**(1–2): 1-11.

Lloyd, D. R., Kinzer, K. E. and Tseng, H. S. (1990). "Microporous membrane formation via thermally induced phase separation. I. Solid-liquid phase separation." Journal of Membrane Science **52**(3): 239-261.

Loeb, S. and Sourirajan, S. (1964). High flow porous membranes for separating water from saline solutions. U.S. Pat. 3, 133, 132, Univ, California.

Loh, C. and Wang, R. (2014). "Fabrication of PVDF hollow fiber membranes: Effects of low-concentration pluronic and spinning conditions." Journal of Membrane Science **466**(0): 130-141.

Loh, C. H. and Wang, R. (2012). "Effects of additives and coagulant temperature on fabrication of high performance PVDF/pluronic F127 blend hollow fiber membranes via nonsolvent induced phase separation." Chinese Journal of Chemical Engineering **20**(1): 71-79.

Loh, C. H. and Wang, R. (2013). "Insight into the role of amphiphilic pluronic block copolymer as pore-forming additive in PVDF membrane formation." Journal of Membrane Science **446**(0): 492-503.

Loh, C. H., Wang, R., Shi, L. and Fane, A. G. (2011). "Fabrication of high performance polyethersulfone UF hollow fiber membranes using amphiphilic pluronic block copolymers as pore-forming additives." Journal of Membrane Science **380**(1–2): 114-123.

Lovinger, A. J. (1982). "Annealing of poly(vinylidene fluoride) and formation of a fifth phase." Macromolecules **15**(1): 40-44.

Lovinger, A. J. and Freed, D. J. (1980). "Inhomogeneous thermal degradation of poly(vinylidene fluoride) crystallized from the melt." Macromolecules **13**(4): 989-994.

Ma, T., Cui, Z., Wu, Y., Qin, S., Wang, H., Yan, F., Han, N. and Li, J. (2013). "Preparation of PVDF based blend microporous membranes for lithium ion batteries by thermally induced phase separation: I. Effect of PMMA on the membrane formation process and the properties." Journal of Membrane Science **444**(0): 213-222.

Ma, W., Chen, S., Zhang, J., Wang, X. and Miao, W. (2008). "Membrane formation of poly(vinylidene fluoride)/poly(methyl methacrylate)/diluents via thermally induced phase separation." Journal of Applied Polymer Science **111**(3): 1235-1245.

Ma, W., Wang, X. and Zhang, J. (2010). "Effect of MMT, SiO2, CaCO3, and PTFE nanoparticles on the morphology and crystallization of poly(vinylidene fluoride)." Journal of Polymer Science Part B: Polymer Physics **48**(20): 2154-2164.

Ma, W., Zhang, J., Bruggen, B. V. d. and Wang, X. (2013). "Formation of an interconnected lamellar structure in PVDF membranes with nanoparticles addition via solid-liquid thermally induced phase separation." Journal of Applied Polymer Science **127**(4): 2715-2723.

Madaeni, S. and Yeganeh, M. (2003). "Microfiltration of emulsified oil wastewater." Journal of Porous Materials **10**(2): 131-138.

Marega, C. and Marigo, A. (2003). "Influence of annealing and chain defects on the melting behaviour of poly(vinylidene fluoride)." European Polymer Journal **39**(8): 1713-1720.

Masuelli, M., Marchese, J. and Ochoa, N. A. (2009). "SPC/PVDF membranes for emulsified oily wastewater treatment." Journal of Membrane Science **326**(2): 688-693.

Matsuyama, H., Berghmans, S. and Lloyd, D. R. (1999). "Formation of anisotropic membranes via thermally induced phase separation." Polymer **40**(9): 2289-2301.

Matsuyama, H., Maki, T., Teramoto, M. and Asano, K. (2002). "Effect of polypropylene molecular weight on porous membrane formation by thermally induced phase separation." Journal of Membrane Science **204**(1–2): 323-328.

Matsuyama, H., Okafuji, H., Maki, T., Teramoto, M. and Kubota, N. (2003). "Preparation of polyethylene hollow fiber membrane via thermally induced phase separation." Journal of Membrane Science **223**(1–2): 119-126.

Matsuyama, H., Takida, Y., Maki, T. and Teramoto, M. (2002). "Preparation of porous membrane by combined use of thermally induced phase separation and immersion precipitation." Polymer **43**(19): 5243-5248.

McGuire, K. S., Lloyd, D. R. and Lim, G. B. A. (1993). "Microporous membrane formation via thermally-induced phase separation. VII. Effect of dilution, cooling rate, and nucleating agent addition on morphology." Journal of Membrane Science **79**(1): 27-34.

Miles, M. J. (1988). Gelation. Developments in Crystalline Polymers. D. C. Bassett, Springer Netherlands**:** 233-295.

Mirko, N., Anke, M. and Carsten, W. (2000). "Immobilization of PEO-PPO-PEO triblock copolymers on PTFE-like fluorocarbon surfaces." Journal of Biomedical Materials Research **50**(3): 340-343.

Moghareh Abed, M. R., Kumbharkar, S. C., Groth, A. M. and Li, K. (2013). "Economical production of PVDF-g-POEM for use as a blend in preparation of PVDF based hydrophilic hollow fibre membranes." Separation and Purification Technology **106**: 47-55.

Mulder, M. J. (1996). Basic principles of membrane technology, Kluwer Academic Publishers.

Nguyen, T. (1985). "Degradation of poly(vinyl fluoride) and poly(vinylidene fluoride)." Journal of Macromolecular Science - Reviews in Macromolecular Chemistry and Physics **C25**(2): 227-275.

Nic, M., Jirat, J. and Kosata, B. (2012). Iupac compendium of chemical terminology (gold book), International Union of Pure and Applied Chemistry.

Oh, S. J., Kim, N. and Lee, Y. T. (2009). "Preparation and characterization of PVDF/TiO2 organic-inorganic composite membranes for fouling resistance improvement." Journal of Membrane Science **345**(1-2): 13-20.

Patterson, A. L. (1939). "The Scherrer Formula for X-Ray Particle Size Determination." Physical Review **56**(10): 978-982.

Pitto-Barry, A. and Barry, N. P. (2014). "Pluronic® block-copolymers in medicine: from chemical and biological versatility to rationalisation and clinical advances." Polymer Chemistry **5**(10): 3291-3297.

Raimo, M. (2011). "Estimation of polymer nucleation and growth rates by overall DSC crystallization rates." Polymer Journal **43**: 78.

Rajabzadeh, S., Liang, C., Ohmukai, Y., Maruyama, T. and Matsuyama, H. (2012). "Effect of additives on the morphology and properties of poly(vinylidene fluoride) blend hollow fiber membrane prepared by the thermally induced phase separation method." Journal of Membrane Science **423–424**(0): 189-194.

Rajabzadeh, S., Maruyama, T., Ohmukai, Y., Sotani, T. and Matsuyama, H. (2009). "Preparation of PVDF/PMMA blend hollow fiber membrane via thermally induced phase separation (TIPS) method." Separation and Purification Technology **66**(1): 76-83.

Rajabzadeh, S., Maruyama, T., Sotani, T. and Matsuyama, H. (2008). "Preparation of PVDF hollow fiber membrane from a ternary polymer/solvent/nonsolvent system via thermally induced phase separation (TIPS) method." Separation and Purification Technology **63**(2): 415-423.

Reichardt, C. and Welton, T. (2011). Solvents and solvent effects in organic chemistry, John Wiley & Sons.

Schneider, S., Drujon, X., Lotz, B. and Wittmann, J. C. (2001). "Self-nucleation and enhanced nucleation of polyvinylidene fluoride (α-phase)." Polymer **42**(21): 8787-8798.

Setiawan, L., Wang, R., Shi, L., Li, K. and Fane, A. G. (2012). "Novel dual-layer hollow fiber membranes applied for forward osmosis process." Journal of Membrane Science **421-422**: 238-246.

Shah, V., Bharatiya, B. and Shah, D. O. (2018). "Effect of molecular weight and diffusivity on the adsorption of PEO-PPO-PEO block copolymers at PTFE-water and oil-water interfaces." Colloid and Polymer Science.

Shah, V., Bharatiya, B., Shah, D. O. and Mukherjee, T. (2015). "Correlation of Dynamic Surface Tension with Sedimentation of PTFE Particles and Water Penetration in Powders." Langmuir **31**(51): 13725-13733.

Shang, M., Matsuyama, H., Teramoto, M., Lloyd, D. R. and Kubota, N. (2003). "Preparation and membrane performance of poly(ethylene-co-vinyl alcohol) hollow fiber membrane via thermally induced phase separation." Polymer **44**(24): 7441-7447.

Sharma, M., Bharatiya, B., Mehta, K., Shukla, A. and Shah, D. O. (2014). "Novel Strategy Involving Surfactant–Polymer Combinations for Enhanced Stability of Aqueous Teflon Dispersions." Langmuir **30**(24): 7077-7084.

She, Q., Tang, C. Y., Wang, Y.-N. and Zhang, Z. (2009). "The role of hydrodynamic conditions and solution chemistry on protein fouling during ultrafiltration." Desalination **249**(3): 1079-1087.

Shi, F., Ma, Y., Ma, J., Wang, P. and Sun, W. (2012). "Preparation and characterization of PVDF/TiO2 hybrid membranes with different dosage of nano-TiO2." Journal of Membrane Science **389**(0): 522-531.

Shi, F., Ma, Y., Ma, J., Wang, P. and Sun, W. (2012). "Preparation and characterization of PVDF/TiO< sub> 2</sub> hybrid membranes with different dosage of nano-TiO< sub> 2</sub>." Journal of Membrane Science **389**: 522-531.

Shi, L., Wang, R. and Cao, Y. (2009). "Effect of the rheology of poly(vinylidene fluoride-co-hexafluropropylene) (PVDF-HFP) dope solutions on the formation of microporous hollow fibers used as membrane contactors." Journal of Membrane Science **344**(1-2): 112-122.

Shi, L., Wang, R., Cao, Y., Feng, C., Liang, D. T. and Tay, J. H. (2007). "Fabrication of poly(vinylidene fluoride-co-hexafluropropylene) (PVDF-HFP) asymmetric microporous hollow fiber membranes." Journal of Membrane Science **305**(1–2): 215-225.

Shi, L., Wang, R., Cao, Y., Liang, D. T. and Tay, J. H. (2008). "Effect of additives on the fabrication of poly(vinylidene fluoride-co-hexafluropropylene) (PVDF-HFP) asymmetric microporous hollow fiber membranes." Journal of Membrane Science **315**(1–2): 195-204.

Shinohara, H. (1979). "Fluorination of polyhydrofluoroethylenes - 2. Formation of perfluoroalkyl carboxylic acids on the suface region of poly(vinylidene fluoride) film by oxyfluorination, fluorination, and hydrolysis." J Polym Sci Polym Chem Ed **17**(5): 1543-1556.

Smolders, K. and Franken, A. C. M. (1989). "Terminology for membrane distillation." Desalination **72**(3): 249-262.

Solvay (2014). Solef 6020 PVDF Technical Data Sheet.

Song, S.-W. and Torkelson, J. M. (1995). "Coarsening effects on the formation of microporous membranes produced via thermally induced phase separation of polystyrene-cyclohexanol solutions." Journal of Membrane Science **98**(3): 209-222.

Song, Y., Wang, Z., Wang, Q., Li, B. and Zhong, B. (2016). "Preparation of PVDF/CaCO3 hybrid hollow fiber membranes for direct contact membrane distillation through TIPS method." Journal of Applied Polymer Science **133**(18): n/a-n/a.

Song, Z., Xing, M., Zhang, J., Li, B. and Wang, S. (2012). "Determination of phase diagram of a ternary PVDF/γ-BL/DOP system in TIPS process and its application in preparing hollow fiber membranes for membrane distillation." Separation and Purification Technology **90**(0): 221-230.

Su, M., Teoh, M. M., Wang, K. Y., Su, J. and Chung, T.-S. (2010). "Effect of inner-layer thermal conductivity on flux enhancement of dual-layer hollow fiber membranes in direct contact membrane distillation." Journal of Membrane Science **364**(1–2): 278-289.

Su, Y., Chen, C., Li, Y. and Li, J. (2007). "PVDF membrane formation via thermally induced phase separation." Journal of Macromolecular Science, Part A: Pure and Applied Chemistry **44**(1): 99-104.

Tanaka, T. (1992). Polyelectrolyte gels, American Chemical Society.

Tao, M.-m., Liu, F., Ma, B.-r. and Xue, L.-x. (2013). "Effect of solvent power on PVDF membrane polymorphism during phase inversion." Desalination **316**: 137-145.

Teipel, U. (2006). Energetic materials: particle processing and characterization, John Wiley & Sons.

Teoh, M. M. and Chung, T.-S. (2009). "Membrane distillation with hydrophobic macrovoid-free PVDF–PTFE hollow fiber membranes." Separation and Purification Technology **66**(2): 229-236.

Teoh, M. M., Chung, T.-S. and Yeo, Y. S. (2011). "Dual-layer PVDF/PTFE composite hollow fibers with a thin macrovoid-free selective layer for water production via membrane distillation." Chemical Engineering Journal **171**(2): 684-691.

United-Nations (2012). The millennium development goals report 2012.

Vadnere, M., Amidon, G., Lindenbaum, S. and Haslam, J. L. (1984). "Thermodynamic studies on the gel-sol transition of some pluronic polyols." International Journal of Pharmaceutics **22**(2): 207-218.

van de Witte, P., Dijkstra, P. J., van den Berg, J. W. A. and Feijen, J. (1996). "Phase separation processes in polymer solutions in relation to membrane formation." Journal of Membrane Science **117**(1–2): 1-31.

Van Oss, C. J., Good, R. J. and Chaudhury, M. K. (1986). "The role of van der Waals forces and hydrogen bonds in “hydrophobic interactions” between biopolymers and low energy surfaces." Journal of Colloid and Interface Science **111**(2): 378-390.

Vasilescu, M. and Bandula, R. (2011). "Aggregation of Pluronic F127 and polydimethylsiloxane-graft-polyether block copolymers in water and microstructure of aggregates as evaluated by molecular probe techniques." Rev Roum Chim **56**(1): 57-64.

Voorhees, P. W. (1992). "Ostwald ripening of two-phase mixtures." Annual Review of Materials Science **22**(1): 197-215.

Wang, K. Y., Chung, T.-S. and Gryta, M. (2008). "Hydrophobic PVDF hollow fiber membranes with narrow pore size distribution and ultra-thin skin for the fresh water production through membrane distillation." Chemical Engineering Science **63**(9): 2587-2594.

Wang, K. Y., Fei Li, D., Chung, T.-S. and Bor Chen, S. (2004). "The observation of elongation dependent macrovoid evolution in single- and dual-layer asymmetric hollow fiber membranes." Chemical Engineering Science **59**(21): 4657-4660.

Wang, K. Y., Foo, S. W. and Chung, T.-S. (2009). "Mixed matrix PVDF hollow fiber membranes with nanoscale pores for desalination through direct contact membrane distillation." Industrial & Engineering Chemistry Research **48**(9): 4474-4483.

Wang, L., Huang, D., Wang, X., Meng, X., Lv, Y., Wang, X. and Miao, R. (2015). "Preparation of PVDF membranes via the low-temperature TIPS method with diluent mixtures: The role of coagulation conditions and cooling rate." Desalination **361**: 25-37.

Wang, P. and Chung, T.-S. (2015). "Recent advances in membrane distillation processes: Membrane development, configuration design and application exploring." Journal of Membrane Science **474**(0): 39-56.

Wang, R., Shi, L., Tang, C. Y., Chou, S., Qiu, C. and Fane, A. G. (2010). "Characterization of novel forward osmosis hollow fiber membranes." Journal of Membrane Science **355**(1–2): 158-167.

Wang, X. Q., Chen, D. R., Han, J. C. and Du, S. Y. (2002). "Crystallization behavior of polytetrafluoroethylene (PTFE)." Journal of Applied polymer science **83**(5): 990-996.

Wang, Y.-N. and Tang, C. Y. (2011). "Fouling of Nanofiltration, Reverse Osmosis, and Ultrafiltration Membranes by Protein Mixtures: The Role of Inter-Foulant-Species Interaction." Environmental Science & Technology **45**(15): 6373-6379.

Wang, Y.-q., Wang, T., Su, Y.-l., Peng, F.-b., Wu, H. and Jiang, Z.-y. (2005). "Remarkable Reduction of Irreversible Fouling and Improvement of the Permeation Properties of Poly(ether sulfone) Ultrafiltration Membranes by Blending with Pluronic F127." Langmuir **21**(25): 11856-11862.

Wang, Z., Sun, L., Wang, Q., Li, B. and Wang, S. (2014). "A novel approach to fabricate interconnected sponge-like and highly permeable polyvinylidene fluoride hollow fiber membranes for direct contact membrane distillation." European Polymer Journal **60**(0): 262-272.

Wei, Y., Chu, H.-Q., Dong, B.-Z., Li, X., Xia, S.-J. and Qiang, Z.-M. (2011). "Effect of TiO< sub> 2</sub> nanowire addition on PVDF ultrafiltration membrane performance." Desalination **272**(1): 90-97.

Wongchitphimon, S., Wang, R., Jiraratananon, R., Shi, L. and Loh, C. H. (2011). "Effect of polyethylene glycol (PEG) as an additive on the fabrication of polyvinylidene fluoride-co-hexafluropropylene (PVDF-HFP) asymmetric microporous hollow fiber membranes." Journal of Membrane Science **369**(1-2): 329-338.

Xiao, T., Wang, P., Yang, X., Cai, X. and Lu, J. (2015). "Fabrication and characterization of novel asymmetric polyvinylidene fluoride (PVDF) membranes by the nonsolvent thermally induced phase separation (NTIPS) method for membrane distillation applications." Journal of Membrane Science **489**: 160-174.

Xiong, X. Y., Tam, K. C. and Gan, L. H. (2003). "Synthesis and Aggregation Behavior of Pluronic F127/Poly(lactic acid) Block Copolymers in Aqueous Solutions." Macromolecules **36**(26): 9979-9985.

Xu, H.-P., Lang, W.-Z., Yan, X., Zhang, X. and Guo, Y.-J. (2014). "Preparation and characterizations of poly(vinylidene fluoride)/oxidized multi-wall carbon nanotubes membranes with bi-continuous structure by thermally induced phase separation method." Journal of Membrane Science **467**(0): 142-152.

Yan, L., Li, Y. S., Xiang, C. B. and Xianda, S. (2006). "Effect of nano-sized Al2O3-particle addition on PVDF ultrafiltration membrane performance." Journal of Membrane Science **276**(1-2): 162-167.

Yang, J., Li, D. W., Lin, Y. K., Wang, X. L., Tian, F. and Wang, Z. (2008). "Formation of a bicontinuous structure membrane of polyvinylidene fluoride in diphenyl ketone diluent via thermally induced phase separation." Journal of Applied Polymer Science **110**(1): 341-347.

Yang, J., Wang, X. L., Tian, F., Lin, Y. K. and Wang, Z. (2008). "Diluent selection of PVDF membrane prepared via thermally induced phase separation." Gaodeng Xuexiao Huaxue Xuebao/Chemical Journal of Chinese Universities **29**(9): 1895-1900.

Yang, X., Wang, R., Shi, L., Fane, A. G. and Debowski, M. (2011). "Performance improvement of PVDF hollow fiber-based membrane distillation process." Journal of Membrane Science **369**(1–2): 437-447.

Yuan, Z. and Dan-Li, X. (2008). "Porous PVDF/TPU blends asymmetric hollow fiber membranes prepared with the use of hydrophilic additive PVP (k30)." Desalination **223**(1–3): 438-447.

Zhang, F., Zhang, W., Yu, Y., Deng, B., Li, J. and Jin, J. (2013). "Sol–gel preparation of PAA-g-PVDF/TiO2 nanocomposite hollow fiber membranes with extremely high water flux and improved antifouling property." Journal of Membrane Science **432**: 25-32.

Zhang, M., Zhang, A.-Q., Zhu, B.-K., Du, C.-H. and Xu, Y.-Y. (2008). "Polymorphism in porous poly(vinylidene fluoride) membranes formed via immersion precipitation process." Journal of Membrane Science **319**(1): 169-175.

Zhang, Y., Lin, R., Yuan, M. and Yue, X. (2013). "Effects of pore-forming additives on structures and properties of PVDF/Fe3+/Cu2+ hollow fiber membranes." Desalination and Water Treatment **51**(19-21): 3903-3908.

Zhang, Z., Guo, C., Li, X., Liu, G. and Lv, J. (2013). "Effects of PVDF Crystallization on Polymer Gelation Behavior and Membrane Structure from PVDF/TEP System via Modified TIPS Process." Polymer-Plastics Technology and Engineering **52**(6): 564-570.

Zhang, Z., Guo, C., Liu, G., Li, X., Guan, Y. and Lv, J. (2014). "Effect of TEP content in cooling bath on porous structure, crystalline and mechanical properties of PVDF hollow fiber membranes." Polymer Engineering & Science **54**(9): 2207-2214.

Zhao, J., Shi, L., Loh, C. H. and Wang, R. (2018). "Preparation of PVDF/PTFE hollow fiber membranes for direct contact membrane distillation via thermally induced phase separation method." Desalination **430**: 86-97.

Zhao, W., Su, Y., Li, C., Shi, Q., Ning, X. and Jiang, Z. (2008). "Fabrication of antifouling polyethersulfone ultrafiltration membranes using Pluronic F127 as both surface modifier and pore-forming agent." Journal of Membrane Science **318**(1): 405-412.